DNA-TR-84-219-V1

SIMULATION DEVELOPMENT FOR SILO TEST PROGRAM (STP)

Volume I—Design and Evaluation of a Variable HEST for STP 3.5A Experiment

M. Sanai
J.D. Colton
SRI International
333 Ravenswood Avenue
Menlo Park, CA 94025

31 March 1984

Technical Report

CONTRACT No. DNA 001-82-C-0103

THIS WORK WAS SPONSORED BY THE DEFENSE NUCLEAR AGENCY
UNDER RDT&E RMSS CODE B344083466 Y99QAXSD00046 H2590D.

Prepared for
Director
DEFENSE NUCLEAR AGENCY
Washington, DC 20305-1000

Destroy this report when it is no longer needed. Do not return to sender.

PLEASE NOTIFY THE DEFENSE NUCLEAR AGENCY, ATTN: STTI, WASHINGTON, DC 20305-1000, IF YOUR ADDRESS IS INCORRECT, IF YOU WISH IT DELETED FROM THE DISTRIBUTION LIST, OR IF THE ADDRESSEE IS NO LONGER EMPLOYED BY YOUR ORGANIZATION.

UNCLASSIFIED
SECURITY CLASSIFICATION OF THIS PAGE

AD-A163 274

REPORT DOCUMENTATION PAGE

Form Approved
OMB No. 0704-0188
Exp. Date: Jun 30, 1986

1a REPORT SECURITY CLASSIFICATION UNCLASSIFIED	1b RESTRICTIVE MARKINGS
2a SECURITY CLASSIFICATION AUTHORITY	3 DISTRIBUTION/AVAILABILITY OF REPORT Approved for public release; distribution is unlimited.
2b DECLASSIFICATION/DOWNGRADING SCHEDULE N/A since UNCLASSIFIED	
4 PERFORMING ORGANIZATION REPORT NUMBER(S) SRI Project PYU-4015	5 MONITORING ORGANIZATION REPORT NUMBER(S) DNA-TR-84-219-V1
6a NAME OF PERFORMING ORGANIZATION SRI International 6b OFFICE SYMBOL (If applicable)	7a NAME OF MONITORING ORGANIZATION Director Defense Nuclear Agency
6c ADDRESS (City, State, and ZIP Code) 333 Ravenswood Avenue Menlo Park, CA 94025	7b ADDRESS (City, State, and ZIP Code) Washington, DC 20305-1000
8a NAME OF FUNDING/SPONSORING ORGANIZATION 8b OFFICE SYMBOL (If applicable)	9 PROCUREMENT INSTRUMENT IDENTIFICATION NUMBER DNA 001-82-C-0103
8c ADDRESS (City, State, and ZIP Code)	10 SOURCE OF FUNDING NUMBERS PROGRAM ELEMENT NO: 62715H; PROJECT NO: Y99QAXS; TASK NO: D; WORK UNIT ACCESSION NO: DH006596

11 TITLE (Include Security Classification)
SIMULATION DEVELOPMENT FOR SILO TEST PROGRAM (STP)
Volume I—Design and Evaluation of a Variable HEST for STP 3.5A Experiment

12 PERSONAL AUTHOR(S)
M. Sanai J.D. Colton

13a TYPE OF REPORT	13b TIME COVERED	14 DATE OF REPORT (Year, Month, Day)	15 PAGE COUNT
Technical	FROM 820111 TO 840331	840331	108

16 SUPPLEMENTARY NOTATION
This work was sponsored by the Defense Nuclear Agency under RDT&E RMSS Code B344083466 Y99QAXSD00046 H2590D.

17 COSATI CODES			18 SUBJECT TERMS (Continue on reverse if necessary and identify by block number)
FIELD	GROUP	SUB-GROUP	Airblast Simulation; Simulation of Weapon Effects; Ground Shock Simulation; High Explosive Simulation Technique (HEST)
14	2		
16	1		

19 ABSTRACT (Continue on reverse if necessary and identify by block number)

In support of the Defense Nuclear Agency (DNA) Silo Test Program (STP), we designed and evaluated the performance of a variable high explosive simulation technique (HEST) to simulate the airblast environment resulting from a 1.95-kt (1/8-scale of 1 MT) nuclear surface burst over a pressure range of 500 MPa (5 kbar) to 7 MPa (1000 psi). Our final design consisted of a variable HEST in which Iremite-60 explosive is used predominantly in the pressure range from 500 to 100 MPa, and 0.085 kg/m (400 grain/ft) primacord explosive is used in the pressure range from 100 to 7 MPa. The overburden height increases linearly with range from 0.64 to 1.15 m. The cavity height increases linearly with the range from 38 mm to the 500-MPa location to 70 mm at the 35-MPa location. Beyond this point, the cavity height remains constant at 70 mm.

The above HEST simulator was used in the STP 3.5A experiment performed by WES at Fort Knox. On the basis of photopole, airblast, and near surface soil stress gage data,

20 DISTRIBUTION/AVAILABILITY OF ABSTRACT	21 ABSTRACT SECURITY CLASSIFICATION
☐ UNCLASSIFIED/UNLIMITED ☒ SAME AS RPT ☐ DTIC USERS	UNCLASSIFIED
22a NAME OF RESPONSIBLE INDIVIDUAL Betty L. Fox	22b TELEPHONE (Include Area Code) (202) 325-7042
	22c OFFICE SYMBOL DNA/STTI

DD FORM 1473, 84 MAR 83 APR edition may be used until exhausted
All other editions are obsolete

SECURITY CLASSIFICATION OF THIS PAGE
UNCLASSIFIED

19. ABSTRACT (Continued)

the impulse from the HEST agreed, to within measurement error, with the design goals for both short (10 ms) and long (90 ms) time frames. Hence, the full positive phase of a 1.95-kt surface burst was successfully simulated by the HEST.

PREFACE

This is one of two reports on investigations performed for the Defense Nuclear Agency (DNA) under Contract DNA001-82-C-0103 during the period 11 January 1982 to 31 March 1984. Technical monitors for this work were Major M. E. Furbee (now at BMO) and Dr. K. Goering.

Most of the experiments reported here were performed by the Waterways Experiment Station (WES) under the supervision of Mr. R. Welch and Mr. J. Balsara. Mr. J. Gran and Mr. C. Romander from SKI supervised the gage placement and participated in the evaluation of the data in the STP 3.5A experiment.

The two-dimensional calculations reported here were performed by Mr. T. Cooper of SRI. Dr. L. Seaman provided support for the one-dimensional PUFF calculations, and Mr. J. Kempf and Ms. B. Lew performed the one-dimensional and the TIGER calculations.

Mr. R. Port from RDA was the chairman of the Simulation Working Group for the Silo Test Program (STP). He provided constructive leadership as well as technical and moral support throughout the work presented here. We dedicate this report to his memory.

TABLE OF CONTENTS

TABLE OF CONTENTS (Continued)

LIST OF ILLUSTRATIONS

LIST OF ILLUSTRATIONS (Continued)

LIST OF ILLUSTRATIONS (Continued)

LIST OF ILLUSTRATIONS (Continued)

LIST OF ILLUSTRATIONS (Concluded)

SECTION 1

INTRODUCTION AND SUMMARY

In support of the Defense Nuclear Agency (DNA) Silo Test Program (STP), we designed and evaluated the performance of a variable high explosive simulation technique (HEST) to simulate the airblast environment resulting from a 1.95-kt (1/8-scale of 1 MT) nuclear surface burst over a pressure range of 500 MPa (5 kbar) to 7 MPa (1000 psi). Figure 1(a) shows the weapon effects and Figure 1(b) shows the schematics of a HEST used to simulate the surface airblast. The HEST consists of an explosive charge inside a cavity that is tamped with a soil overburden. The explosive charge usually consists of high explosive cords placed inside the grooves of rigid foam plates. The impulse applied to the test bed is controlled mainly by the areal density of the explosives, and the pulse width is determined mainly by the initial height of the explosive cavity. The overburden height influences both the impulse and the pulse width.

In a nuclear blast, the peak pressure attenuates and the pressure pulse widens with increasing range from ground zero. To simulate the airblast environment at all ranges, we designed a variable HEST in which the explosive loading density, cavity height, and overburden height varied with range. The design criterion is to match at all ranges the positive phase of the impulse history of the reference Brode-Speicher nuclear environment. This implies that the pressure history is also matched at all ranges. The peak pressure, however, may not match exactly because of the familiar pressure spikes produced by the HEST.

The first step in our design procedure was to perform a parametric series of calculations to determine the effects on the HEST impulse of adjustable parameters such as the explosive areal density, charge density, and cavity and overburden heights (Section 2). The one-dimensional PUFF finite-difference hydrocode was used to model the HEST

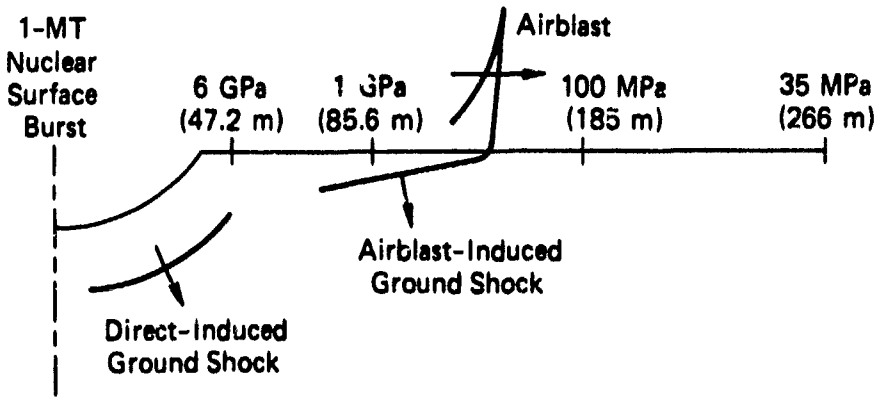

(a) Weapon Effects

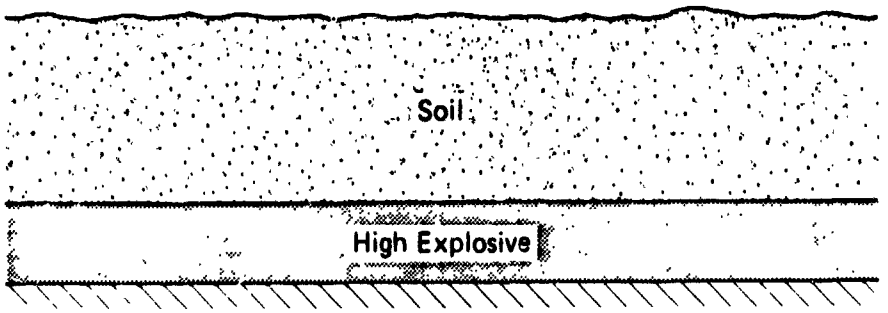

(b) Conventional HEST

JA-4015-4

Figure 1. Weapon effects and a conventional HEST for simulating the airblast-induced ground shock.

cavity expansion and motion of the berm and the loaded medium. The SRI TIGER code was used to calculate equilibrium states of the explosive and foam products during expansion to establish an expansion isotrope for each explosive/foam ratio used in the HEST cavity. We also performed a series of two-dimensional calculations to determine the extent to which the boundaries of a finite-size HEST affect the pressure and impulse histories.

From the preliminary calculations discussed above, we determined the HEST configuration that produced the impulse history of the reference environment at several discrete ranges and then developed a design curve that allowed us to interpolate the HEST design at other ranges of interest. Our final design (Section 3) consists of a variable HEST in which Iremite-60 explosive is used predominantly in the pressure range from 500 to 100 MPa, and 0.085 kg/m (400 grain/ft) primacord explosive is used in the pressure range from 100 to 7 MPa. The overburden height increases linearly with range from 0.64 to 1.15 m. The cavity height increases linearly with range from 38 mm at the 500-MPa location to 70 mm at the 35-MPa location. Beyond this point, the cavity height remains constant at 70 mm.

To check the HEST designs, Waterways Experiment Station (WES) performed calibration experiments that represented the HEST designs at the 1000-, 100-, and 35-MPa peak pressures (Section 4). Iremite-60 explosive was used in the 1000-MPa experiment and primacord explosive was used in the other experiments. By comparing the calculations and the experimental data, we deduced a relationship between the explosion pressure and the charge density. This relationship was then used to adjust the amount of the explosives in the final design of the STP 3.5A experiment.

The variable HEST simulator was used in the STP 3.5A experiment (Section 5). On the basis of photopole, airblast, and near surface soil stress gage data, the impulse from the HEST agreed, to within measurement error, with the design goals for both short (10 ms) and long (90 ms) time frames. Hence, the full positive phase of a 1.95-kt surface burst was successfully simulated by the HEST.

SECTION 2

PARAMETRIC INVESTIGATION OF HEST

A parametric series of one-dimensional and two-dimensional hydrocode calculations was performed to determine the effect of various parameters on the performance of a HEST. To put the calculations in prospective, we show in Figure 2 the setup in a typical foam HEST experiment. High explosive cords are placed in a foam cavity and tamped with a soil overburden. As shown in Figure 2(b), the foam holds the explosive strands in place and provides the desired initial cavity height. We expect the areal density of the explosives to determine the impulse applied to the test bed, and the initial cavity height to determine the pulse width. The overburden height should influence both the impulse and pulse width.

The parameters discussed here are the expansion characteristics of the explosive products (Section 2.1), charge initiation schemes (Section 2.2), adjustable HEST parameters such as the explosion pressure and charge areal density (Section 2.3), charge placement in the cavity (Section 2.4), tailoring of the overburden for pulse shaping (Section 2.5), comparison of loads on a sand test bed with those on a buried structure (Section 2.6), and relief waves generated at the edges of the HEST cavity (Section 2.7). We used the SRI version of the PUFF computer code[1] for the one-dimensional calculations and the TDL computer code[2] for the two-dimensional calculations.

2.1 EQUATION OF STATE OF EXPLOSIVE PRODUCTS

We used the TIGER computer code[3] to characterize the expansion of the explosive products. Figure 3 shows the relationship between the pressure and specific volume for equilibrium expansion of a 0.085 kg/m (400 gr/ft) primacord and 16 kg/m^3 (1 lb/ft^3) foam from explosion pressures of 91, 35, and 9.5 MPa. The plastic and binding materials

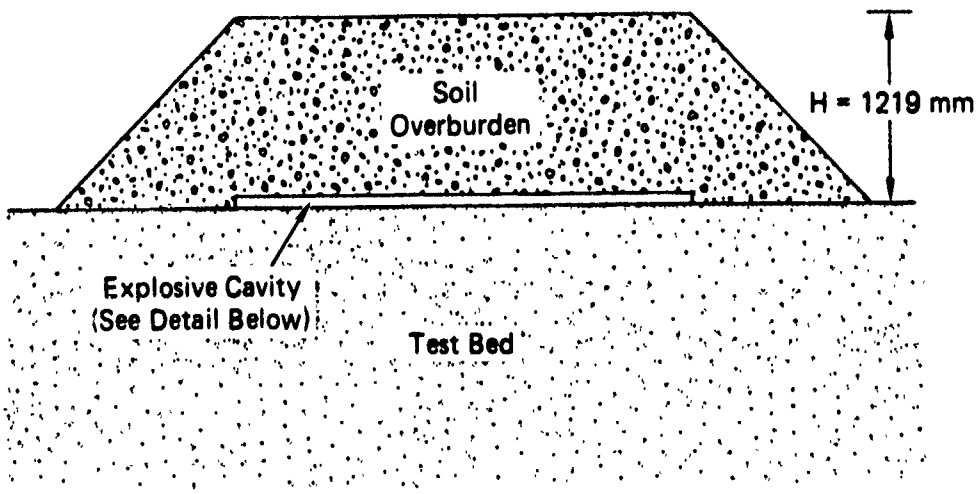

(a) HEST Configuration

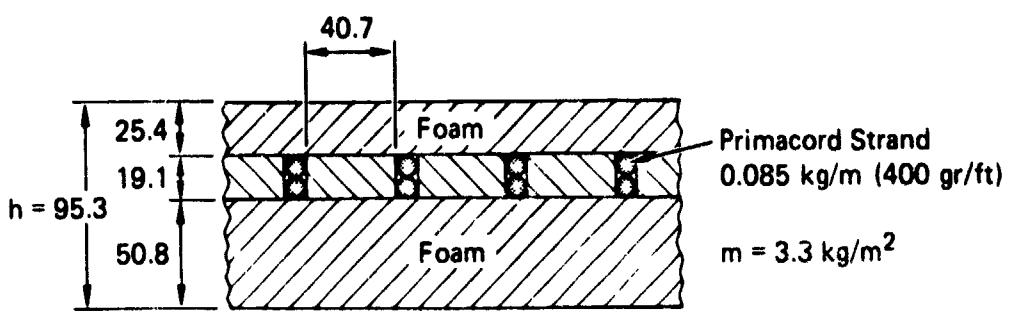

(b) Detail of Explosive Cavity
(STP 2.5 Calibration Experiment)

(Dimensions in mm)

JA-4015-5

Figure 2. A typical foam HEST experiment.

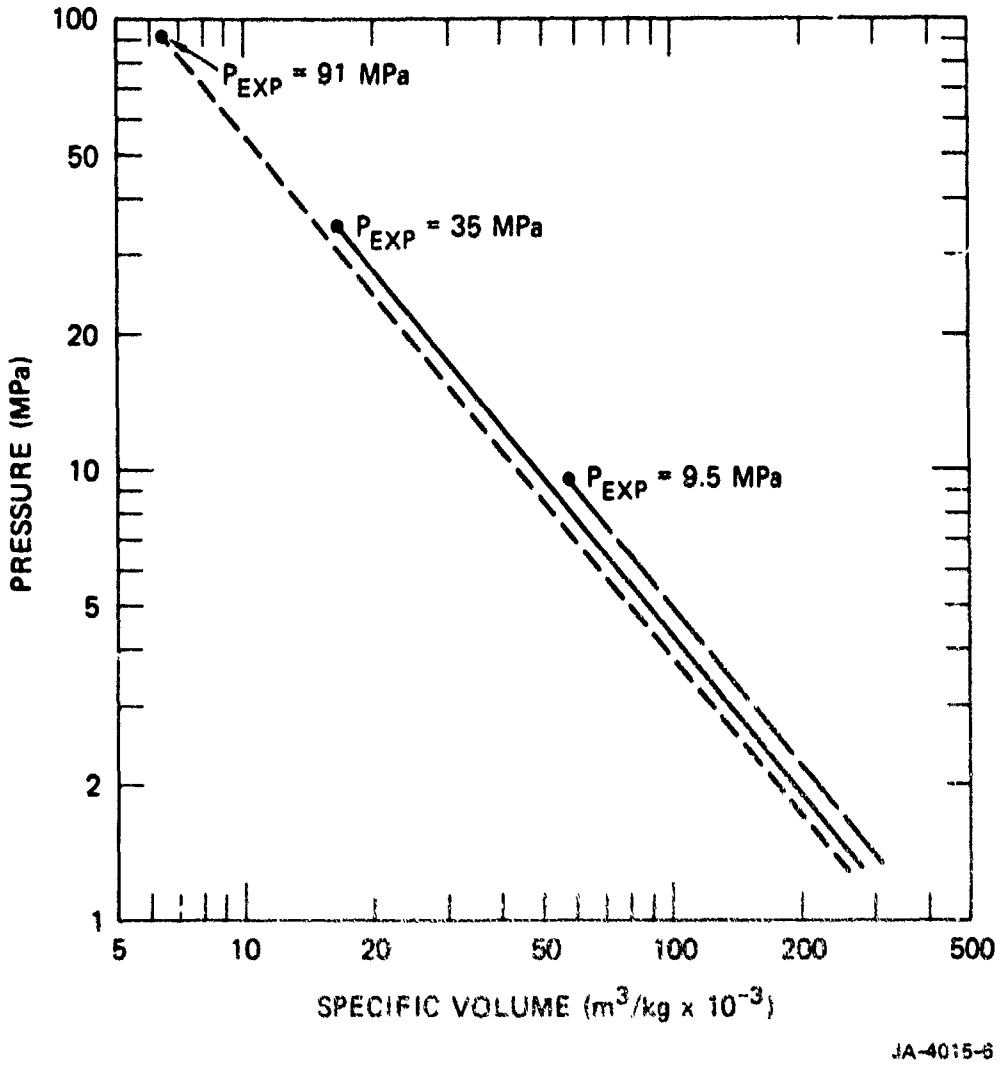

Figure 3. Equation of state for equilibrium expansion of 0.085 kg/m (400 gr/ft) primacord explosives and 16 kg/m^3 (1 lb/ft^3) foam from different explosive pressures. The middle curve (solid line) corresponds to the STP 2.5 HEST experiment shown in Figure 2(b).

used in the construction of the primacord are included in these calculations. The straight lines in the log-log plot of Figure 3 indicate that, for pressures below 100 MPa, the expansion states of the explosive products can be described by the equation of states of an ideal gas with a constant specific heat ratio of $\gamma = 1.18$.

To determine the adequacy of the constant-γ law in HEST calculations, we calculated the impulse from a primacord/foam charge for expansions from initial explosion pressures of 58 and 270 MPa using the ideal and TIGER equations of state. For the 58-MPa case [Figure 4(a)], the calculated impulses are essentially identical, whereas for the 270 MPa case [Figure 4(b)], the constant-γ equation of state overestimates the impulse at 10 ms by about 18%. This corresponds to about a 30% error in the explosive weight and indicates that a more complete equation of state must be used in the design of a HEST with above 100 MPa.

We also compared the TIGER calculations against the JWL[4] model using an amonium nitrate/fuel oil (ANFO) explosive, which is similar to the Iremite-60 explosive used in the STP experiments. Figure 5 shows the TIGER and the JWL equations of state, and Figure 6 shows the stress histories resulting from a 0.92-m-thick bare ANFO charge using the two models. The waveforms appear to be very similar, but the peak stress is higher and the pulse width is smaller for the TIGER model. Figure 7 shows the impulse histories on the surface of the test bed and indicates that both models predict the same total impulse at 10 ms.

Results of the present calculations may be regarded as an indirect verification of the TIGER code against experiments because the JWL model is based on an extensive series of experiments in which the measured motion of a cylindrical shell surrounding the explosive charge is matched by hydrocode calculations. Direct comparison with experimental results are discussed in Section 4.1 where the 1000-MPa Iremite calibration experiment is discussed.

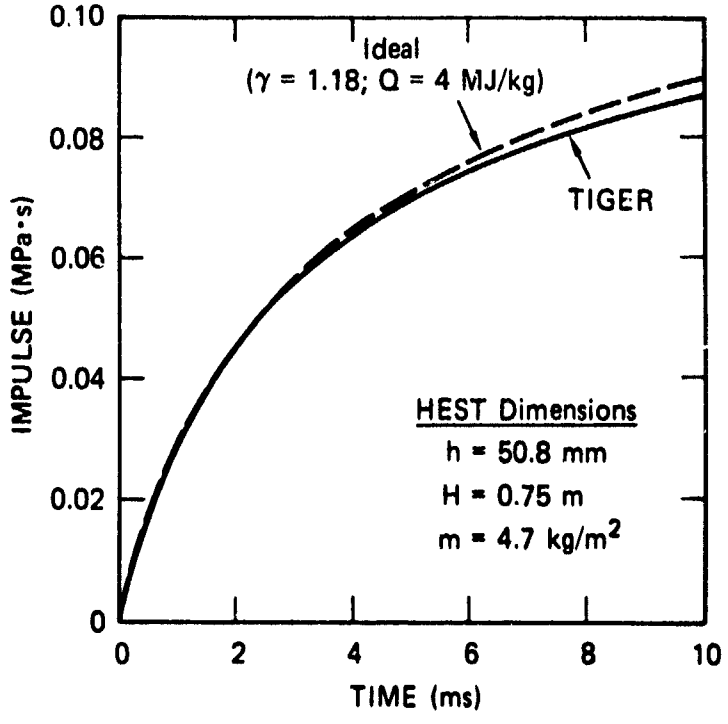

(a) 58-MPa Explosion Pressure

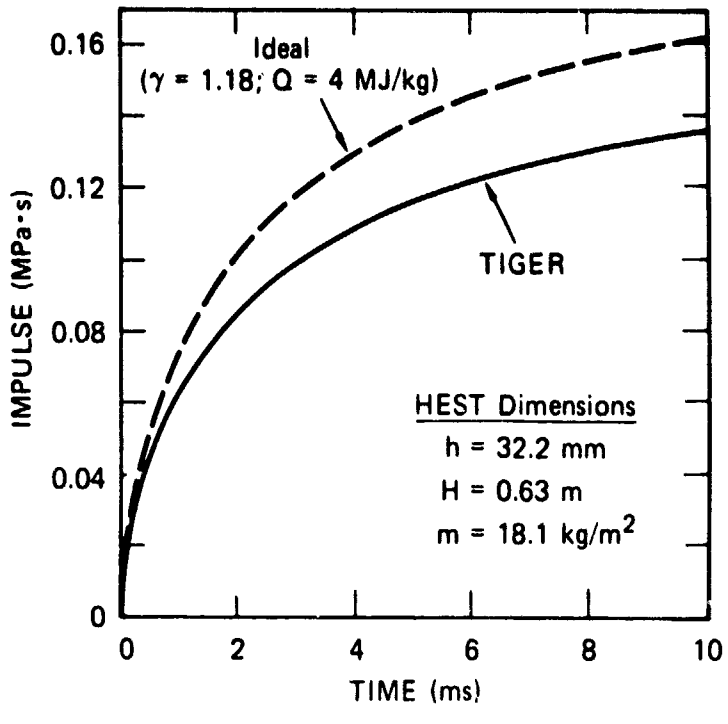

(b) 270-MPa Explosion Pressure

JA-4015-7

Figure 4. Impulse histories from an ireinite HEST based on TIGER and ideal (constant-γ) equations of state.

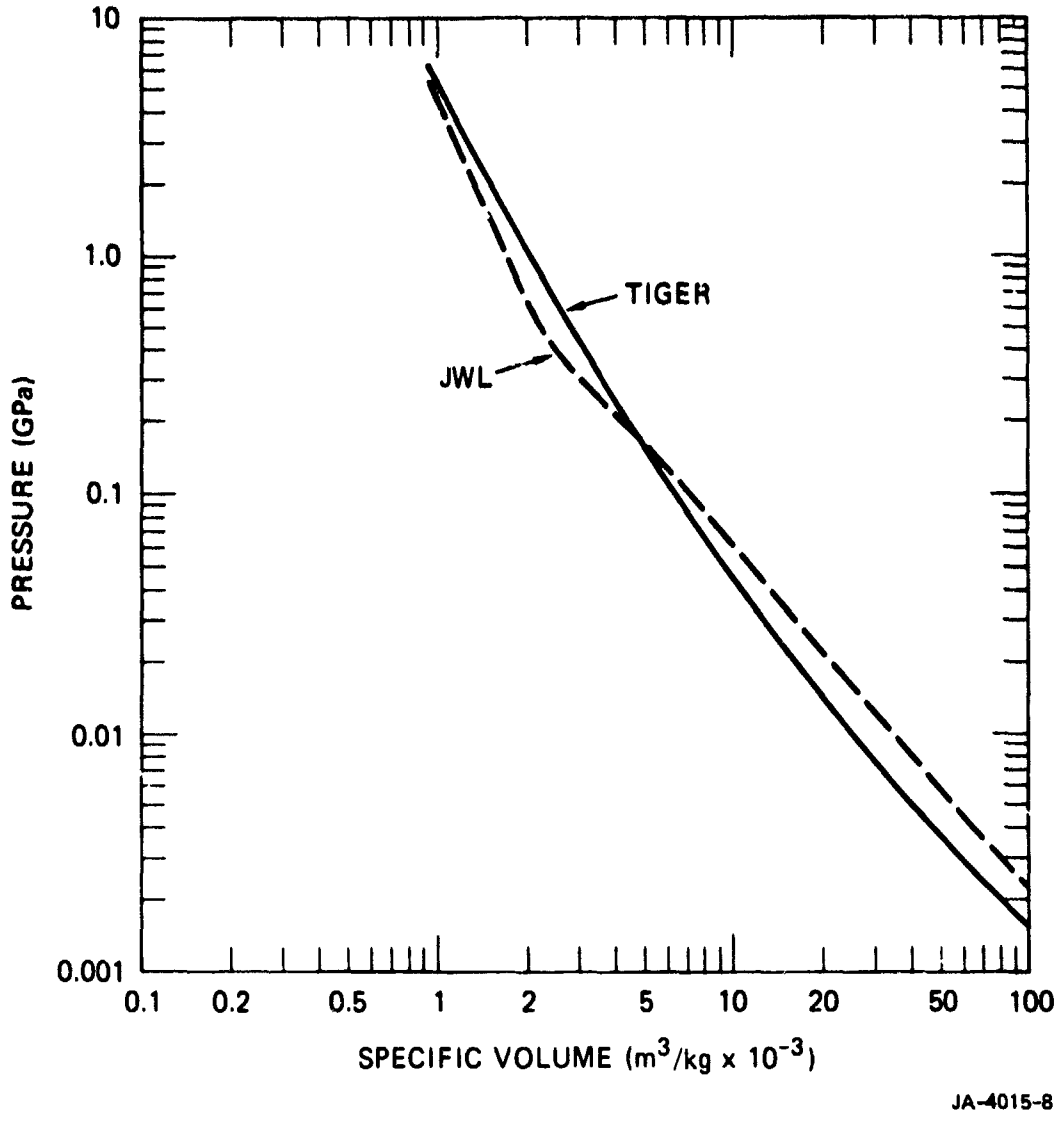

Figure 5. TIGER and JWL equations of state for equilibrium expansion of ANFO from Chapman-Jouget detonation pressure.

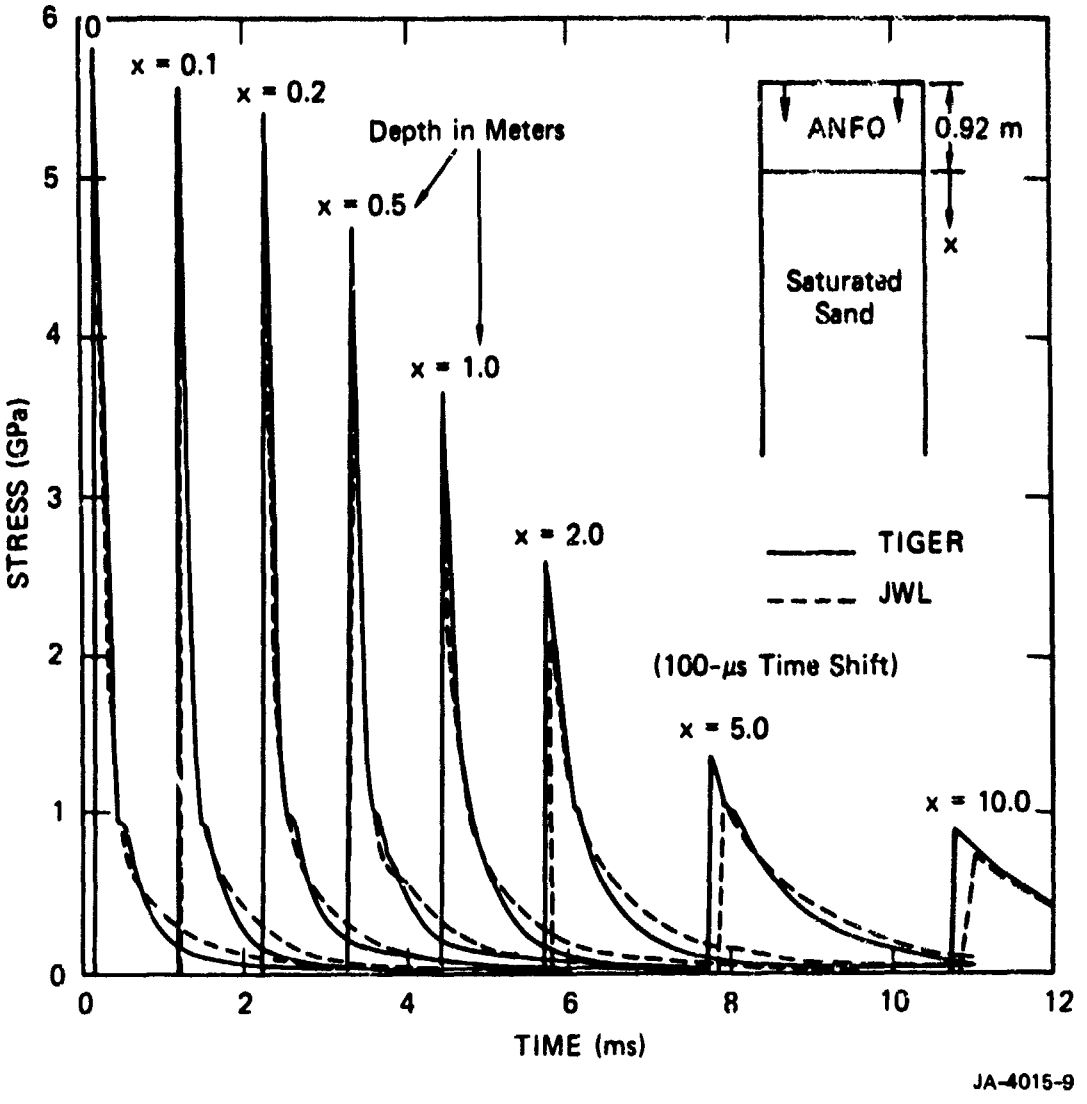

Figure 6. Stress histories at various depths for a 0.92-m ANFO charge based on TIGER and JWL equations of state.

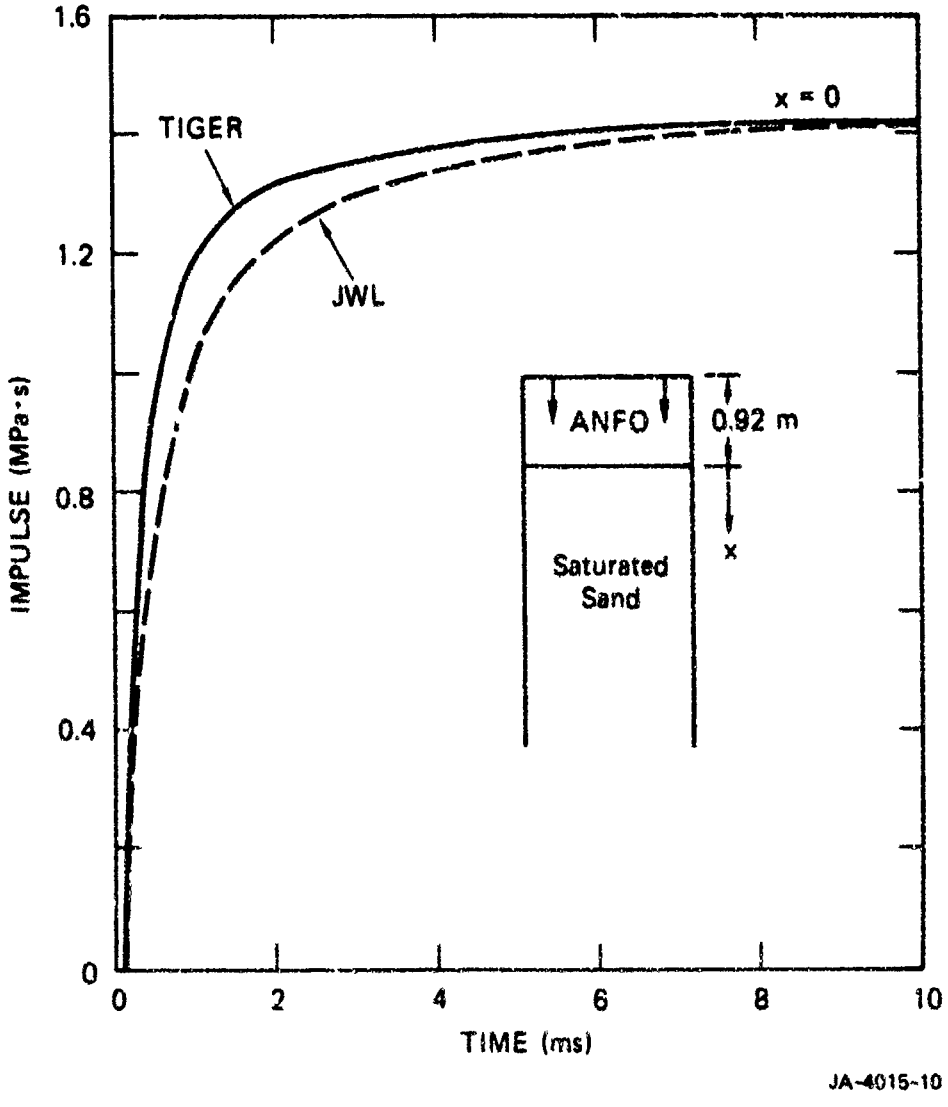

Figure 7. Impulse histories from a 0.92-m ANFO charge based on TIGER and JWL equations of state.

2.2 CHARGE INITIATION SCHEME

We compared different schemes of initiation of a HEST charge based on one-dimensional calculation of the cavity pressure. Figure 8 shows the cavity pressure and impulse histories resulting from a 0.92-m ANFO charge initiated simultaneously throughout the volume, at the top, or at the bottom. The pressure waveforms are different from each other, although the impulse delivered by the explosive is identical. This indicates that different initiation schemes significantly modify the HEST pressure history, but do not change the impulse ultimately delivered by the explosive.

It is expected that the details of the initiation scheme should become less discernible as the stress wave propagates into the soil. Figure 9 shows the peak stress versus depth for the three initiation schemes of the ANFO charge. Close to the charge, the peak stresses are quite different from each other, but at about 32 times the charge height (30 m depth), the peak stresses become equal and remain the same with further propagation. Figure 10 shows that the waveforms at this point are also identical.

The present calculations therefore indicate that the details of a HEST waveform do not propagate to locations that are beyond 30 times the initial cavity height. The propagation distance required to "clean up" the waveform depends strongly on the geology (saturated sand in the present calculations) and is expected to be much shorter (ten times cavity height, say) for a drier geology.

2.3 ADJUSTABLE HEST PARAMETERS

The three main parameters that can be adjusted in a HEST design to match given pressure and impulse histories are the initial explosion pressure P_{exp}, the cavity height h, and the overburden height H. The explosion pressure is related to the initial charge density ρ_c, defined as the mass of the explosive per unit cavity volume.* The total

*The relationship between P_{exp} and ρ_c is obtained separately from TIGER calculations or from cylindrical calibrator (C^2) experiments. See Section 4.5 for more detail.

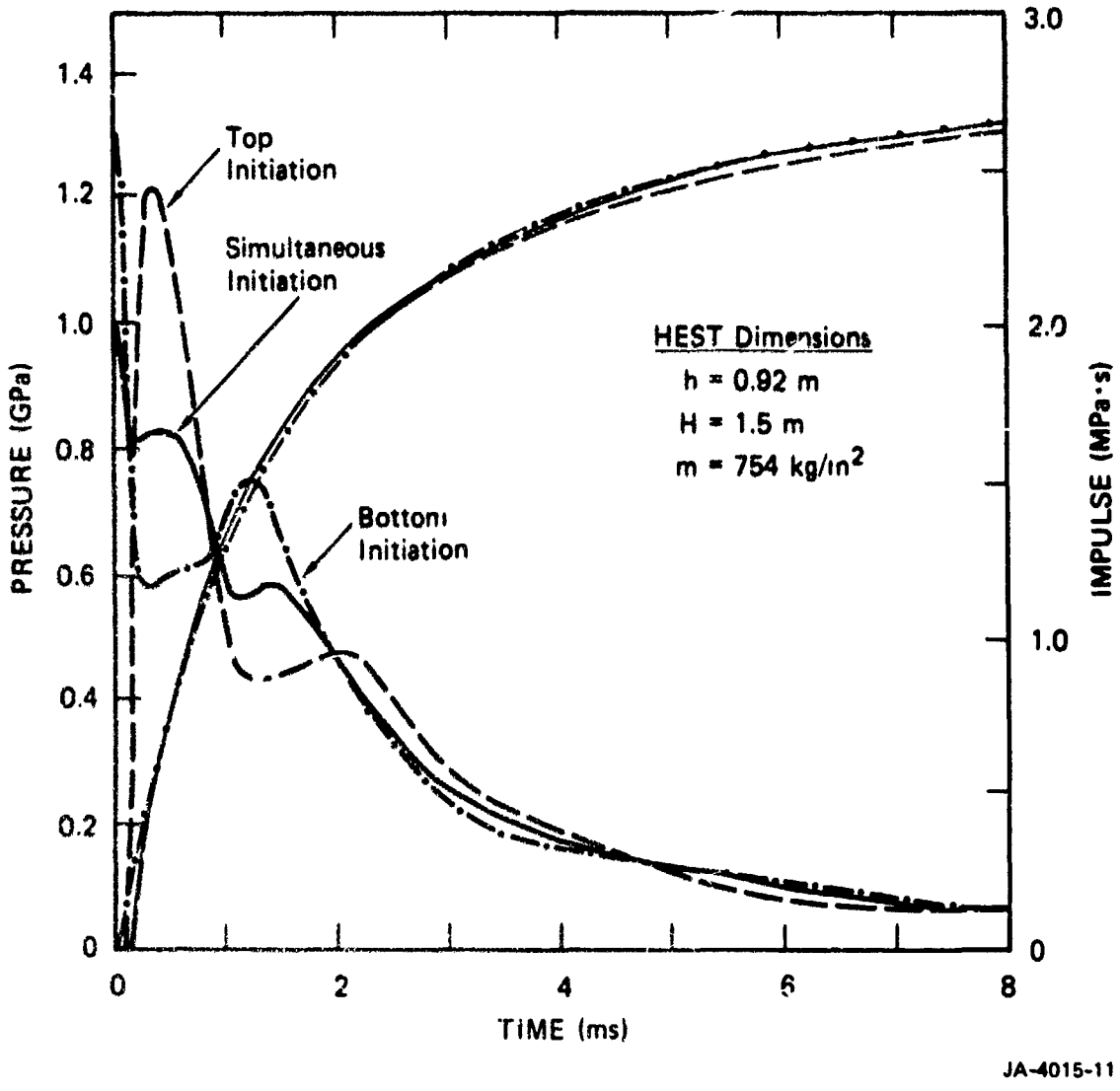

Figure 8. Cavity pressure and impulse histories for three initiation schemes of an ANFO HEST.

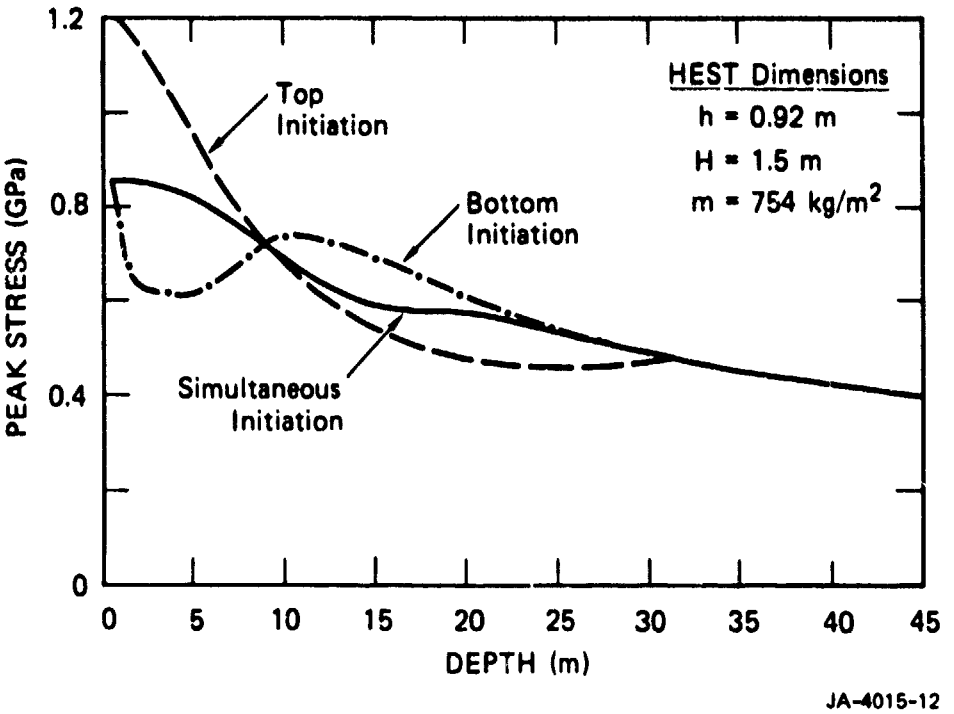

Figure 9. Variation of peak stress with depth for three initiation schemes of an ANFO HEST.

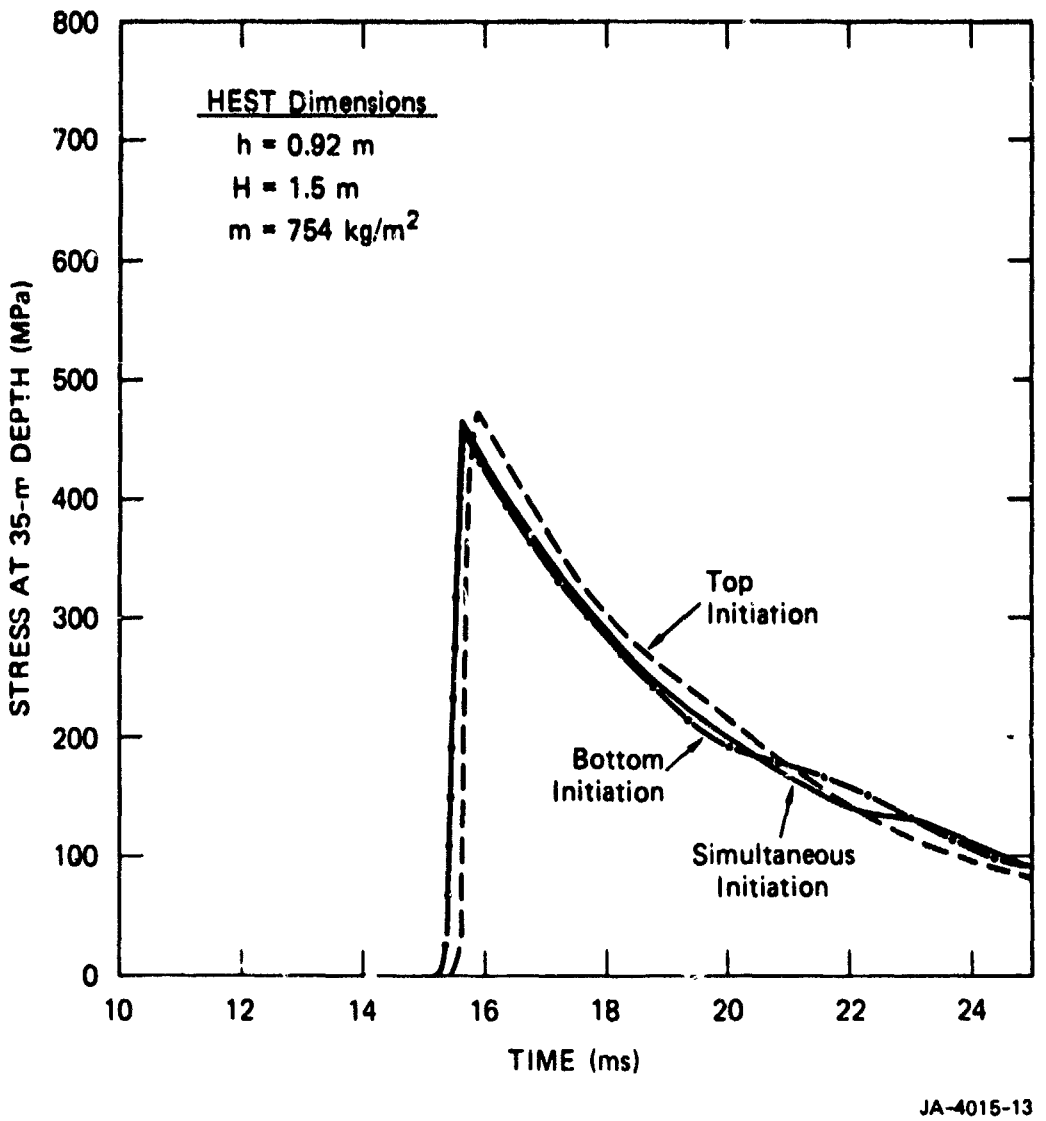

Figure 10. Pressure histories at 35 m below an ANFO HEST for three initiation schemes.

explosive mass per unit area m is then determined by $m = \rho_c h$ and the spacing, between explosive strands is determined by $s = t/m$, where t is the linear density (mass per unit length) of the explosive strands.

2.3.1 Explosion Pressure

Figure 11 shows the pressure and impulse histories resulting from different initial explosion pressures of an ideal explosive charge (constant specific heat ratio of 1.18). An increase of 94% in the explosion pressure from 17 to 33 MPa has resulted in a 65% increase in impulse at 5 ms and a 49% increase in impulse at 20 ms. These increases are consistent with the familiar rule that the total impulse from a one-dimensional HEST is proportional to the square root of the explosion pressure.*

2.3.2 Charge Areal Density

Figure 12 shows the pressure and impulse histories from a HEST with four explosive areal densities ranging from $m = 2.29$ kg/m^2 to $m = 4.57$ kg/m^2. The charge density and explosion pressure are constant in all cases ($\rho_c = 90$ kg/m^3, $P_{exp} = 100$ MPa), so the charge areal density is directly proportional to the cavity height. The calculations show that a 100% increase in charge areal density (from 2.29 to 4.57 kg/m^2) results in a 48% increase in impulse at 5 ms. Also, the width of the pressure waveform at half the peak pressure (50 MPa) increases by 93% from 0.14 to 0.27 ms, which is roughly the same as the 100% increase in cavity height from 25.4 to 50.8 mm. This increase is consistent with the familiar rule that, for equal explosion pressures, the width of a HEST pulse is nearly proportional to the height of the cavity.

---

*This rule follows from equating the kinetic energy of the overburden to the initial internal energy of the explosives.

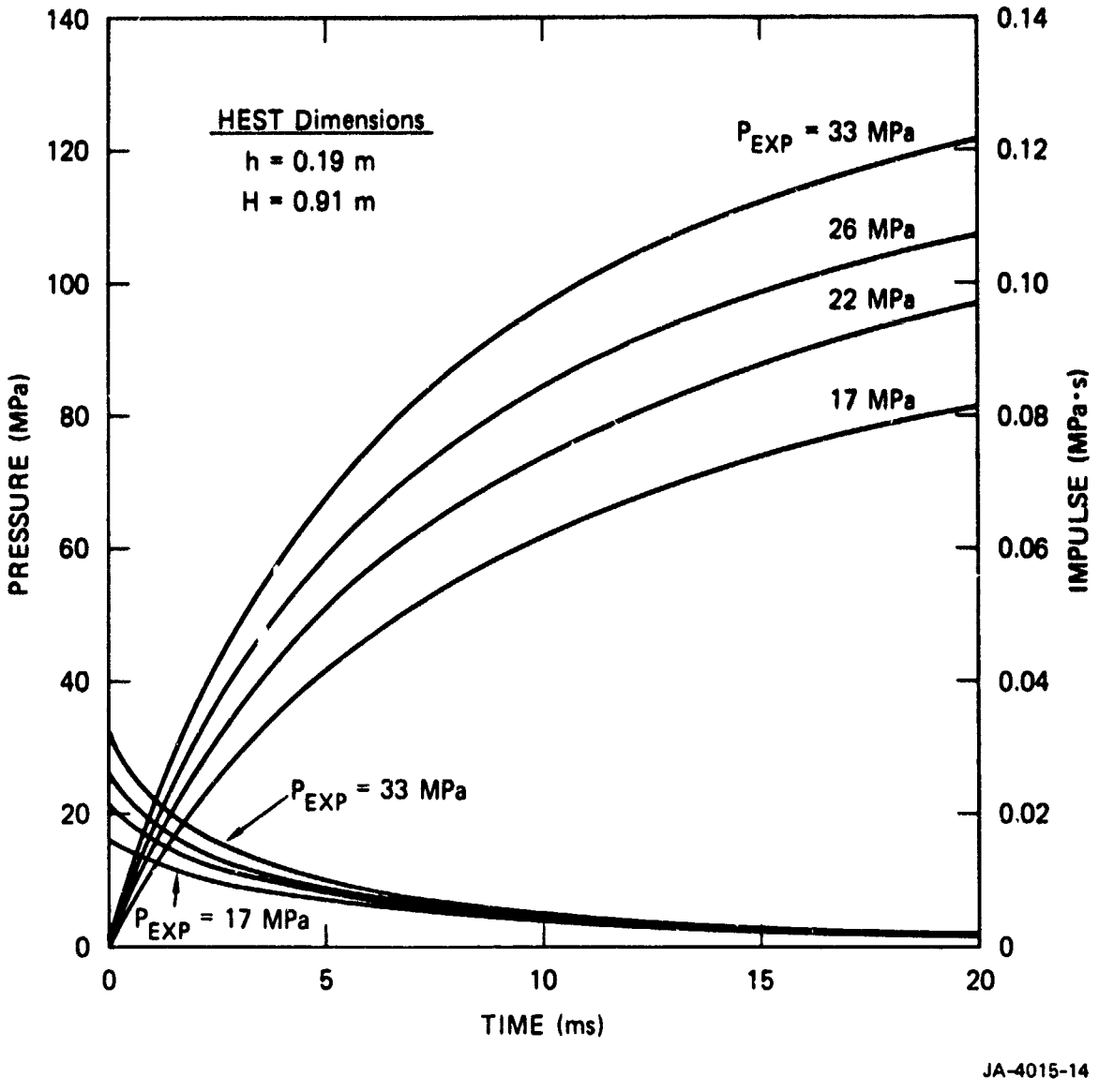

Figure 11. Pressure and impulse histories for different initial explosion pressures P_{exp}.

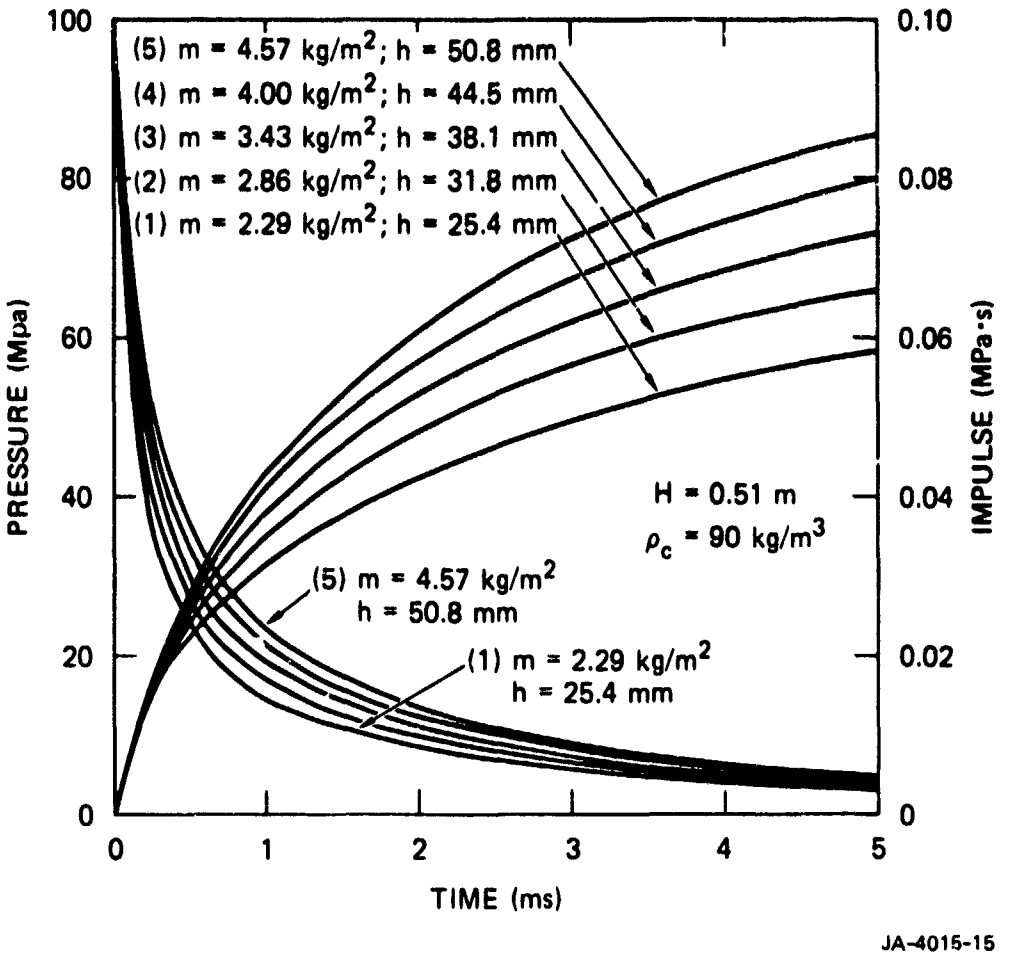

Figure 12. Pressure and impulse histories for different charge areal densities m.

2.3.3 Cavity Height

Figure 13 shows the pressure and impulse histories from a HEST with initial cavity heights of 25.4 mm (1 in.), 50.8 mm (2 in.), and 101.6 mm (4 in.). The areal density of the explosives is constant in all calculations ($m = 3.36\ kg/m^2$), but the charge density varies according to $\rho_c = m/h$. The calculations show that the reduction in cavity height leads to an increase in peak pressure, but the impulse at 20 ms remains essentially unchanged. This result indicates that the total impulse is controlled mainly by the areal density of the explosive weight and is essentially independent of the details of the HEST cavity.

2.3.4 Overburden Height

Figure 14 shows the pressure and impulse histories from an ANFO HEST with overburden heights ranging from H = 0 (bare charge) to H = 3.0 m. The trend is a substantial increase in impulse with increasing overburden height. For example, compared with the case of bare charge, the impulse at 8 ms increases 2.8 times when a 3-m (3.3 times the cavity height) soil berm is placed on top of the explosives.

2.4 CHARGE PLACEMENT

In the calculations presented so far, we have assumed that the explosive is uniformly distributed throughout the HEST cavity. To investigate the limitation of this assumption, we performed the three calculations shown at the top of Figure 15 in which the same amount of explosive is assumed to be (1) uniformly distributed throughout the cavity, (2) concentrated in 25% of the cavity near the top, and (3) concentrated in 25% of the cavity near the bottom. The calculated pressures for the concentrated charges show repeated oscillations due to the reflection of the pressure waves from the top and bottom of the cavity. The impulse, however, is essentially the same for all three cases, except for about the first 0.2 ms after charge initiation.

We therefore conclude that the overall impulse is essentially independent of the explosive configuration inside the HEST cavity.

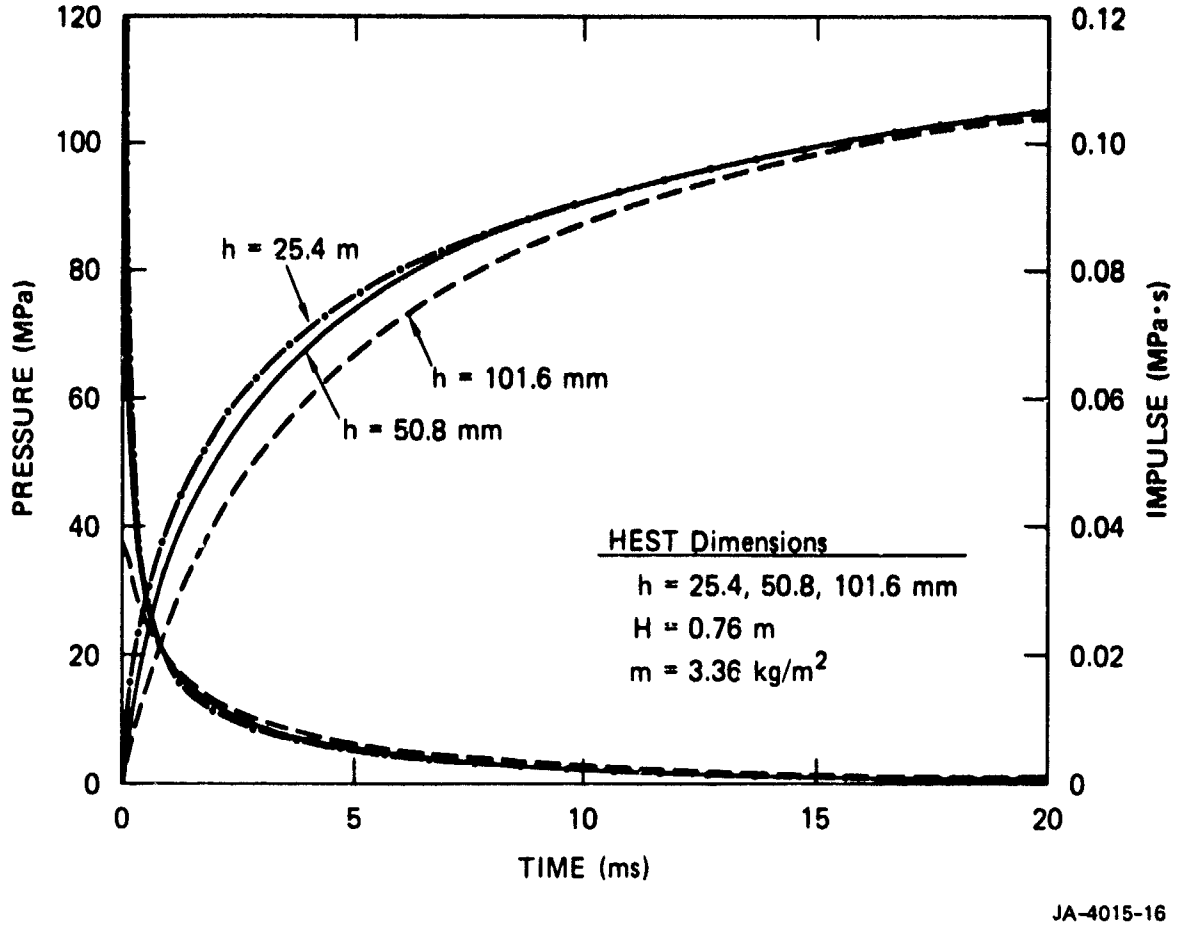

Figure 13. Pressure and impulse histories for different cavity heights h.

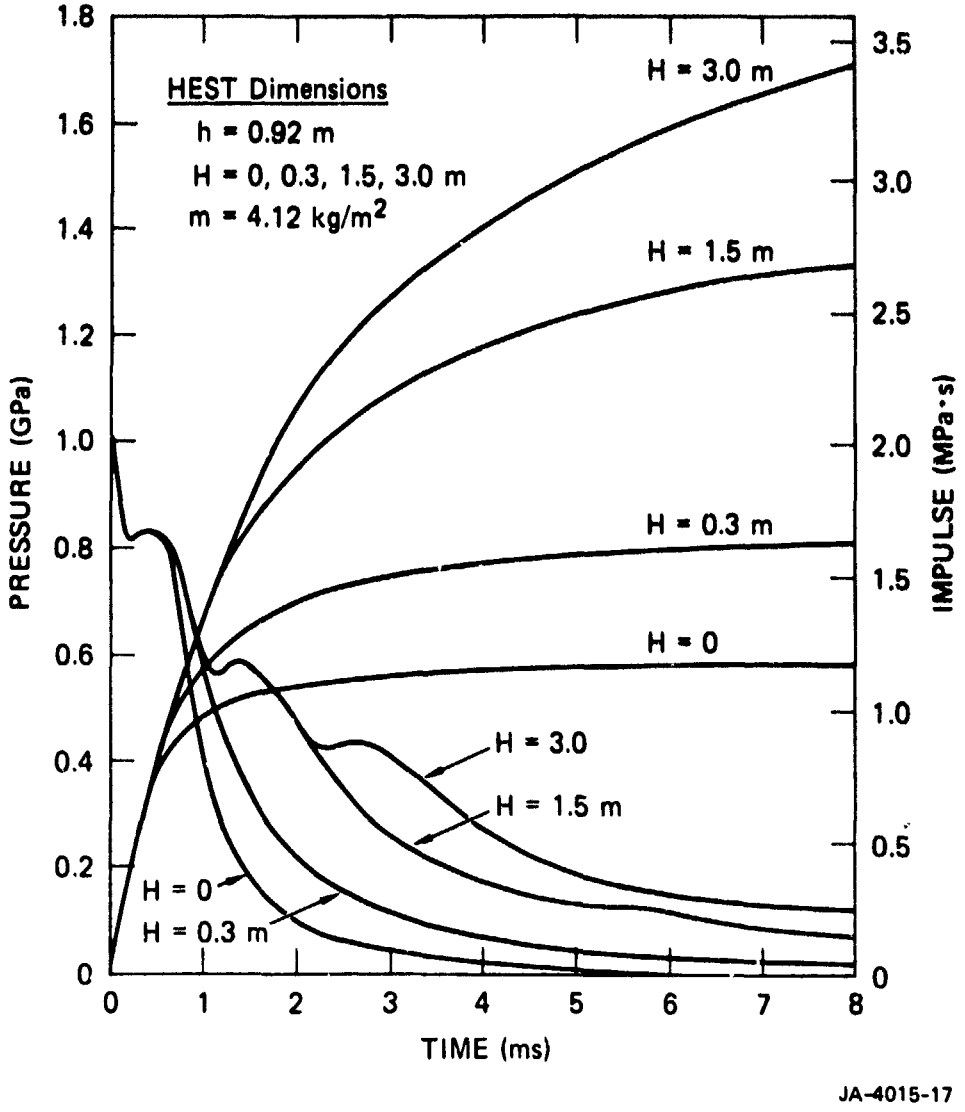

Figure 14. Pressure and impulse histories for different overburden heights H.

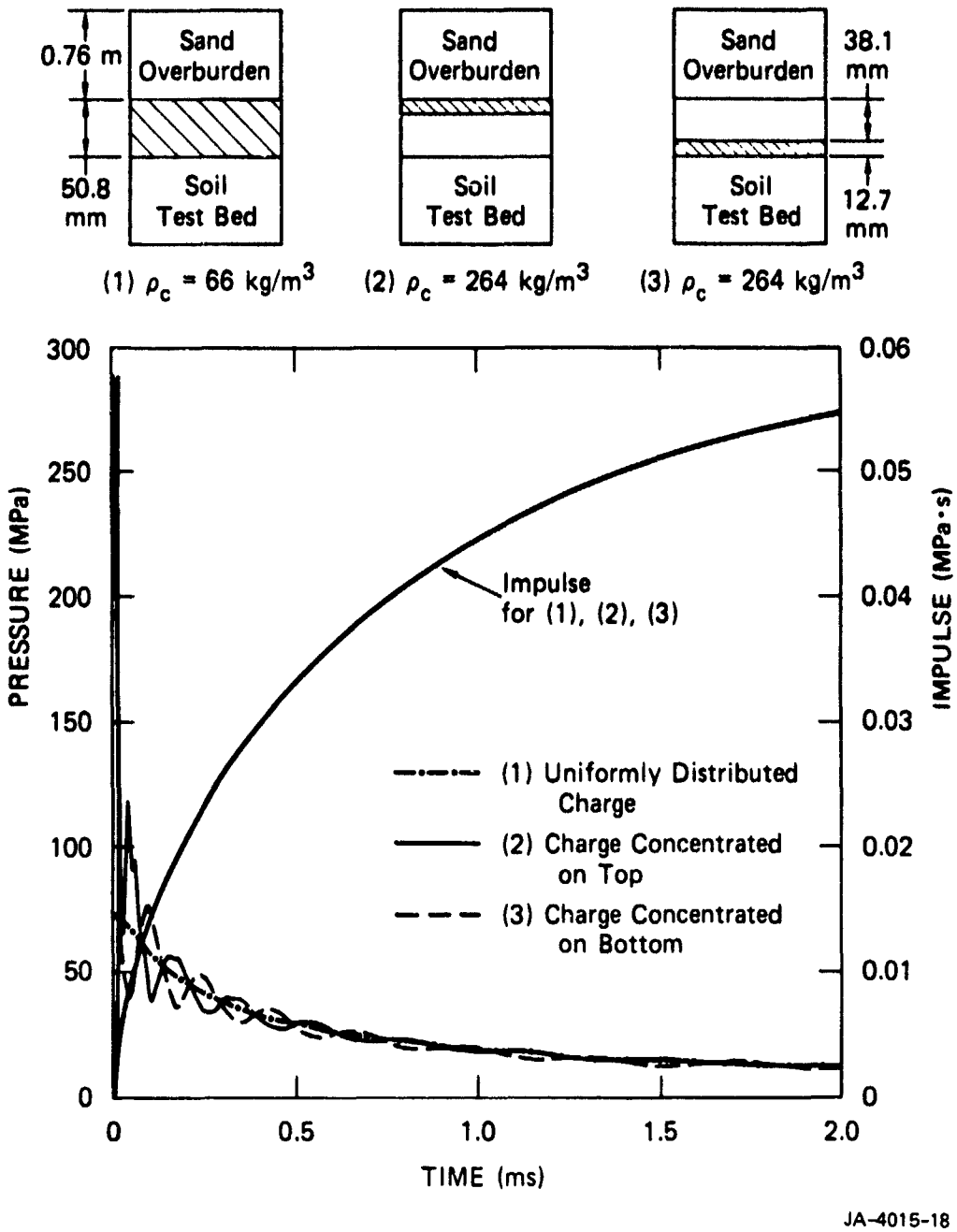

Figure 15. Pressure and impulse histories for different charge placements.

This further supports the conclusion that, for equal overburden height, the HEST impulse is determined mainly by the explosive areal density and is not sensitive to such cavity design details as the detonation point (Section 2.2), cavity height (Section 2.3.3), or charge placement.

2.5 TAILORED OVERBURDEN

The modified Brode-Speicher nuclear environment, which is used as the simulation objective in the present program,[5] is characterized by a very rapid decay from peak pressure immediately after the shock arrival. To simulate the rapid pressure decay, we designed a HEST with a tailored overburden that consists of layers of sand and foam. The immediate crush of the foam layers would result in a rapid expansion of the cavity volume and a rapid decay of the cavity pressure.

Figure 16 shows the pressure histories for two thicknesses of a 16 kg/m^3 (1 lb/ft^3) foam layer placed above a HEST cavity. Compared with the reference case with no foam (F = 0), the cavity pressure for the foam/sand overburden decays faster and results in a narrower pulse. For example, at 60 MPa, the pulse width for a foam/sand overburden is about one half of the reference case.

Figure 17 shows a generic design for simulating the Brode-Speicher pressure history at the 100-MPa peak pressure. Both the pressure and impulse are closely matched by the HEST. Note that use of a tailored overburden may not be appropriate in a conventional HEST because the pressure spikes typically seen in conventional HEST produce deviations from the ideal nuclear waveforms that are much more significant than the improvements provided by a tailored overburden. Thus, the use of a tailored overburden should probably be limited to a high-fidelity HEST in which the spikes are removed by, for example, using a dilute explosive that fills the cavity uniformly.

2.6 LOADS ON BURIED SILO STRUCTURES

When a buried silo structure is loaded with a HEST (Figure 18), the cavity expansion above the silo will be slightly smaller than the free-

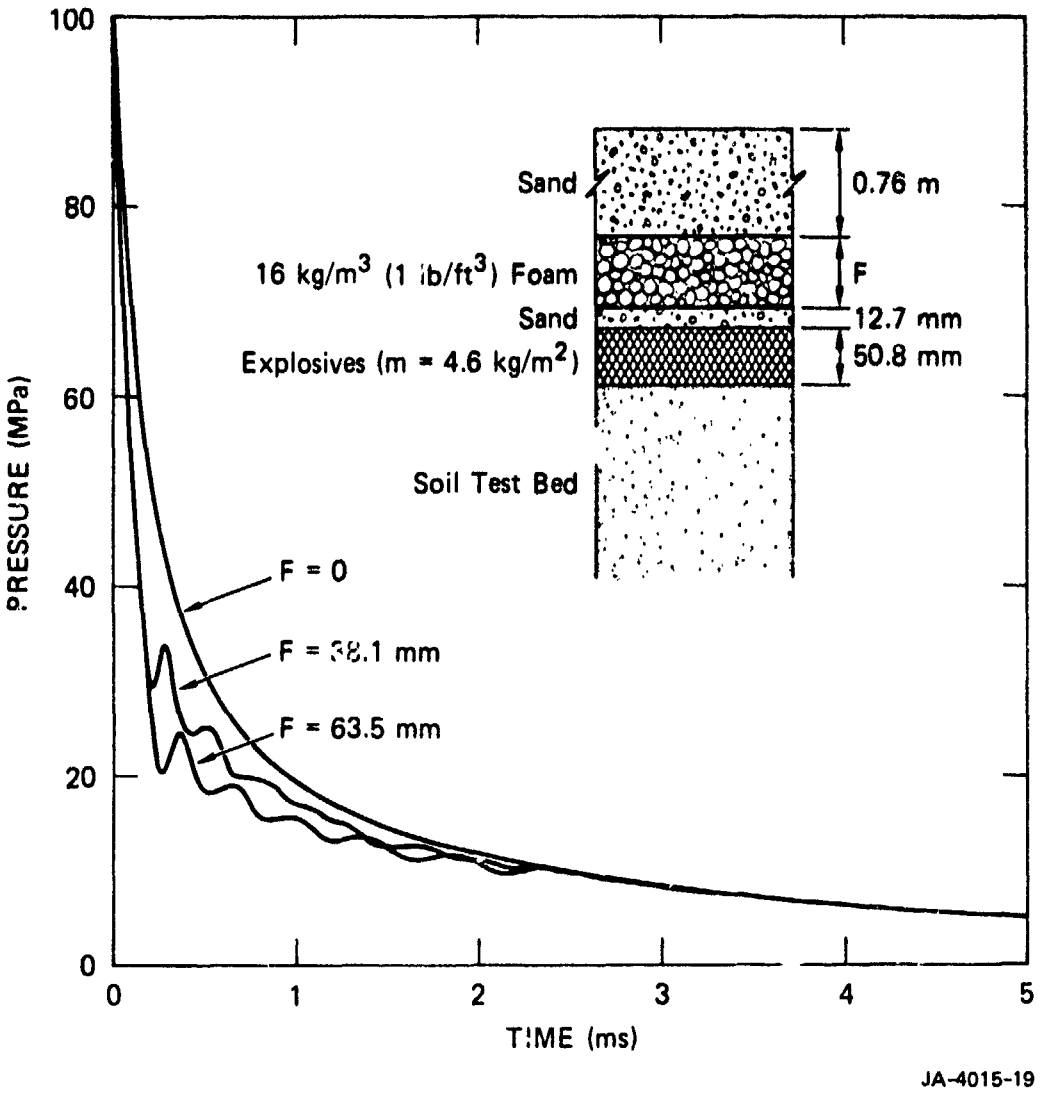

Figure 16. Pressure histories for different tailored foam/sand overburdens.

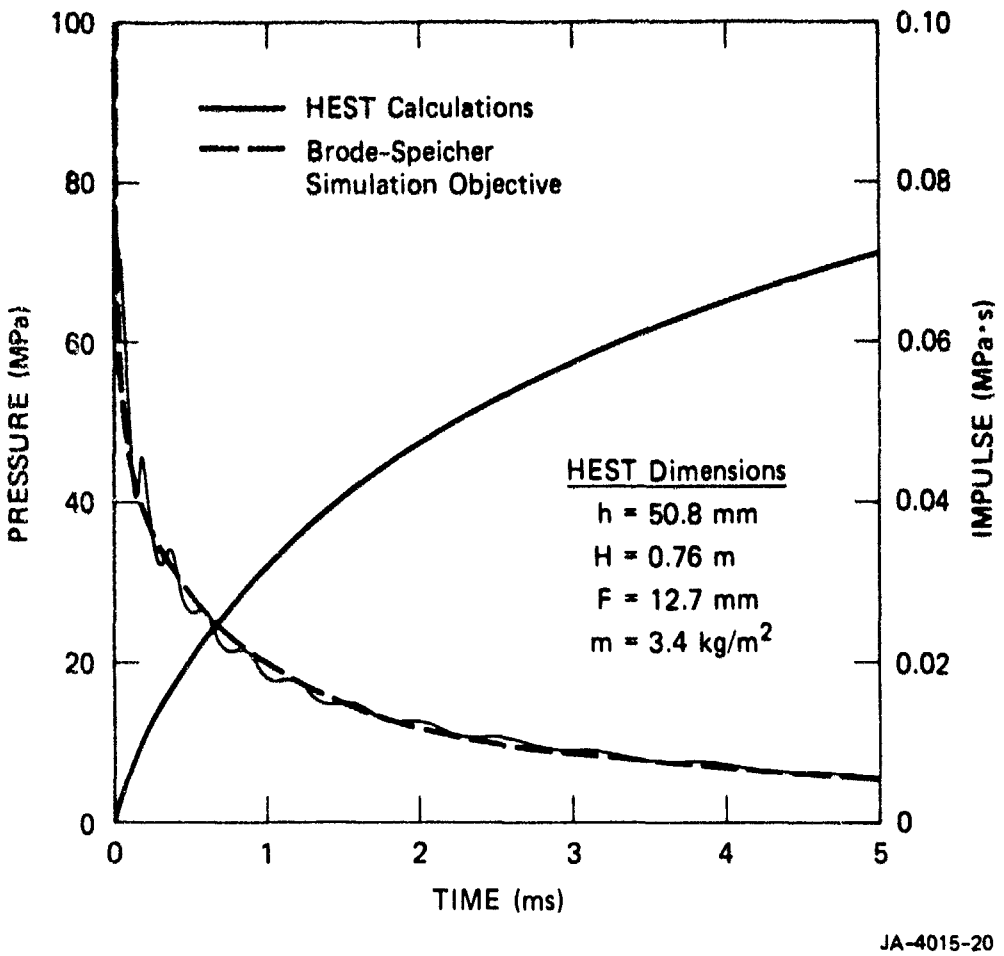

Figure 17. Pressure and impulse from a HEST with a foam/sand overburden tailored to match the Brode-Speicher simulation objective at 100-MPa peak pressure.

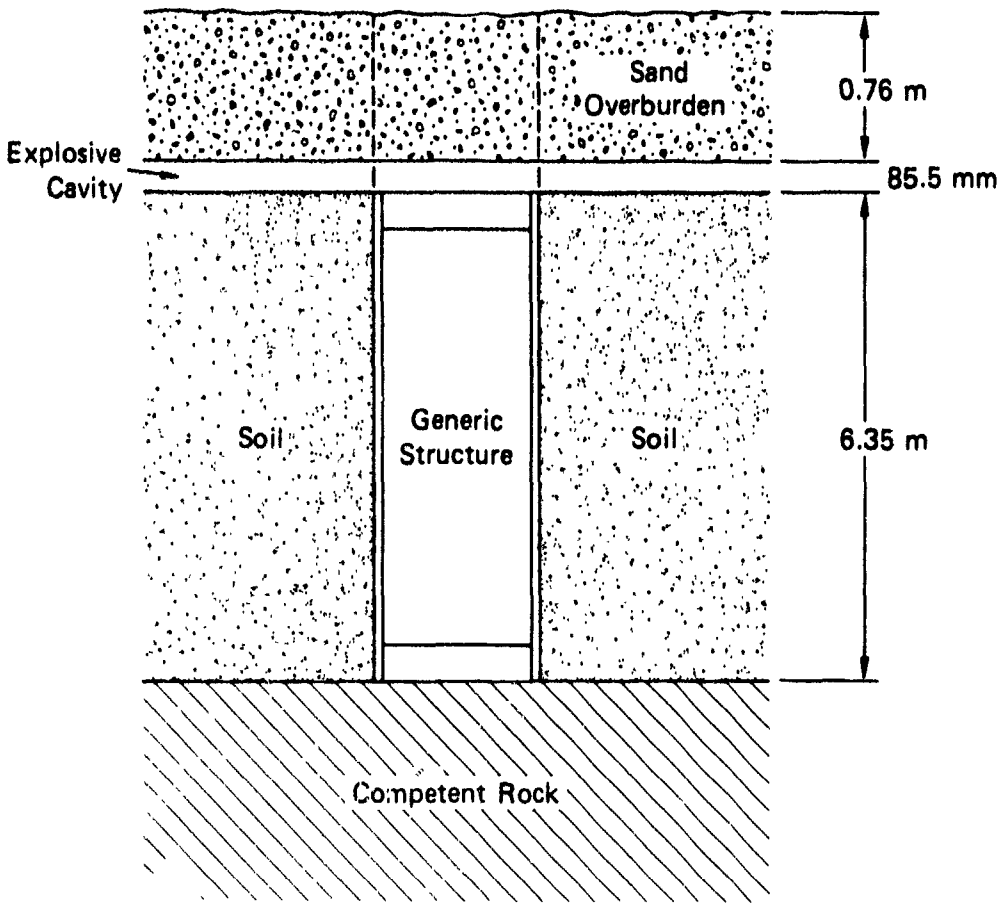

Figure 18. Test configuration assumed for calculating the difference in loads applied by a HEST to a soil surface or a buried structure.

field expansion because the silo is stronger than the soil and therefore does not move down as much as the surrounding soil does. This leads to a higher pressure over the silo and may result in an overtest of the structure.

We performed two separate one-dimensional calculations to determine the loads on a generic silo structure and on a soil test bed. The calculations correspond to vertical expansion of the flow over the structure (region between the two dashed lines in Figure 18) and the vertical expansion of the flow over the soil test bed (region outside the dashed lines). These one-dimensional calculations in which no lateral flow is allowed give an upper bound to the difference of HEST pressures in the free-field and over silo structures, because in an actual experiment, a lateral flow occurs in the cavity, which tends to equilibrate the pressures.

Figure 19 shows the cavity expansion of a 35-MPa HEST placed over a generic structure (dashed curves) and over a generic soil test bed (full curves). At 10 ms, the bottom surface of the cavity has moved down 170 mm for the soil test bed, but only 10 mm for the structure (a net difference of 160 mm). The cavity height at this time, however, is different by only 90 mm (750 mm over soil compared with 660 mm over structure) because a smaller cavity height results in a higher pressure, which in turn, results in a more rapid expansion of the cavity. This self-correcting mechanism tends to equalize the HEST pressure over a buried silo structure and the surrounding free-field.

Figure 20 shows the calculated pressure and impulse histories for the two cases. The impulse at 12 ms is 12% higher over the structure than over the soil test bed. As mentioned earlier, this is an upper-bound estimate of the overtest. Experimental data reported in Reference 6 tend to indicate that the impulse over a concrete pad (representing a generic structure) is, to within the spread of the HEST data, the same as the free-field impulse.

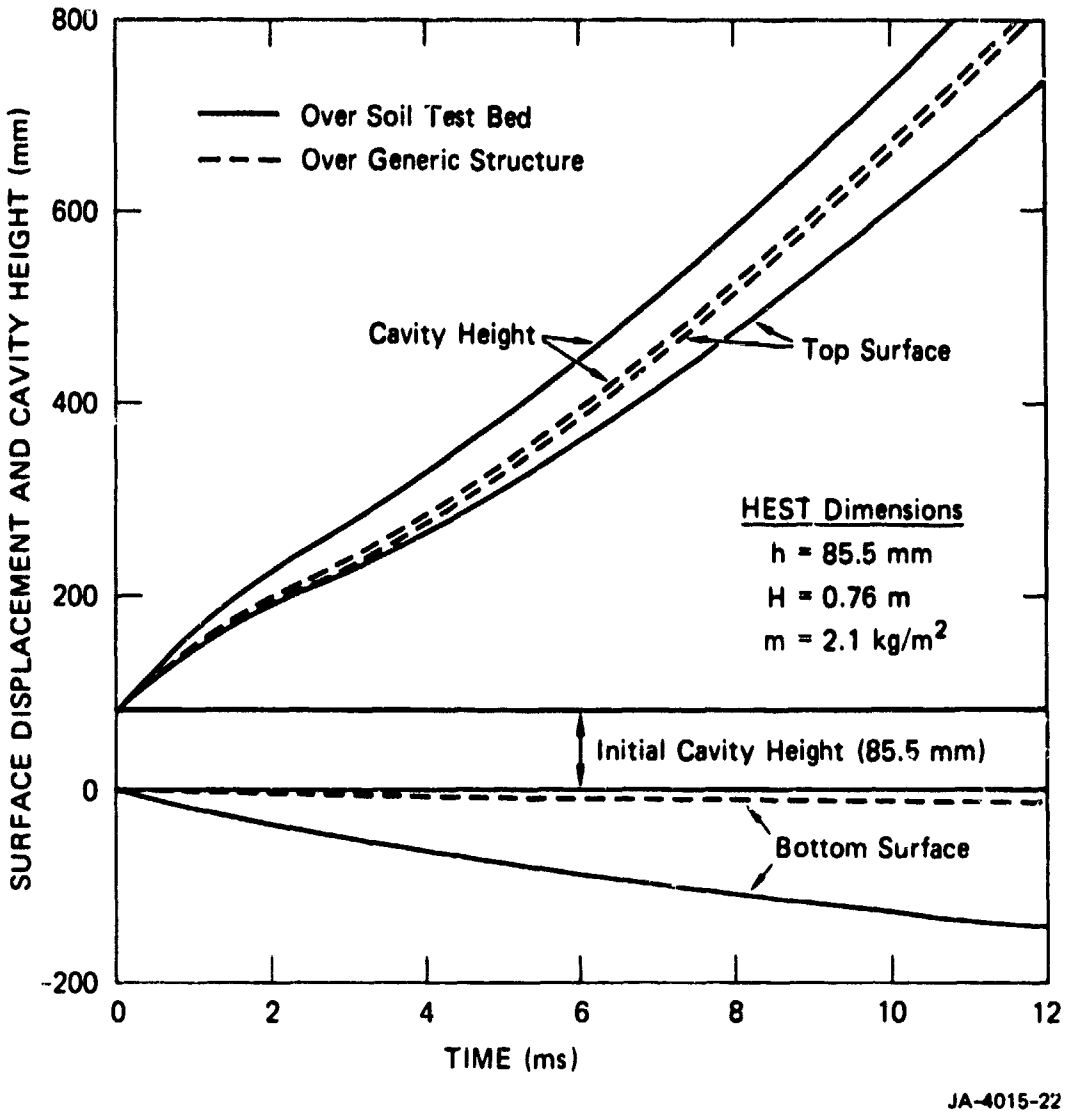

Figure 19. Displacement and cavity height histories of the top and bottom surfaces of a HEST placed over a soil test bed and over a generic structure.

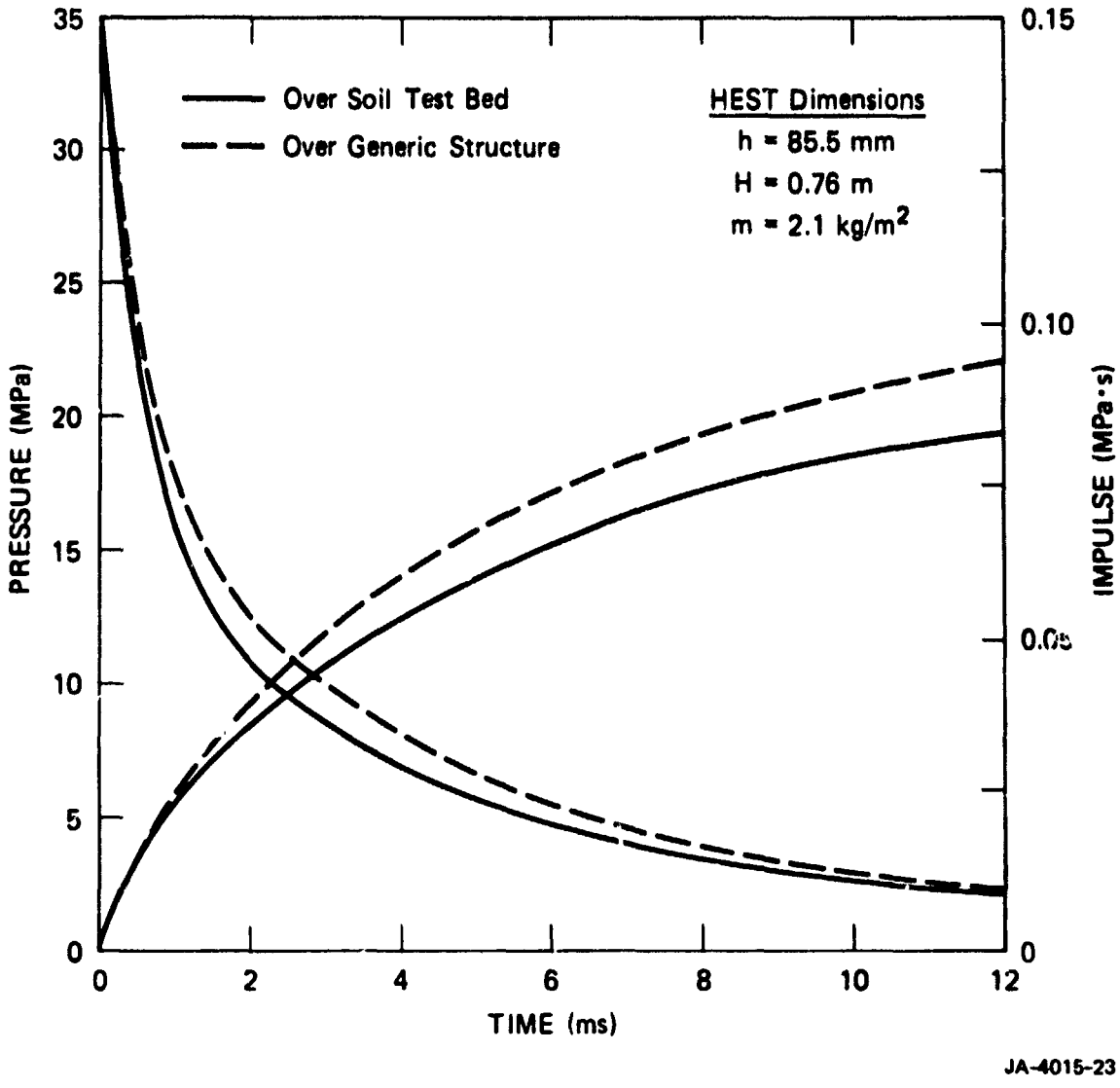

Figure 20. Pressure and impulse histories resulting from a HEST placed over a soil test bed and over a generic structure.

2.7 EDGE EFFECTS

Near the edges of a HEST cavity, the pressure drops faster than the free-field pressure because of the lateral expansion of the cavity. This results in a lower total impulse than that obtained from one-dimensional calculations.

To estimate the edge effects in a typical HEST, we performed a series of two-dimensional axisymmetric calculations using the SRI TDL computer code.[2] Figure 21 shows the cavity expansion 10 ms after the detonation for a nominal HEST design. The initial charge cavity (shown as a dashed lines in Figure 21) is 1.5 m in radius and 70 mm high. The charge is center-initiated with an explosion pressure 18.5 MPa, which corresponds to the HEST design in STP 3.5A experiment at the 35-MPa range. We note that the cavity contour at 10 ms (shown as a heavy solid line in Figure 21) is not straight near the edge. The depression observed at the radius of 1.4 m indicates a high-pressure zone due to the reflection and focusing of the wave near the edge.

Figure 22 shows the pressure histories calculated for simultaneous and center initiation of the charge. For comparison, pressure histories from a one-dimensional calculation representing an infinite HEST are shown as dashed curves in Figure 22. For the case of simultaneous initiation, Figure 22(a), a relief wave propagates from the edge toward the center. The arrival of the wave is manifested in Figure 22(a) by a deviation of the two-dimensional calculation (solid curves) from the reference one-dimensional calculation (dashed curves). The geometric focusing of the relief wave enhances the relative drop in pressure as the center of the charge is approached. For example, the relative pressure drop when the wave arrives at R = 1.4 m is about 18%, whereas the pressure drops by about 30% for R = 0.8 m.

When the charge is initiated at the center [Figure 22(b)], the relief wave from the edge is preceded by the reflection of the outward running wave from the edge, which shows as a second peak on the pressure histories. As before, geometric focusing has enhanced the magnitude of the second peak at R = 0.2 m over that at R = 1.4 m.

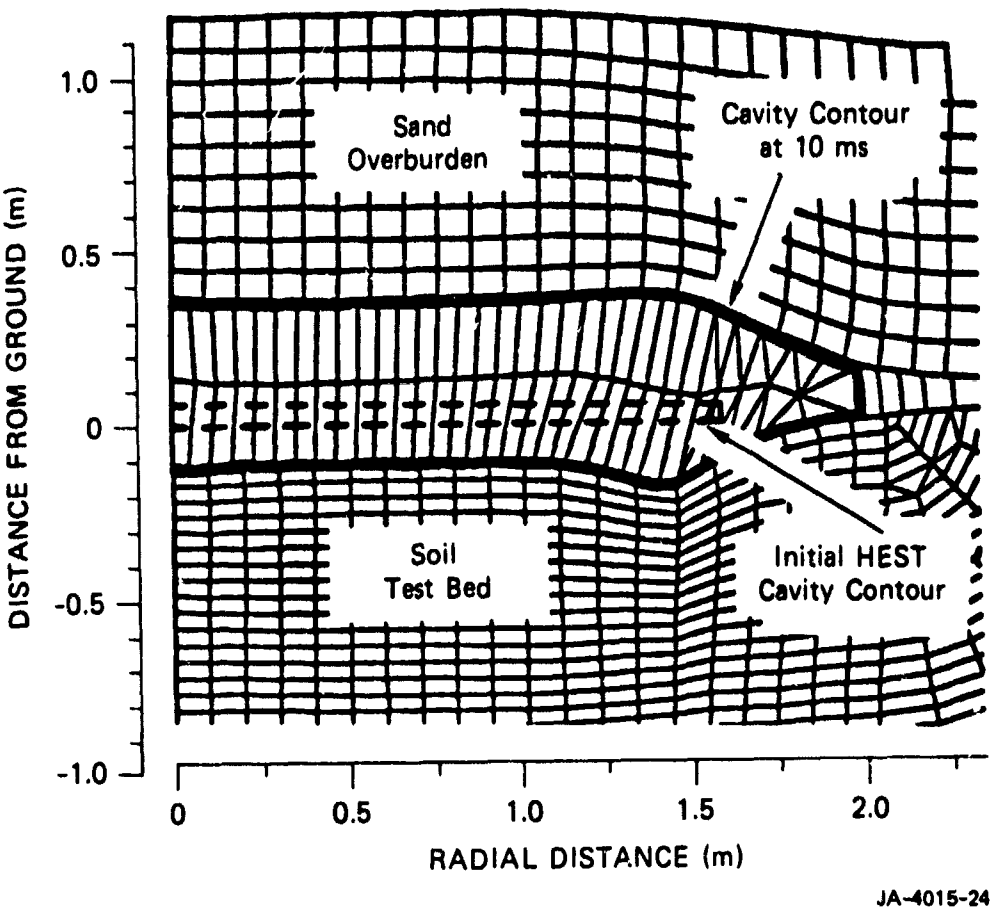

Figure 21. Two-dimensional axisymmetric calculation of HEST expansion. (Initial radius of 1.6 m, initial cavity height of 70 mm, and charge areal density of 2.1 kg/m^2).

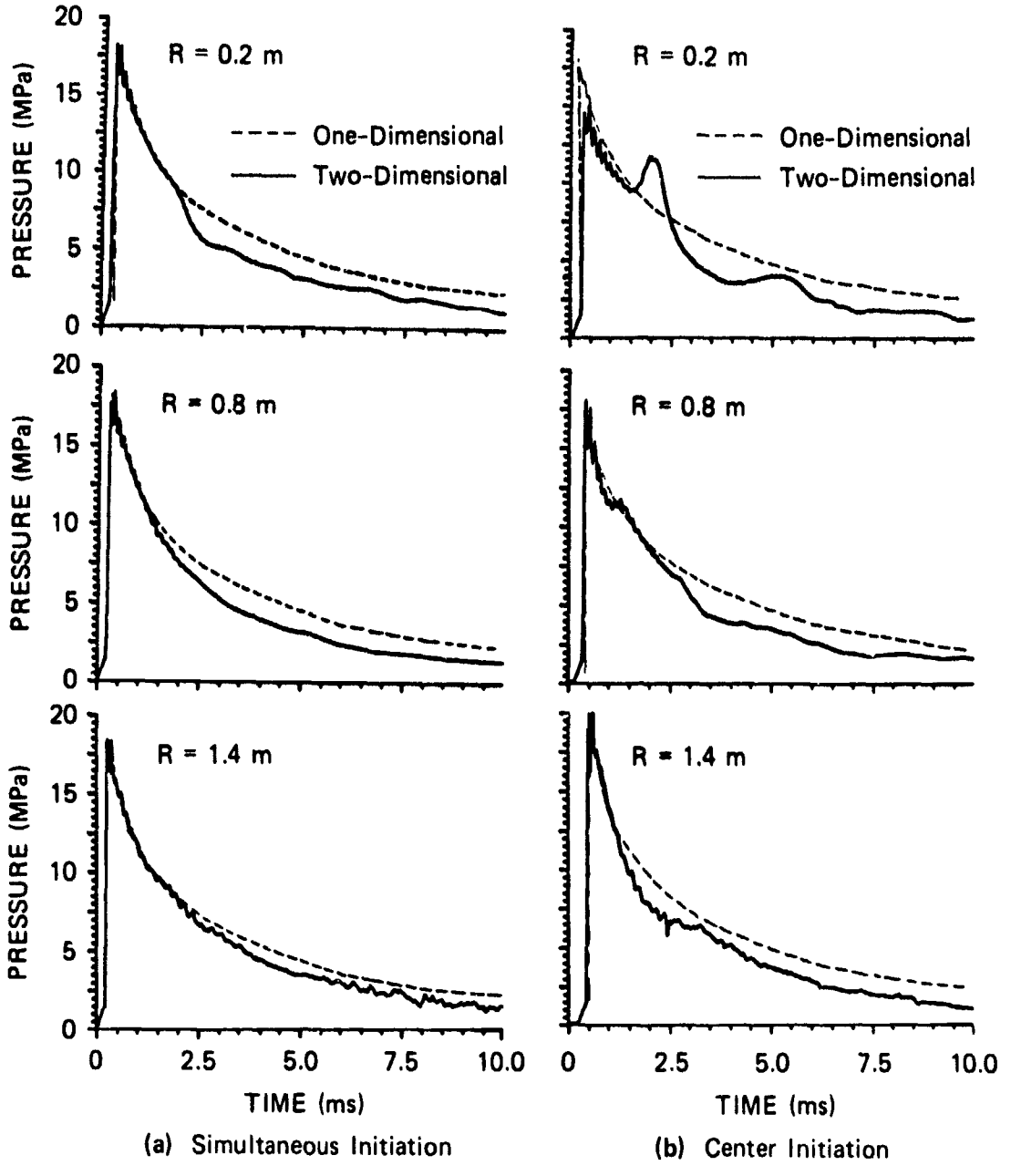

Figure 22. Pressure histories from one-dimensional and two-dimensional HEST calculations for (a) simultaneous initiation and (b) center initiation of the explosive charge. (Initial radius of 1.6 m, initial cavity height of 70 mm, charge areal density of 2.1 kg/m^2, and detonation velocity of 6200 m/s).

The impulse histories calculated from the six pressure histories shown in Figure 22 are compared in Figure 23 with the one-dimensional reference calculation. The impulse from both of the two-dimensional calculations are nearly identical (5% spread at 10 ms), indicating that the detonation scheme modifies the pressure histories but does not change the overall impulse. This result is consistent with our previous conclusion that the overall impulse is determined mainly by the charge weight and not by the charge configuration or the detonation scheme.

Compared with an infinite HEST (dashed curve in Figure 23), the impulse at 10 ms is reduced by about 18% due to the lateral expansion at the edges. This estimate may be regarded as typical of the edge effects in small HEST experiments. For a larger HEST calibration experiment, such as the 6.1-m-radius DISK HEST experiment discussed in Section 4.4, the calculated impulse at 10 ms is only 9% lower than the reference one-dimensional calculation.

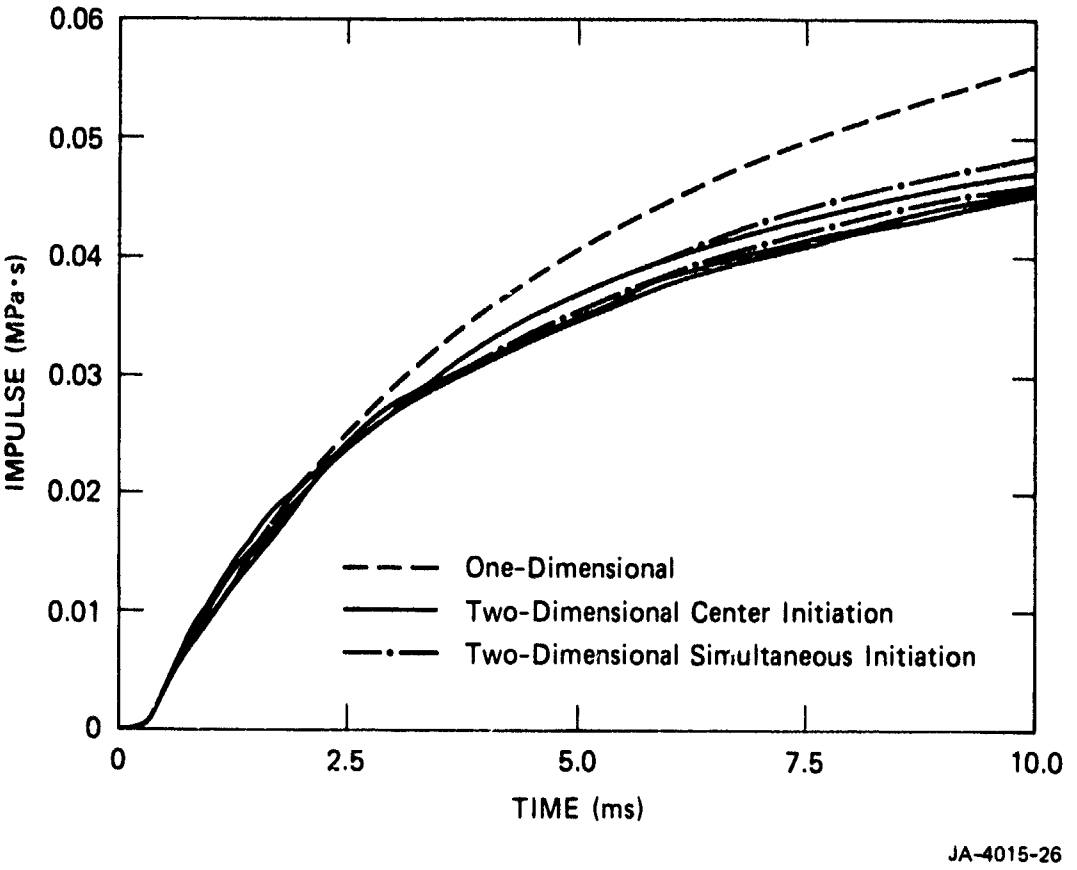

Figure 23. Impulse histories from one-dimensional and two-dimensional HEST calculations. (Initial radius of 1.6 m, initial cavity height of 70 mm, charge areal density of 2.1 kg/m^2, and detonation velocity of 6200 m/s).

SECTION 3

DESIGN CALCULATIONS FOR STP 3.5A EXPERIMENT

In this section, we present the methodology and the design calculations for the variable HEST used in the STP 3.5A experiment.

3.1 DESIGN CRITERIA

The ultimate objective of a HEST simulator would be to match exactly a desired nuclear pressure history throughout the simulation time. The HEST pressure, however, includes many oscillations and spikes due to reflections from the cavity walls and interaction of pressure waves from the explosive strands. Figure 24 shows typical pressure histories measured in the STP 2.5 experiment and a comparison with one-dimensional PUFF calculations. The desired peak pressure for this HEST design was 35 MPa (5 ksi), which is the same as the initial explosion pressure assumed in the calculations. The measured peak pressures of 117 MPa in Figure 24(a) and 85 MPa in Figure 24(b) are, respectively, 3.3 and 2.4 times higher than the 35-MPa explosion pressure. The impulse history, however, matches the calculated impulse very well. The present comparison shows that the peak pressure measured in a conventional HEST is not the same as the initial explosion pressure that must be used in one-dimensional calculations to match the measured impulse history.

The above discrepancy between the measured HEST peaks and the explosion pressure suggests that the HEST design criterion should not be based on matching the peak pressure. The criterion we chose is to match the pressure waveform (excluding its peak) and the impulse history throughout the desired simulation time. Even though our criterion does not require a match to the peak pressure, we do not expect a degradation of the fidelity of the resulting HEST simulator, especially if the HEST is intended to simulate the airblast-induced ground shock. Calculations

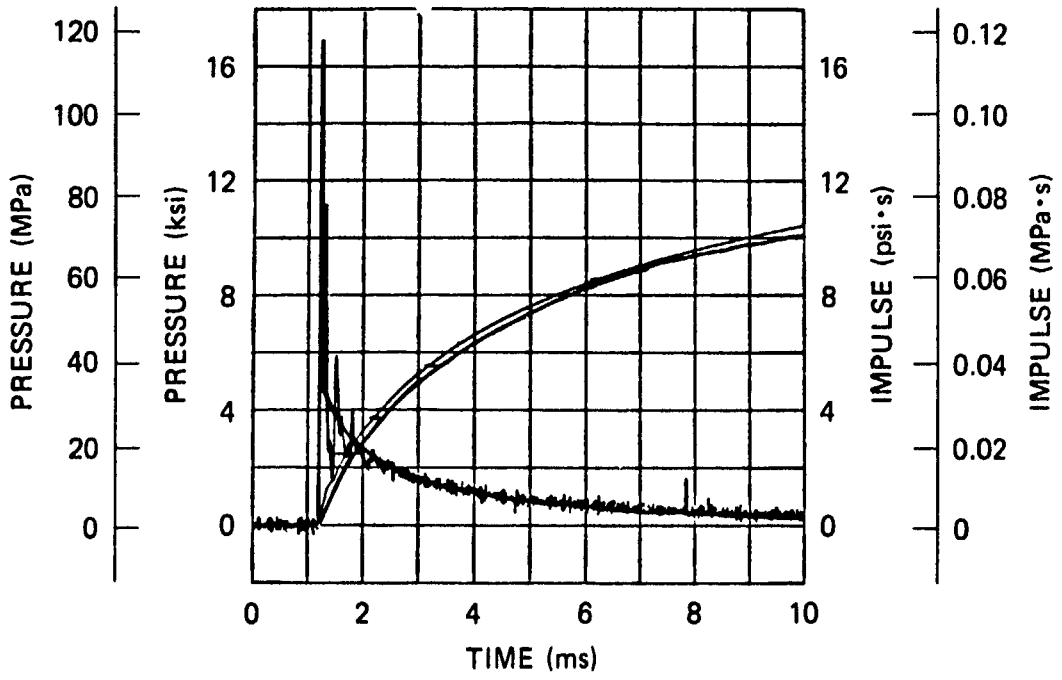

(a) Free-field (Gage BP-15)

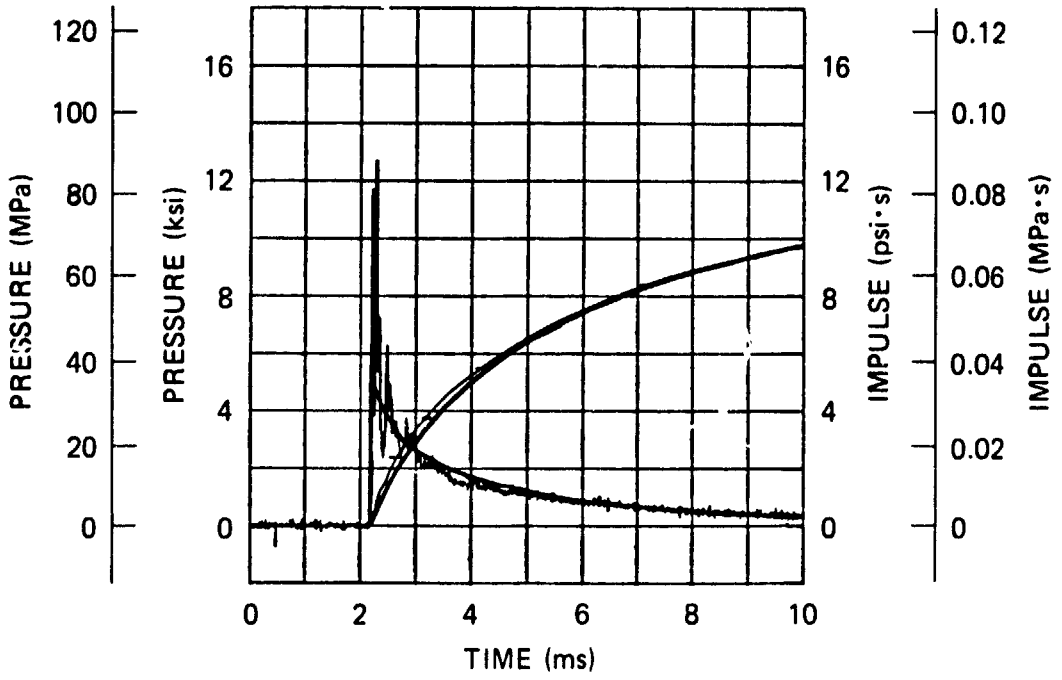

(b) Over Structure (Gage 5)

JA-4015-27

Figure 24. Comparison of calculated pressure histories (heavy solid lines) with typical pressure measurement made in the STP 2.5 experiment.

discussed in Section 2.2 show that two pressure waveforms with different peaks but the same impulse become identical after a propagation distance of about 35 times the cavity height. In other words, the peak stress that occurs in soil at distances far enough from the explosive cavity is insensitive to the peak pressure initially applied to the soil surface. Because most of the HEST waveforms in the STP experiments arrive at the test structure after traveling a distance that is large compared with the initial cavity height, we conclude that a discrepancy in peak pressure on the soil surface does not measurably impair the fidelity of the ground shock simulation.

The criterion discussed above should lead to a reasonable simulation of the ground shock. However, if a HEST is used to simulate the direct airblast loads on a responding structure, the pressure spikes must be considered in determining an equivalent pressure-yield combination and in assessing the simulation fidelity. This topic is under investigation in the simulation development community. Several fitting routines, including the SRI shock spectrum method,[7] are discussed in Reference 8.

We have observed that any of the fitting routines applied to a HEST pressure record result in a higher equivalent pressure than the explosion pressure used in our one-dimensional calculations. For example, the average equivalent pressure calculated by WES for the STP 2.5 experiment is about 48 MPa, which is 37% higher than the explosion pressure of 35 MPa. This indicates that, if the HEST design is based on an explosion pressure that is about 35% lower than the simulation objective, the equivalent pressure of the resulting HEST should then approach the simulation objective. This rule is used as a guide in designing the HEST for the STP experiments.

3.2 STP 3.5A VARIABLE HEST DESIGN

We designed a variable HEST for the STP 3.5A experiment based on the criterion that the airblast pressure (excluding the peak) and impulse are matched throughout the desired simulation time. The overburden and test bed materials were represented by pressure-density

relationships in our calculations. The relationship for the crushed limestone overburden was based on the stress-strain data provided by WES (Figure 25). A generic unsaturated soil with 3% void ratio was used to represent the HEST test bed at Fort Knox.[6]

Our design methodology was to determine the HEST configuration at several discrete ranges based on one-dimensional calculations of the cavity expansion. The areal density of the explosive, m, and the overburden height, H, were determined such that the total impulse from the HEST matched the total positive impulse of the reference nuclear environment. We then obtained a "best" match to the desired pressure and impulse histories by varying the cavity height while keeping m and H constant.

Figure 26 shows the results of such calculations for a nominal 35-MPa HEST. Comparison of the impulse histories shows that the reference impulse, designated as the simulation objective in Figure 26, is best matched by the 70-mm-high cavity (P_{exp} = 18.5 MPa). We also note that a good match with the simulation objective would not be possible with an initial explosion pressure of 35 MPa (long-dashed curves in Figure 26). The calculated impulse for P_{exp} = 35 MPa always lies above the simulation objective throughout the 20-ms-window shown in Figure 26, and at 2.5 ms it is about 50% higher than the simulation objective.

We repeated similar one-dimensional calculations for several other ranges and then interpolated the HEST variables at other ranges based on these calculations. Figure 27 shows a schematic of our final design of the variable HEST for the STP 3.5A experiment covering the pressure range of 500 to 7 MPa (5 kbar to 1000 psi). Iremite-60 explosive is used for the pressure ranges of 500 to 100 MPa, and primacord explosive is used for the lower pressure ranges. We found that the overburden height could be chosen to vary linearly with range from 0.64 m at the 500-MPa location to 1.15 m at the 7-MPa location. The cavity height increases linearly with range from 38 mm at the 500-MPa location to 70 mm at the 35-MPa location. Beyond this location, the cavity height remains constant at 70 mm.

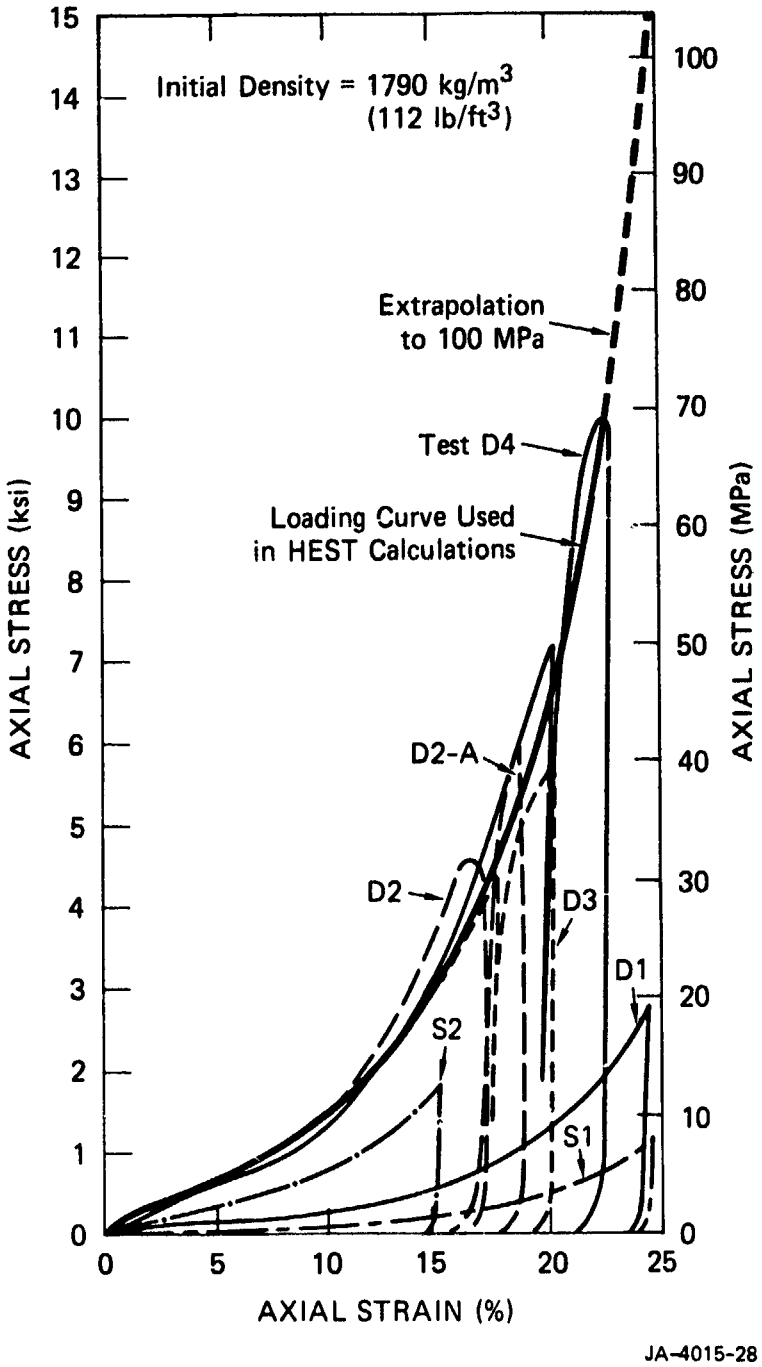

Figure 25. Stress-strain data from uniaxial compression tests performed by WES on Fort Knox crushed limestone. (The loading curve used in STP 3.5A HEST design calculations is shown as a heavy solid line.

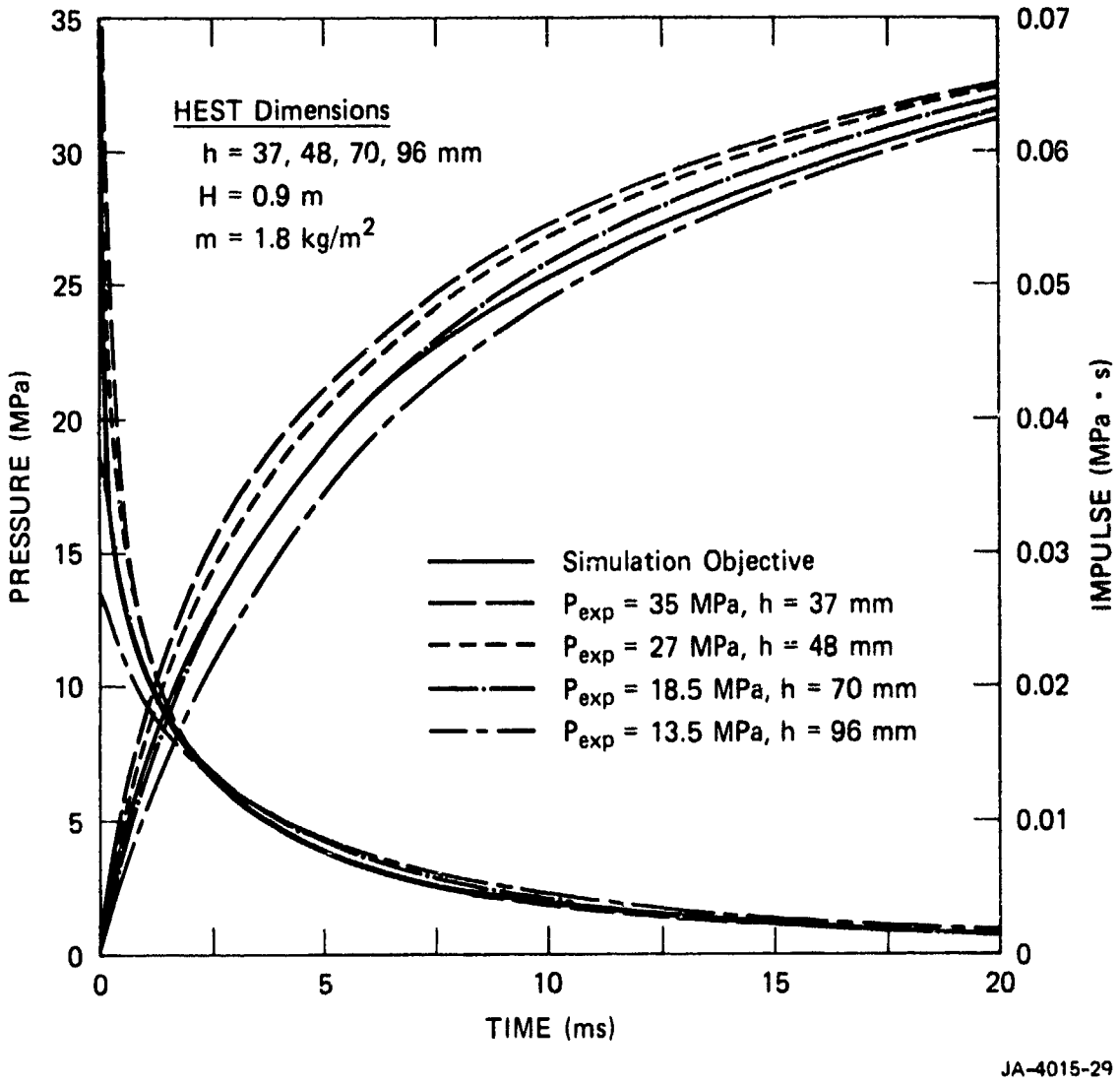

Figure 26. Pressure and impulse histories calculated for different explosion pressure P_{exp} in a nominal 35-MPa HEST.

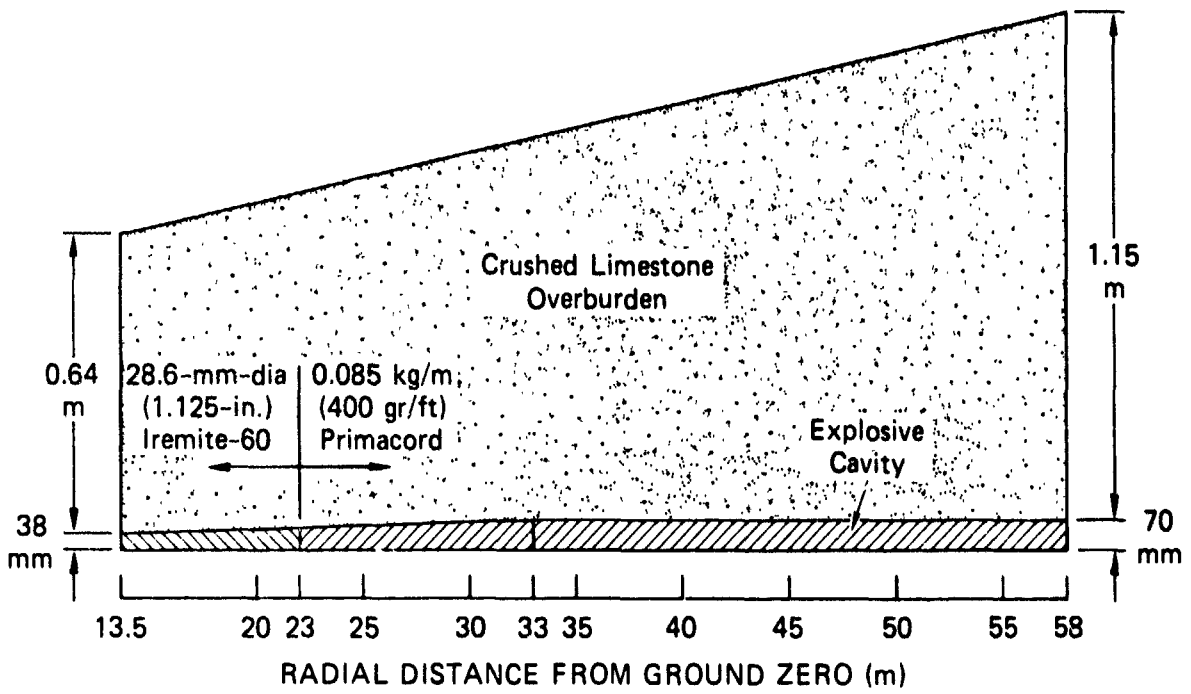

Figure 27. STP 3.5A variable HEST design covering the pressure range of 7-500 MPa (1000 psi-5 kbar).

Figures 28 and 29 show typical comparisons between our calculations and the simulation objective for two segments in which Iremite-60 (Figure 28) and primacord (Figure 29) explosives are used. The difference between the calculated impulse and the simulation objective is less than 5% at all times and ranges.

Figure 30 shows that the discrete primacord and Iremite-60 HEST designs (including those shown in Figures 28 and 29) can be correlated by plotting the total impulse from the HEST versus the product of charge areal density and overburden height, mH. The plot shows that the total impulse is roughly proportional to the square root of mH. The dashed-point line indicates a theoretical limit for the HEST impulse and represents the case in which all the explosive energy is transformed into the kinetic energy of the overburden. The plot in Figure 30 was used to interpolate the value of mH at all ranges in the HEST design and resulted in the variable HEST design shown in Figure 27.

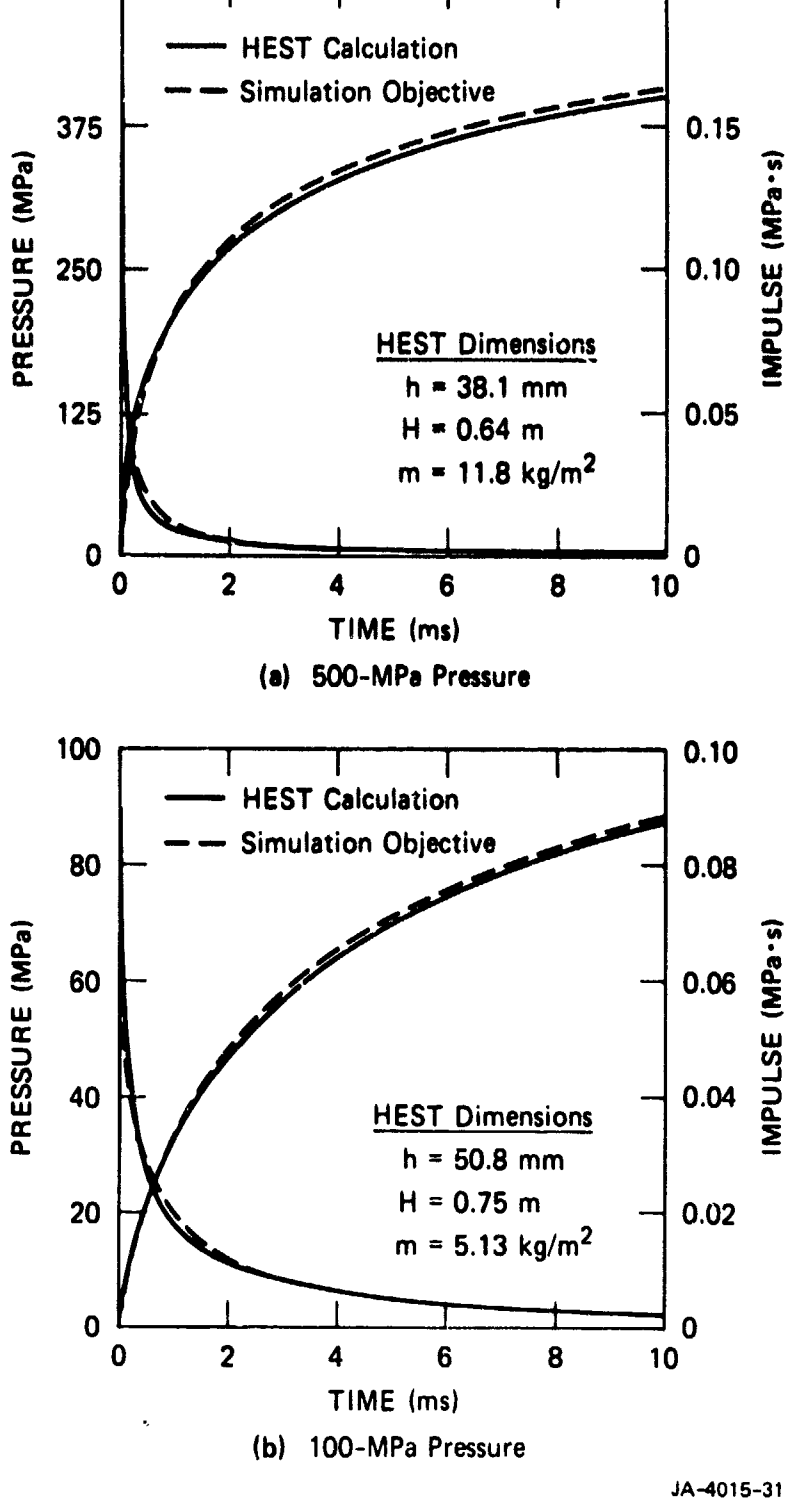

Figure 28. HEST pressure and impulse (using Iremite explosive) compared with simulation objective at 500-MPa and 100-MPa peak pressures.

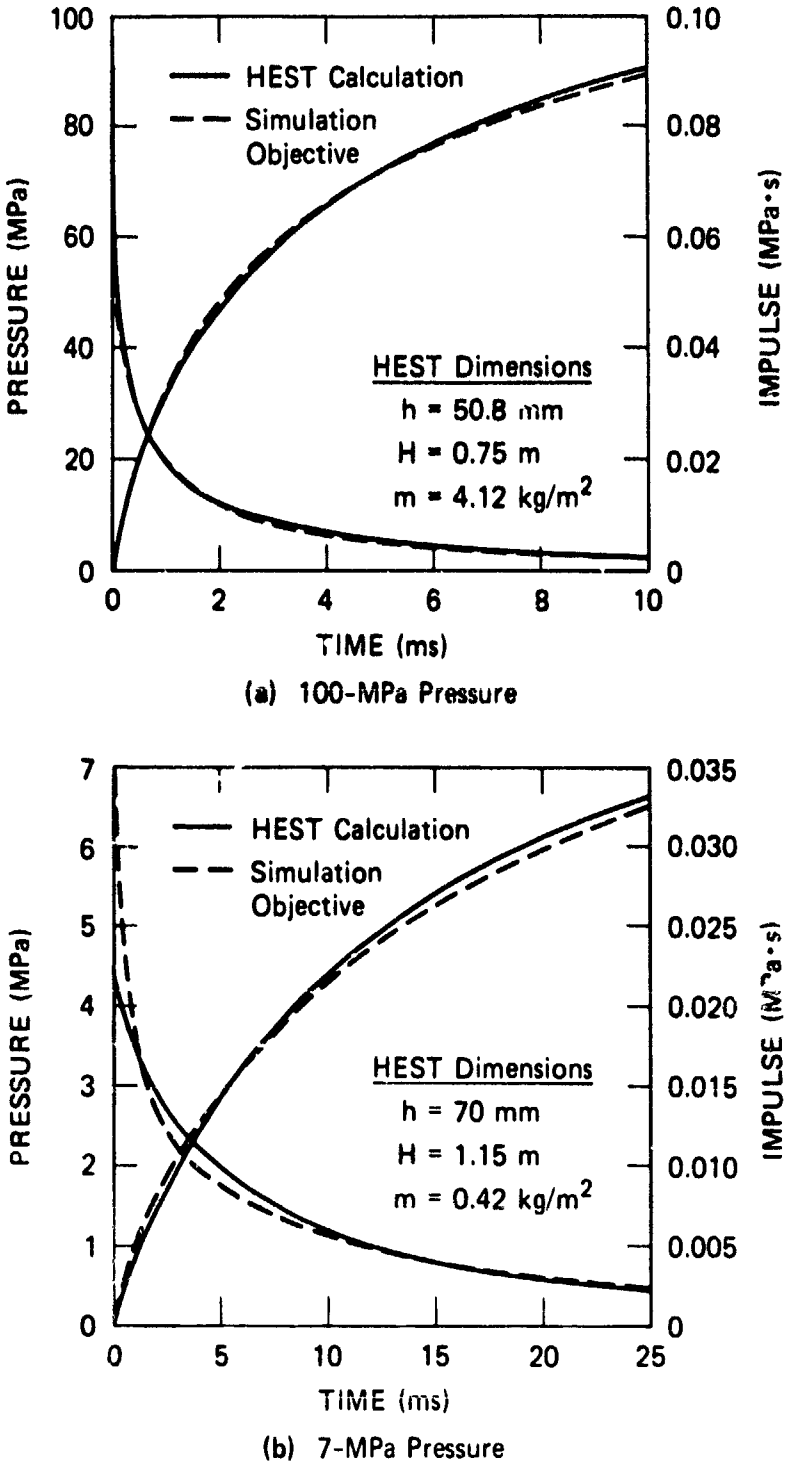

Figure 29. HEST pressure and impulse (using primacord explosive) compared with simulation objective at 100-MPa and 7-MPa peak pressures.

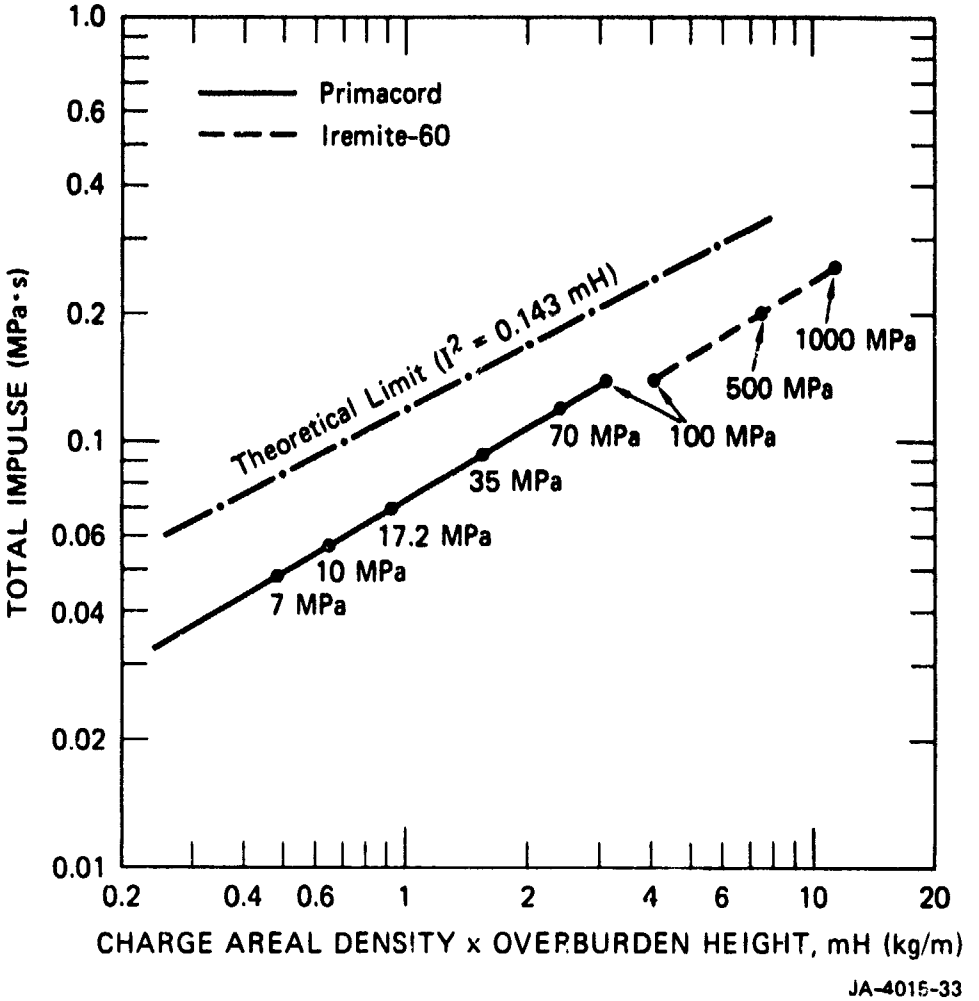

Figure 30. Calculated total impulse versus the product of charge areal density and overburden height for primacord HEST (7-100 MPa) and for iremite-60 HEST (100-1000 MPa).

SECTION 4

CALIBRATION EXPERIMENTS

We designed four uniform HEST calibration experiments to validate our code calculations and obtain a relationship between the charge density and explosion pressure. The calibration experiments represent a constant-pressure segment of the STP 3.5A variable HEST design at 1000, 100, and 35 MPa peak pressure ranges (two calibration experiments were designed at the 35-MPa range). These experiments were performed by WES at Fort Knox near the site of the STP 3.5A main event.

4.1 1000-MPA EXPERIMENT

The 1000-MPa HEST calibration experiment consisted of a 7.9-m (26-ft) square charge placed directly over the in situ soil at Fort Knox. The explosive used was 28.6-mm-diameter (1.125 inch) Iremite-60 placed on 41.3-mm (1.625 inch) centers. (Details of the charge design are given in Reference 5.)

Figure 31 shows a comparison between the pretest HEST calculations and the simulation objective. In this calculation, the SRI TIGER code was used to generate a tabular equation of state for the Iremite/foam explosive charge.

Figure 32 shows a comparison between the calculations and the data from a flatpack ytterbium gage. Because of an uncertainty in the density of the overburden used in this experiment, Figure 32 shows the results of two separate calculations based on probable maximum and minimum overburden densities of 1840 kg/m^3 and 1360 kg/m^3. Also shown is an error bar representing the uncertainty in the measured impulse.*

*Hysteresis and strain effects must be accounted for to obtain stress and impulse data from ytterbium gages. Details of data reduction procedure and the level of uncertainties involved are discussed in Reference 5.

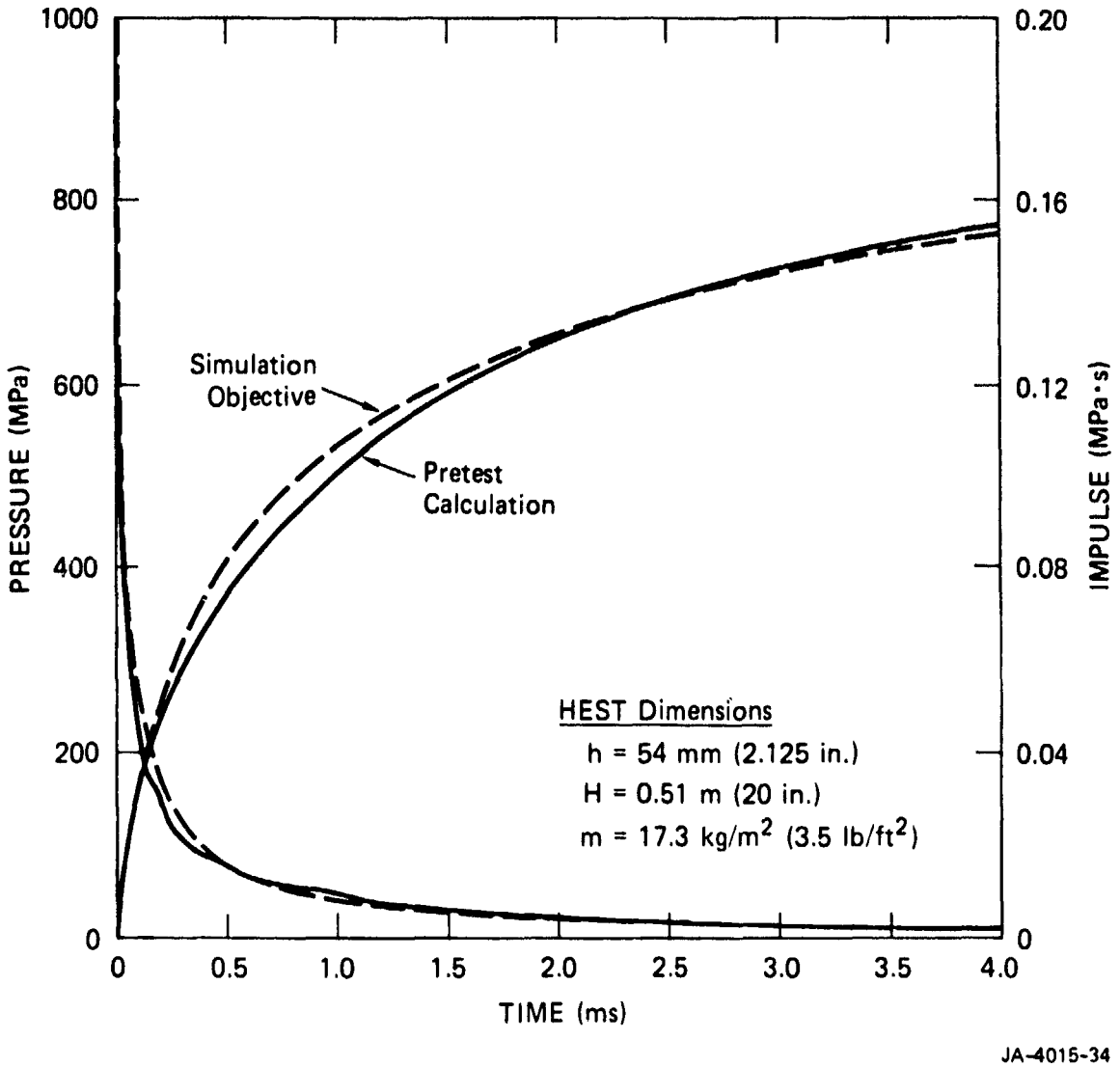

Figure 31. Pretest HEST calculations and the simulation objective for the 1000-MPa Iremite HEST calibration experiment.

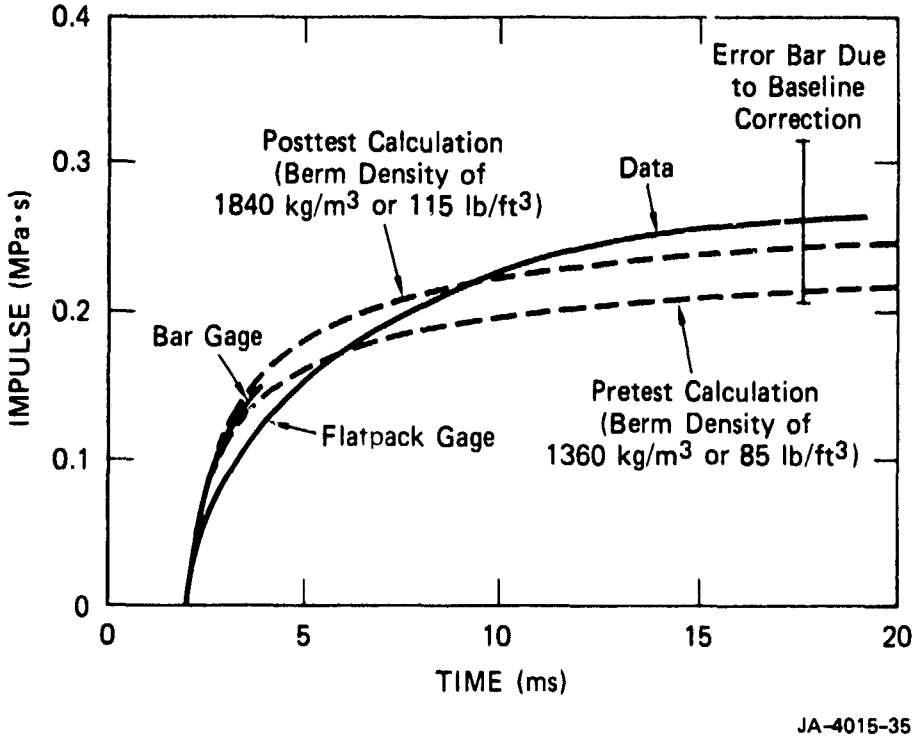

Figure 32. HEST calculations and data from the 1000-MPa Iremite HEST calibration experiment.

The agreement between the predicted and measured impulse is reasonably good after about 10 ms. The impulse at earlier times does not agree as well, possibly due to the measurement errors.

We used the calibration experiment discussed above and several other uniform Iremite HEST experiments at lower pressures to obtain a relationship between the charge density ρ_c and explosion pressure P_{exp}. For each HEST design, we performed several calculations with different explosion pressures and found the value that best matched the impulse measurements.

The explosion pressures obtained in this manner are plotted versus the as-built charge density in Figure 33 and compared with the TIGER calculations. The agreement is very good for the 1000-MPa HEST, but differs as much as 50% for the low pressure experiments. This difference seems to be a manifestation of nonequilibrium effects at low pressures, which is not accounted for in the equilibrium calculations of the TIGER code. The solid curve in Figure 33 is a fit to the experimental points and was used in the design of the STP 3.5A experiment.

4.2 100-MPA EXPERIMENT

The 100-MPa HEST calibration experiment consisted of a 5.0-m (16.4 ft) square charge placed directly over the in situ soil at Fort Knox. The explosive used was 0.085 kg/m (400 grains/ft) primacord placed on 25.4-mm (1 inch) centers. (Details of charge design are given in Reference 5.)

Figure 34 shows a comparison between the pretest calculations, simulation objective, and data obtained from a WES airblast gage. The measured impulse is significantly lower (about 40%) than the calculated impulse or the simulation objective. As shown in Reference 5, this large difference could not be accounted for by either the edge effects from the test bed (also discussed in Section 2.7) or by varying the properties of the overburden or test bed materials within reasonable bounds. The most probable cause for the discrepancy between calculations and measurements was found to be the lack of performance of the primacord explosives used in this experiment.

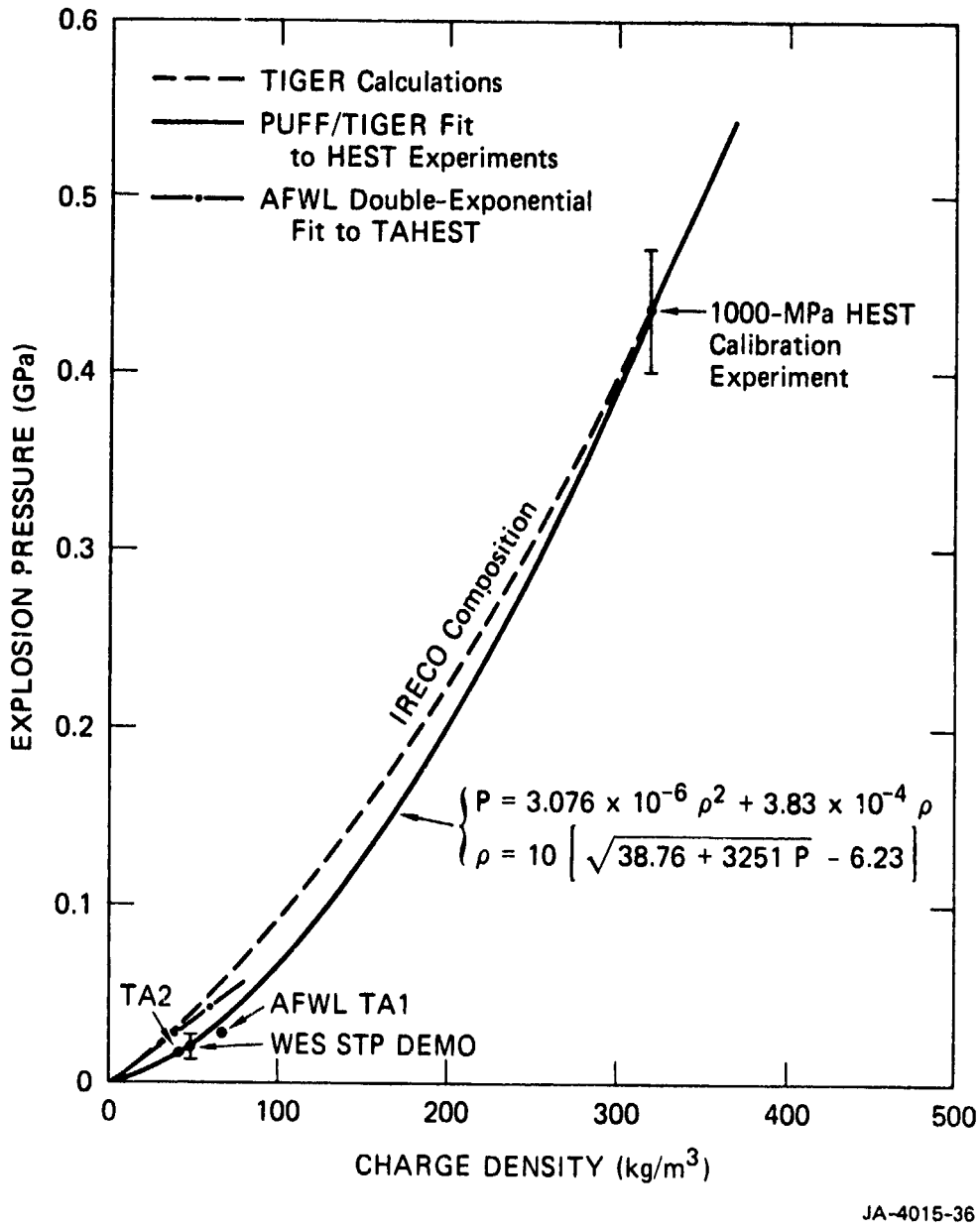

Figure 33. Explosion pressure versus charge density for Iremite-60 explosive.

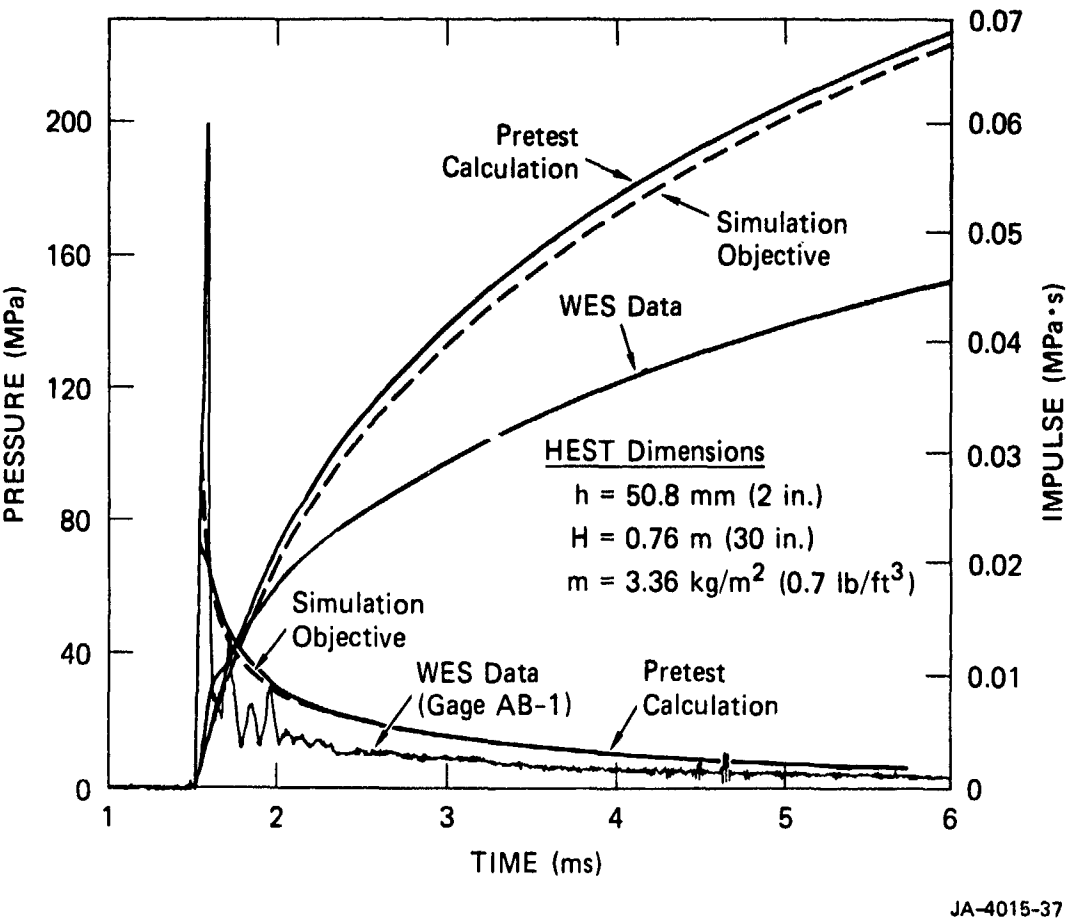

Figure 34. Calculations, simulation objective, and data from the 100-MPa primacord HEST calibration experiment.

As a check on explosive performance, measured impulse-time histories for three similar tests are compared in Figure 35. The highest curve is the simulation objective for which the 100-MPa HEST was designed (left-hand diagram in the figure). As previously indicated, the measured impulse is lower than the objective by 40%. The ACID test has a slightly higher overburden and only 70% of the explosive areal density, but gives an impulse comparable to the 100-MPa experiment. The STP 2.5 test has 60% less overburden and the same amount of explosives, but gives 50% more impulse than the 100-MPa test. This result indicates that the performance of the primacord explosive in the 100-MPa test was lower than in other tests in which primacord explosive of same size was used.

To verify the accuracy of the charge weight, WES measured the weight of some of the primacord that was left over from the calibration experiments. The measured weights from some of the samples were as much as 30% lower than the manufacturer's specification of 0.085 kg/m (400 grain/ft). However, the question of what was actually used in the calibration experiments could not be resolved because the primacord charge had not been weighed before the experiments.

4.3 35-MPA EXPERIMENT

The 35-MPa HEST calibration experiment consisted of a 7.9-m (26-foot) square charge placed directly over the in situ soil at Fort Knox. The explosive used was primarily the 0.085 kg/m (400 grain/ft) primacord from the same batch used in the 100-MPa experiment. The spacing between the primacord strands was 50.8 mm (2 inch). (Details of the charge design are given in Reference 5.)

Figure 36 shows a comparison between the pretest calculation and the simulation objective, and Figure 37 shows a comparison between the pretest calculations and the measured impulse histories from nine of the WES airblast gages. A typical pressure history (from Gage 418) is also shown for comparison. The data shows a 20% spread and the mean impulse is about 40% lower than the simulation objective. The discrepancy seen

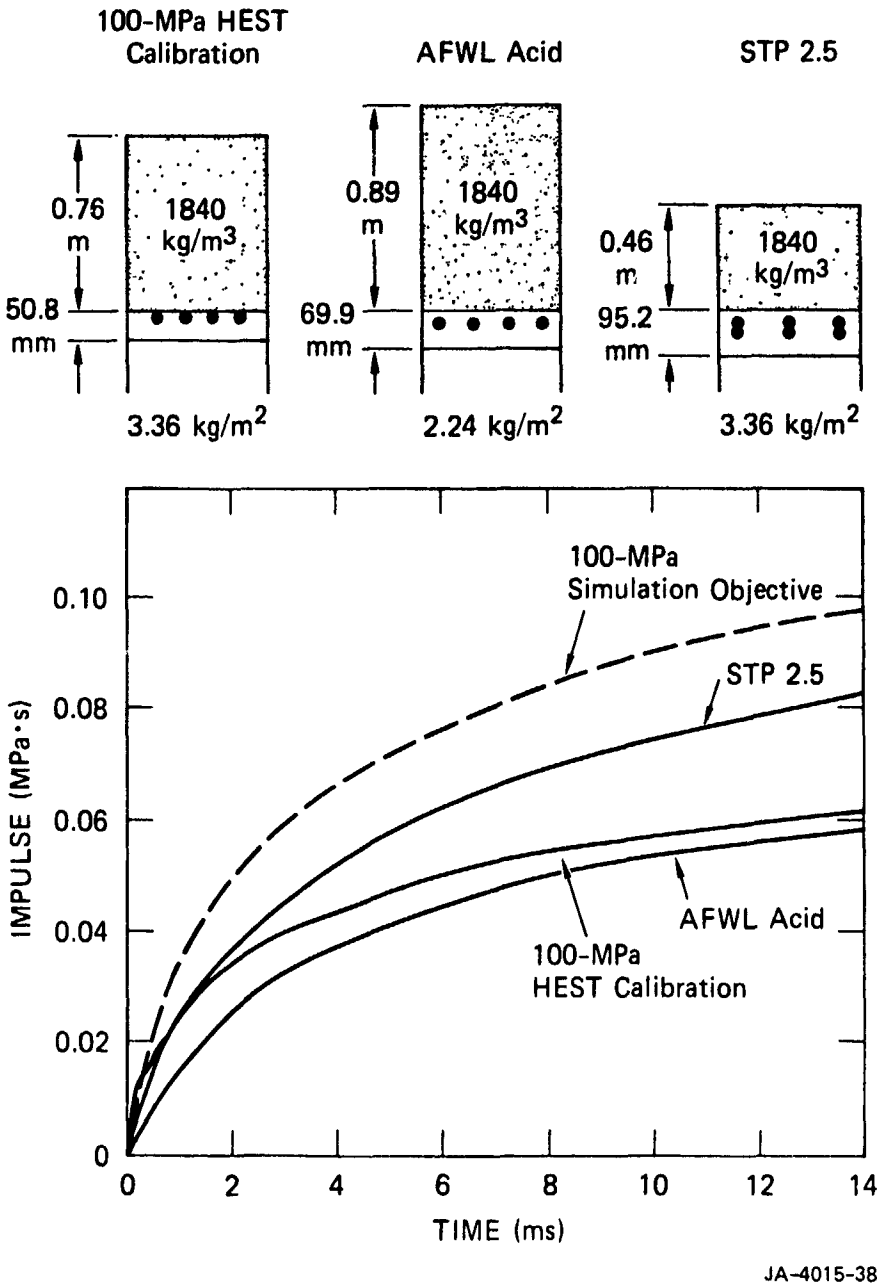

Figure 35. Data from 100-MPa HEST calibration experiment and two other similar HEST experiments in which 0.085 kg/m (400 gr/ft) primacord was used.

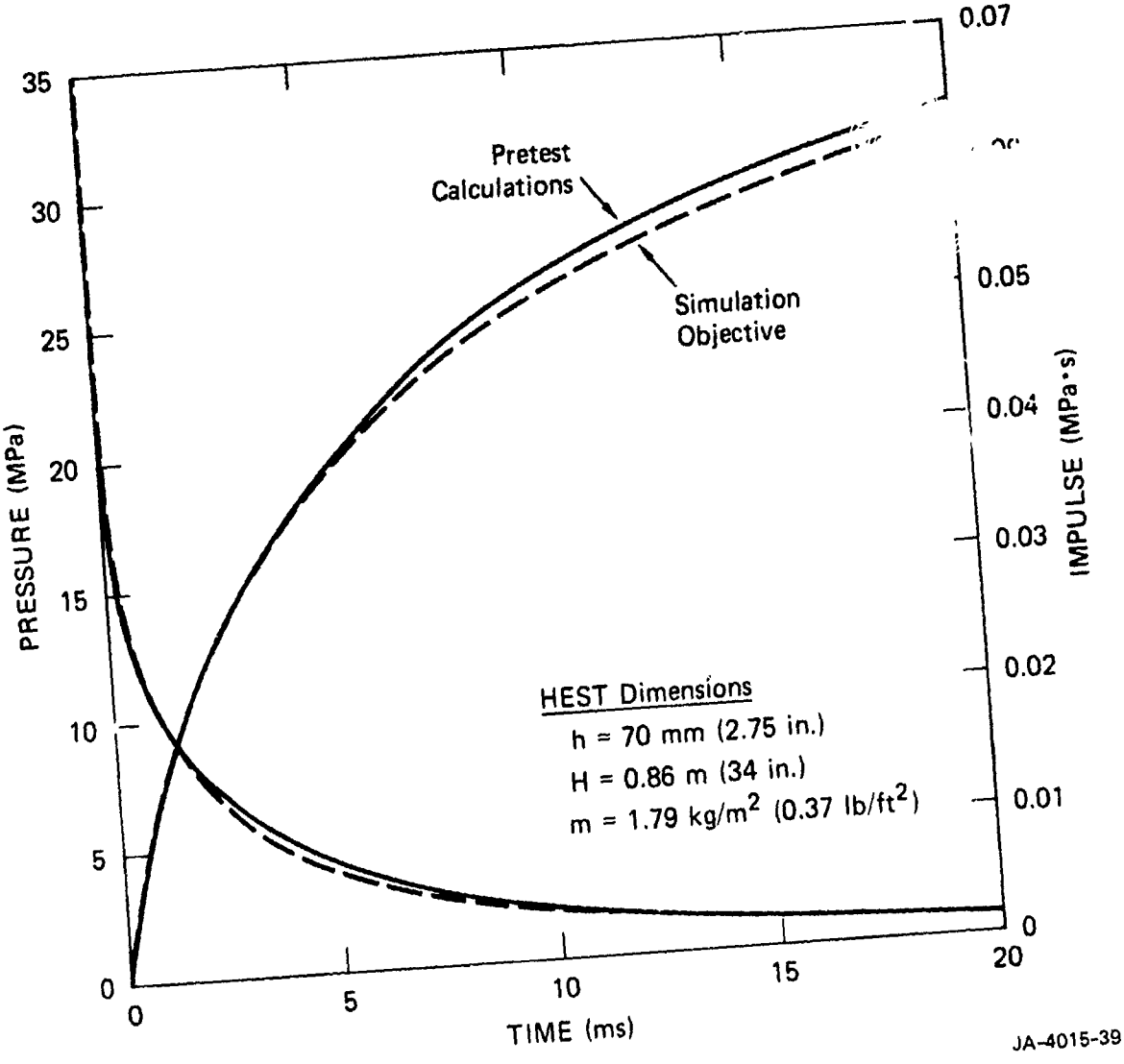

Figure 36. Pretest HEST calculation and simulation objective for the 35-MPa HEST calibration experiment.

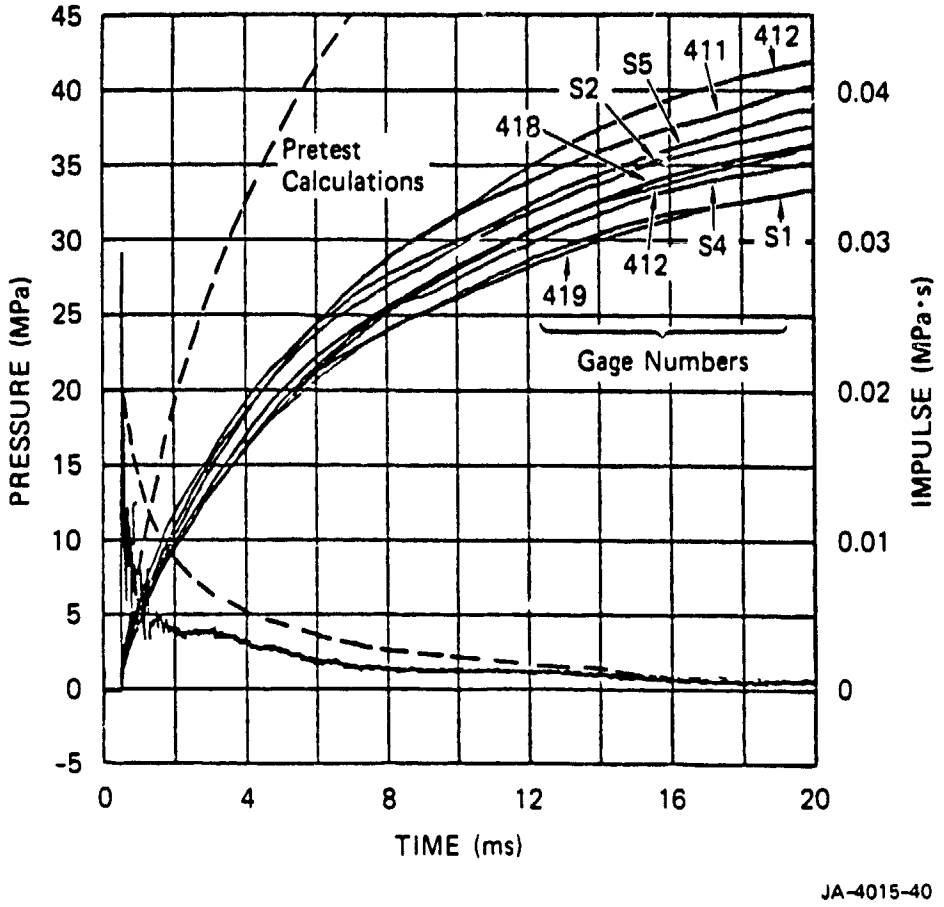

Figure 37. Calculations and data from the 35-MPa primacord HEST calibration experiment.

here again appears to be due to the lack of performance of tne primacord charge similar to that observed in the 100-MPa experiment.

4.4 DISK HEST EXPERIMENT

Because of the uncertainties in the amount of explosives used in the 35- and 100-MPa calibration experiments, results from these experiments could not be used for validating the code calculations. Therefore, WES performed another 35-MPa HEST calibration experiment, designated as DISK HEST, in which the explosives were weighed before being placed in the cavity. Results of this experiment are compared in Figure 38 with one-dimensional and two-dimensional calculations. The agreement between the data and the calculations is within the accuracy of the measurements.

4.5 RELATIONSHIP BETWEEN EXPLOSION PRESSURE AND CHARGE DENSITY

Using the procedure discussed in Section 4.1, we deduced a relationship between the as-built primacord charge density and the explosion pressure based on all the calibration experiments after a posttest correction was made for the charge weight and the STP 2.5 experiment (Figure 39). Because the manufacturer's specification for weight tolerance is ±20% of 0.085 kg/m (400 grain/ft) primacord, we assumed a 20% lower charge weight to account for the low performance of the explosives in the 35- and 100-MPa HEST experiments and a 20% higher charge weight to account for the extra high performance of the charge in the STP 2.5 experiment. This appears reasonable from the resulting smooth solid curve in Figure 39 fit to the experimental points. This curve was used in the design of the variable HEST in the STP 3.5A experiment.

Also shown in Figure 39 are the results from TIGER calculations for a primacord/foam charge and the data from AFWL C^2 experiments. At a charge density of 15 kg/m^3, the effective explosion pressure deduced from the calibration experiments is about 40% lower than the TIGER predictions and about 25% lower than the C^2 data. We believe that the discrepancy observed here is characteristic of a HEST with a thin cavity

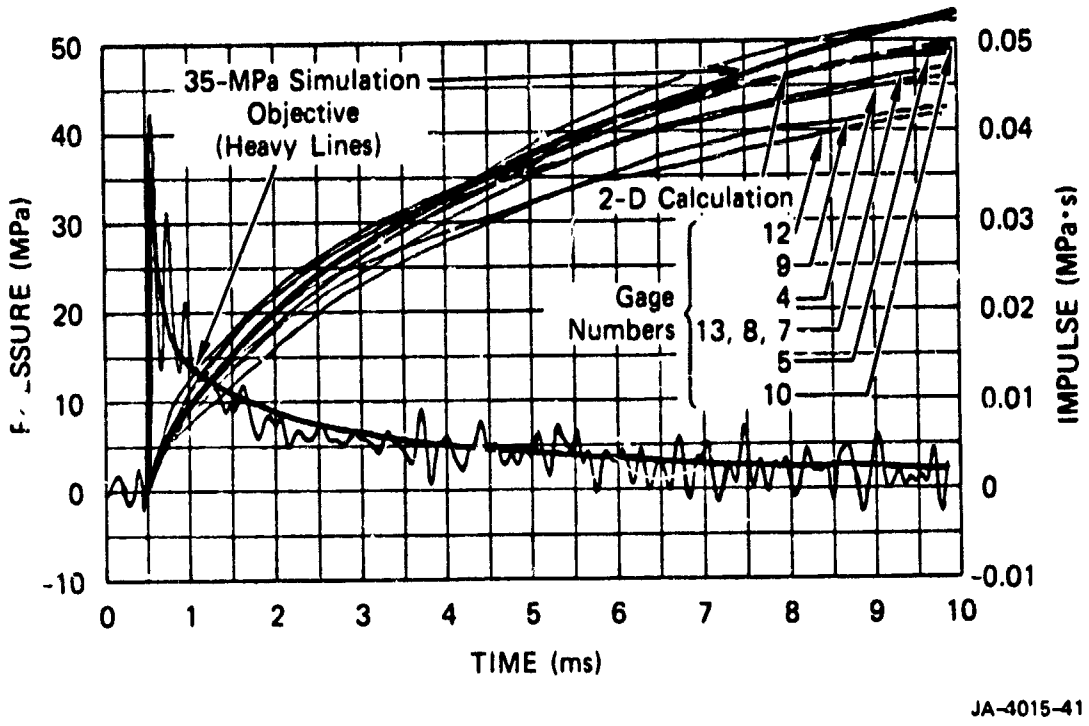

Figure 38. Data from the disk HEST experiment (light solid curves), 35-MPa simulation objective (heavy solid curves), and two-dimensional finite difference calculations (heavy dashed curve).

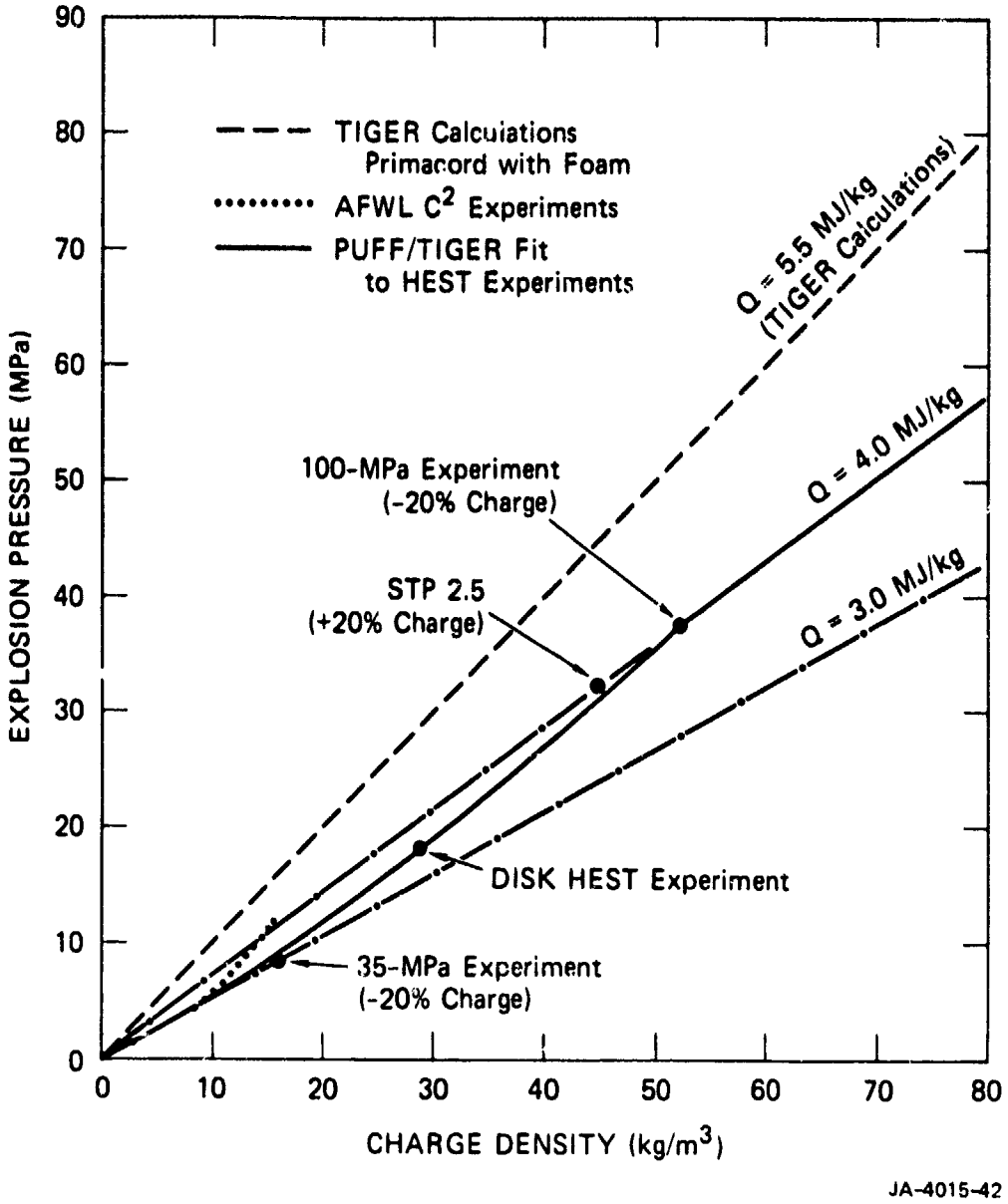

Figure 39. Explosion pressure versus charge density for primacord explosive.

(less than 100 mm, say). In such a HEST, the jetting between the explosive strands tends to penetrate into the soil that surrounds the cavity, thus dissipating part of the explosive energy. The net result is a loss of impulse delivered by the charge, which is represented by a lower effective explosion pressure in Figure 39. This conclusion is also supported by the HPC^2 experiments reported in the Appendix.

Regardless of the actual reasons for the lack of agreement with TIGER calculations or C^2 experiments, the solid curve in Figure 39 represents the combination of measured explosive density in the as-built experiment and the explosion pressure required to give the best match to the measured impulse history. This result was therefore used in conjunction with the one-dimensional calculations to design the STP 3.5A variable HEST discussed in Section 5.

SECTION 5

STP 3.5A MAIN EVENT

In this section, we first discuss the layout of the test bed and then evaluate the performance of the variable HEST by comparing the simulation objective with the data from the airblast and near-source stress gages.

5.1 OVERALL TEST BED LAYOUT

The overall layout of the STP 3.5A experiment is shown in Figure 40. The location of the perimeter of the HEST was specified by ARA.[9] The central strip covers four structures as shown. Iremite (denoted by I) was used in the closer ranges of the central strip (down to 23.2 m or 76 feet) and in the side (down to 39.4 m or 129 feet). The angle of the side zones was chosen to be 22.5° relative to the central zones so that the length of the side zone at the 35-MPa range is normal to a radius from GZ through the center of this zone.

The variation with range R of the explosive areal density m and the cavity height h were obtained from the conceptual design shown in Figure 27 and the explosion pressure-charge density relationship shown in Figure 39. The curves of m versus R and h versus R were then discretized into zones of constant m and constant h. For ease of construction, all zone widths were chosen to be multiples of 1.22 m (4 feet). The zones over the structures (zones 13P, 15P, and 21BP) were selected to be at least 2.44 m (8 feet) wide and centered over the 1.22-m-diameter (4-foot) structures. The remaining zones were chosen to reasonably approximate the m versus R curve.

For each zone, the primacord spacing was calculated according to the explosive areal density required in that zone. A similar procedure was used for selecting spacing for Iremite-60 explosive. The cavity height for each zone was chosen to be a constant and a multiple of 6.35 mm (0.25 inch).

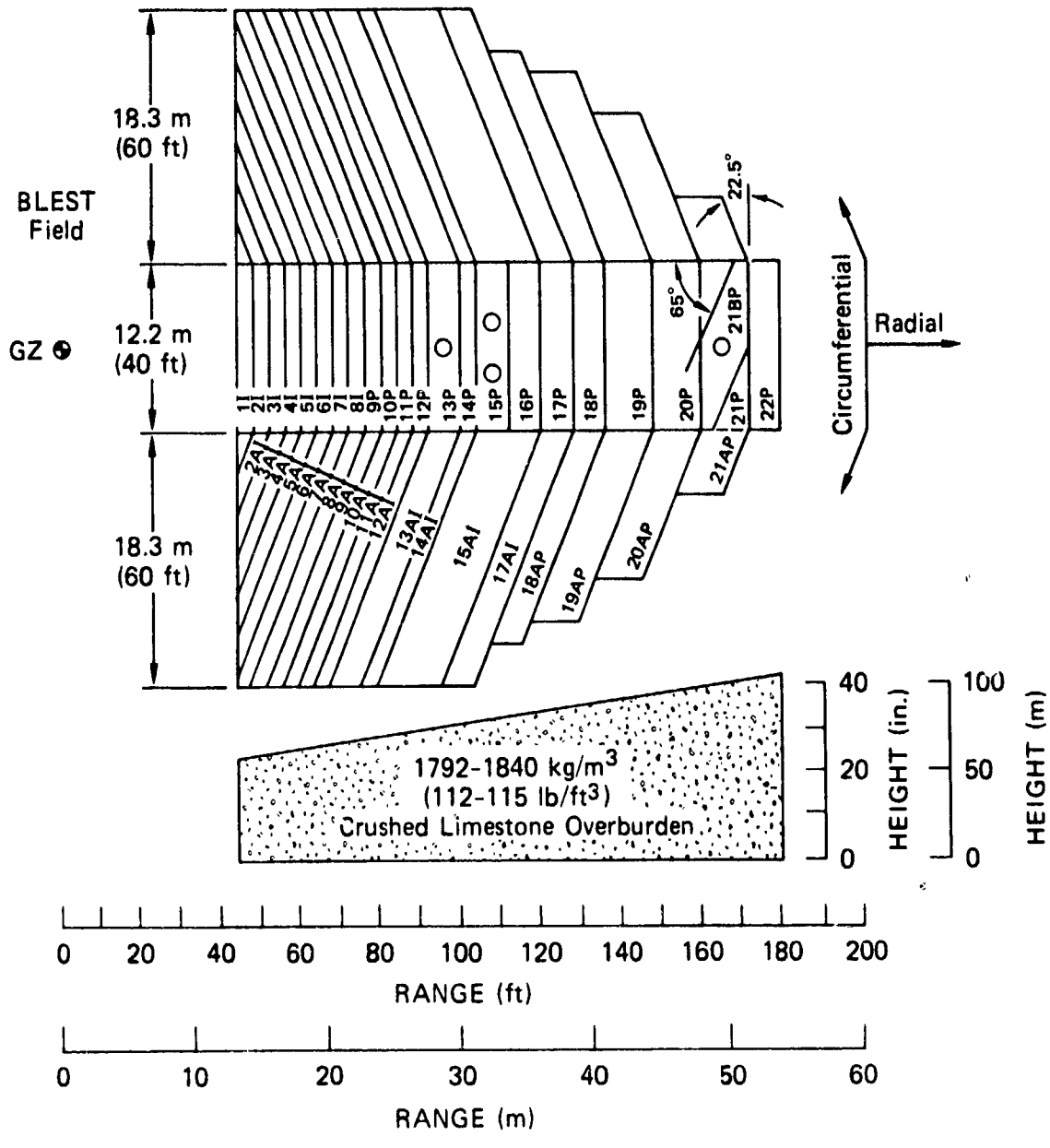

Figure 40. Layout of striptest and STP 3.5A HEST experiments.

The parameters calculated for each zone are shown in Tables 1 and 2. In most zones, the explosive was parallel to the zone length ("circumferential"). In zones 13A through 15P, the explosive was parallel to the zone width ("radial") so that the load ran over the structures at the detonation velocity of the primacord (6100 m/s), which is approximately equal to the air shock velocity of the airblast environment at these ranges. The primacord in zone 21BP was oriented as shown so that the load swept the structure at a velocity of about 3050 m/s, which is approximately the air shock velocity of the airblast environment at this range.

5.2 DATA FROM AIRBLAST GAGES

Twenty airblast gages (8 over the structures and 14 in the free-field) produced usable waveforms. Figure 41 compares the airblast data (solid lines) with the simulation objective (dashed lines) over 10, 20, and 100 ms time windows. The distance from ground zero is given at the top of the plots for each of the gages.

Except for Gage AB-3, which shows an impulse about four times lower than the expected values at this range, the remaining 21 airblast gages compare reasonably well with the simulation objective. There appears to be a late-time cavity flow caused by the horizontal pressure gradients in the cavity. This flow is manifested as low-amplitude ripples visible on some of the pressure records at late times. An example of cavity flow can be seen in the data from gages AB-1 or AB-9. A good match with the simulation objective is obtained in the 20-ms plots. At about 20 ms, the measured impulse rises above the simulation objective due to the arrival of a pressure ripple, signalling the passage of a compression wave from the upstream higher-pressure zone.

The overall performance of the simulator can be assessed by plotting the impulse measured by a gage at a given time versus the gage location. Figure 42 shows the impulses measured from the airblast gages at 5, 10, 50, and 90 ms after the time of shock arrival. For comparison, the simulation objective is shown as the solid line with the 15% band

Table 1

HEST CHARGE DESIGN OF STP 3.5A CENTER STRIP

Zone Number	Range m	Range (ft)	Width m	Width (ft)	Cavity Height mm	Cavity Height (in.)	Centerline Spacing mm	Centerline Spacing (in.)	Explosive	Direction of Explosive	m kg/m^2	m (lb/ft^2)	ρ_o kg/m^3	ρ_o (lb/ft^3)
1I	13.7	(45)	1.2	(4)	38.1	(1.5)	41.9	(1.65)	28.6 mm IREMITE (1.125 inches)	circumferential	17.47	(3.57	459.1	(28.6)
2I	14.9	(49)	1.2	4	38.1	(1.5)	50.8	(2.0)			14.48	(2.96)	380.4	(23.7)
3I	16.2	(53)	1.2	4	38.1	(1.5)	61.0	(2.4)			12.04	(2.46)	316.2	(19.7)
4I	17.4	(57)	1.2	4	38.1	(1.5)	67.8	(2.67)			10.81	(2.21)	284.1	(17.7)
5I	18.6	(61)	1.2	4	44.5	(1.75)	76.2	(3.)			9.56	(1.96)	215.1	(13.4)
6I	19.8	(65)	1.2	4	44.5	(1.75)	87.1	(3.43)			8.42	(1.72)	189.4	(11.8)
7I	21.0	(69)	1.2	4	50.8	(2.0)	101.6	(4.0)			7.19	(1.47)	141.3	(8.8)
8I	22.3	(73)	1.2	4	50.8	(2.0	110.7	(4.36)			6.61	(1.35)	130.0	(8.1)
9P	23.5	(77)	1.2	4	50.8	(2.0)	22.6	(0.89)			3.77	(0.770)	74.1	(4.62)
10P	24.7	(81)	1.2	(4)	57.2	(2.25)	25.4	(1.0)			3.35	(0.685)	58.6	(3.65)
11P	25.9	(85)	1.2	(4)	57.2	(2.25)	28.4	(1.12)			3.00	(0.613)	52.2	(3.25)
12P	27.1	(89)	1.2	(4)	57.2	(2.25)	30.5	(1.20			2.79	(0.570)	48.8	(3.04)
13P	28.3	(93)	2.4	(8)	63.5	(2.5)	33.8	(1.33)	0.085 kg/m primacord (400 gr/ft)	radial	2.51	(0.513)	39.3	(2.45)
14P	30.8	(101	1.2	(4)	69.9	(2.75)	36.8	(1.45			2.30	(0.471)	32.9	(2.05)
15P	32.0	(105	2.4	(8)	69.9	(2.75)	40.6	(1.60)			2.09	(0.428)	29.7	(1.85)
16P	34.4	(113)	2.4	(8)	69.9	(2.75)	48.8	(1.92)			1.75	(0.357)	25.2	(1.57)
17P	36.9	(121)	2.4	(8)	69.9	(2.75)	55.4	(2.18)		circum	1.54	(0.314)	21.7	(1.35)
18P	39.3	(129)	2.4	(8)	69.9	(2.75)	64.3	(2.53)			1.33	(0.271)	19.3	(1.20)
19P	41.8	(137)	3.7	(12)	69.9	(2.75)	71.6	(2.82)			1.19	(0.243)	17.0	(1.06)
20P	45.4	(149)	3.7	(12)	69.9	(2.75)	81.3	(3.20)			1.05	(0.214)	15.2	(0.95)
21P	49.1	(161)	3.7	(12)	69.9	(2.75)	84.3	(3.32)	0.02 kg/m	65° from	1.01	(0.206)	14.4	(0.90)
21BP	49.1	(161)	3.7	(12	69.9	(2.75)	21.1	(0.83)	(100 gr/ft) primacord	radial	1.01	(0.206)	14.4	(0.90)
22P	52.7	173	2.4	(8)	69.9	(2.75)	89.4	3.52)	0.085 kg/M primacord	circum	0.95	(0.195)		(0.83)

Table 2

HEST CHARGE DESIGN OF STP 3.5A SIDE ZONES

Zone Number	m	Width (in.)	Cavity Height mm	(in.)	Centerline Spacing mm	(in.)	Number Charges Per Zone	Explosive	Direction of Explosive	m kg/m^2	(lb/ft^2)	ρ_o kg/m^3	(lb/ft^3)
1AI	13.5	(44.3)	38.1	(1.5)	41.9	(1.65)	27	28.6 mm IREMITE (1.125 inches)	circumferential	17.56	(3.59)	462.3	(28.8)
2AI	13.5	(44.3)	38.1	(1.5	50.8	(2.0)	22			14.38	(2.94)	378.8	(23.6)
3AI	13.5	(44.3)	38.1	(1.5)	61.0	(2.40)	19			12.38	(2.53)	325.9	(20.3)
4AI	13.5	(44.3)	38.1	(1.5)	67.8	(2.67)	17			11.06	(2.26)	290.5	(18.1)
5AI	13.5	(44.3)	44.45	(1.75)	76.2	(3.0)	15			9.74	(1.99)	218.3	(13.6)
6AI	13.5	(44.3)	44.45	(1.75)	87.1	(3.43)	13			8.46	(1.73)	191.0	(11.9)
7AI	13.5	(44.3)	50.8	(2.0)	101.6	(4.0)	11			7.14	(1.46)	139.7	(8.7)
8AI	13.5	(44.3)	50.8	(2.0)	110.7	(4.36)	10			6.51	(1.33)	128.4	(8.0)
9AP	13.5	(44.3)	50.8	(2.0)	135.4	(5.33)	9			5.82	(1.19)	115.6	(7.2)
10AI	13.5	(44.3)	57.15	(2.25)	135.4	(5.33)	9			5.82	(1.19)	102.7	(6.4)
11AI	13.5	(44.3)	57.15	(2.25	152.4	(6.0)	8			5.19	(1.06)	89.9	(5.6)
12AI	13.5	(44.3)	57.15	(2.25)	174.2	(6.86)	7			4.56	(0.931)	80.3	(5.0)
13AI	27.0	(88.7)	63.5	(2.5)	203.2	(8.0)	12			3.90	(0.797)	61.0	(3.8)
14AI	13.5	(44.3)	69.85	(2.75)	203.2	(8.0)	6			3.90	(0.797)	56.2	(3.5)
15AI	54.1	(177.4)	69.85	(2.75)	243.8	(9.60)	19			3.09	(0.631)	44.9	(2.8)
17AI	27.0	(88.7)	69.85	(2.75)	304.8	(12.0)	8			2.60	(0.531)	36.9	(2.3)
18AP	27.0	(88.7)	69.85	(2.75)	64.3	(2.53)	35	0.085 kg/m (400 gr/ft) primacord		1.32	(0.270)	19.3	(1.20)
19AP	42.4	(139.0)	69.85	(2.75)	71.6	(2.82)	50			1.20	(0.246)	26.8	(1.67)
20AP	42.4	(139.0)	69.85	(2.75)	87.1	(3.43)	41			0.99	(0.202)	14.1	(0.88)
21AP	42.4	(139.0)	69.85	(2.75)	101.6	(4.0)	35			0.81	(0.165)	12.2	(0.76)

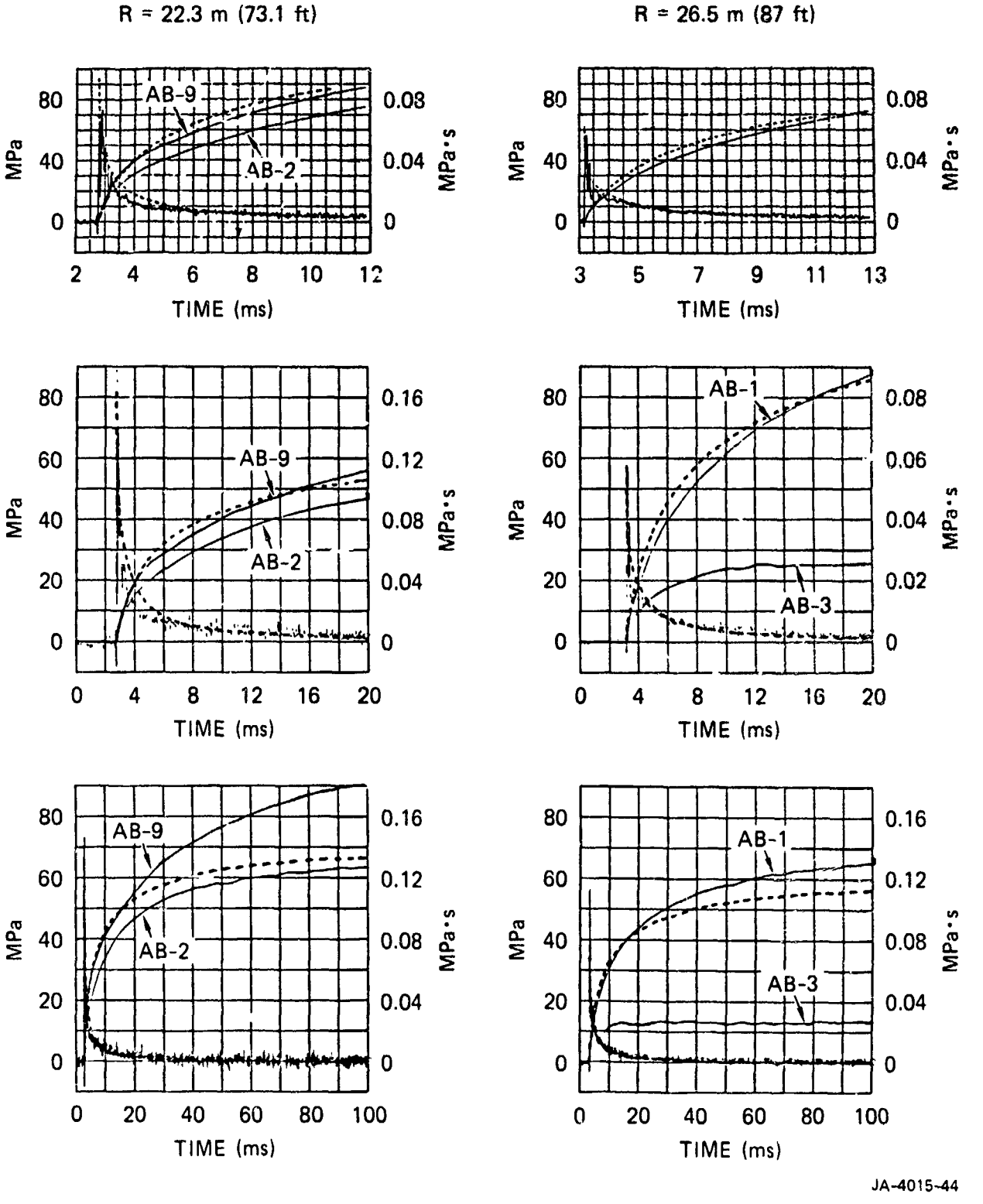

Figure 41. Airblast data from STP 3.5A experiment and simulation objectives (dashed lines).

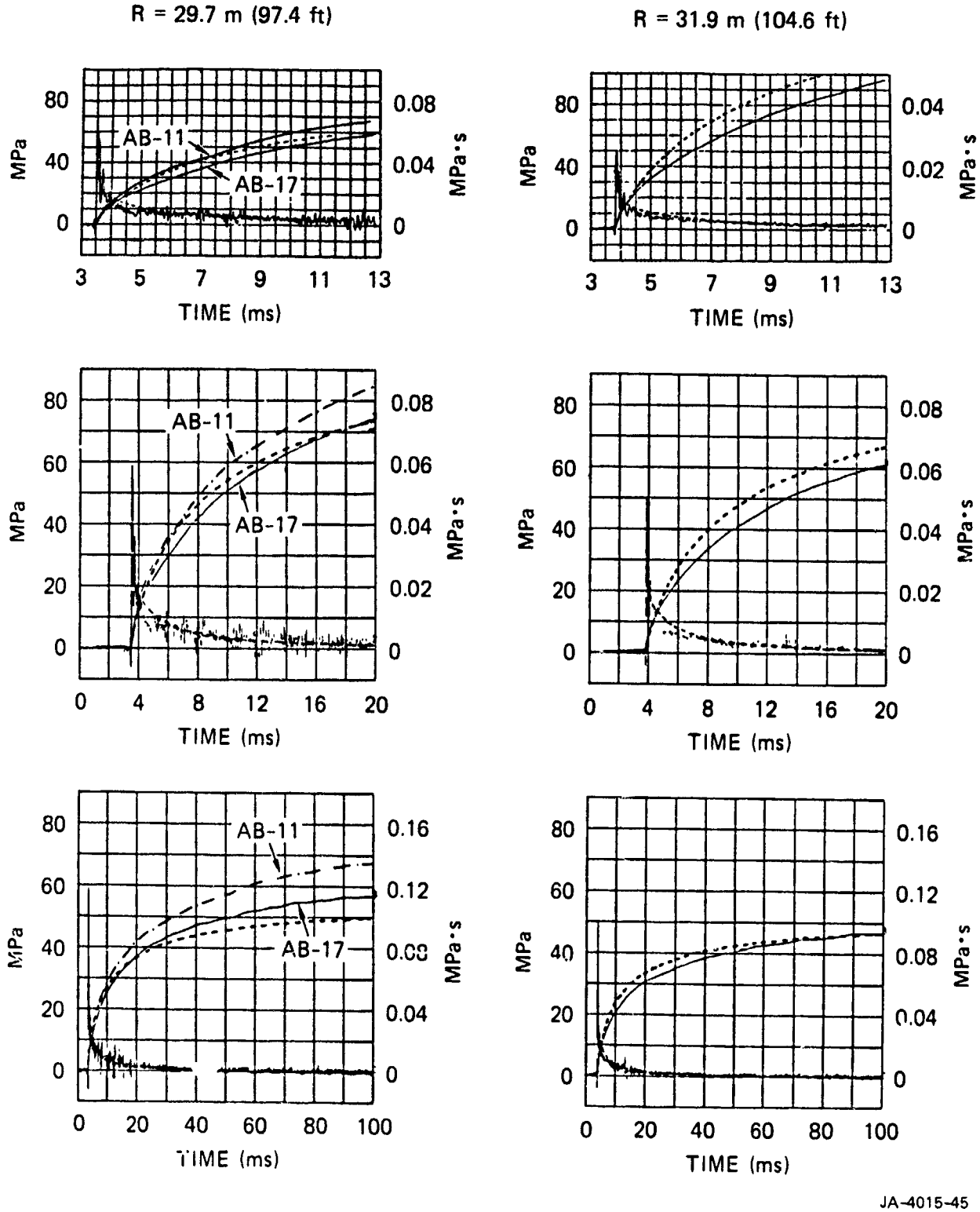

Figure 41. Airblast data from STP 3.5A experiment and simulation objectives (dashed lines). (Continued).

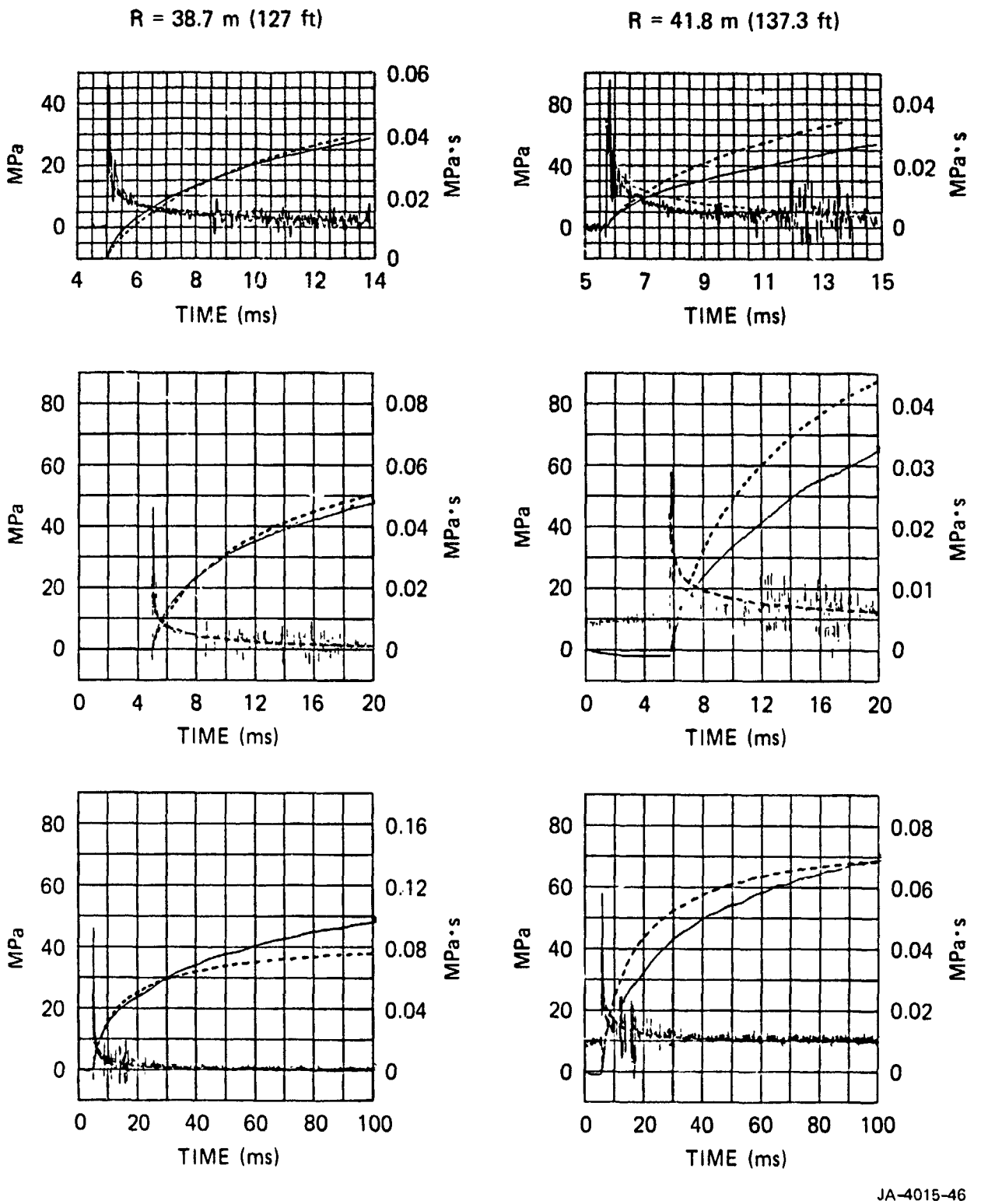

Figure 41. Airblast data from STP 3.5A experiment and simulation objectives (dashed lines). (Continued).

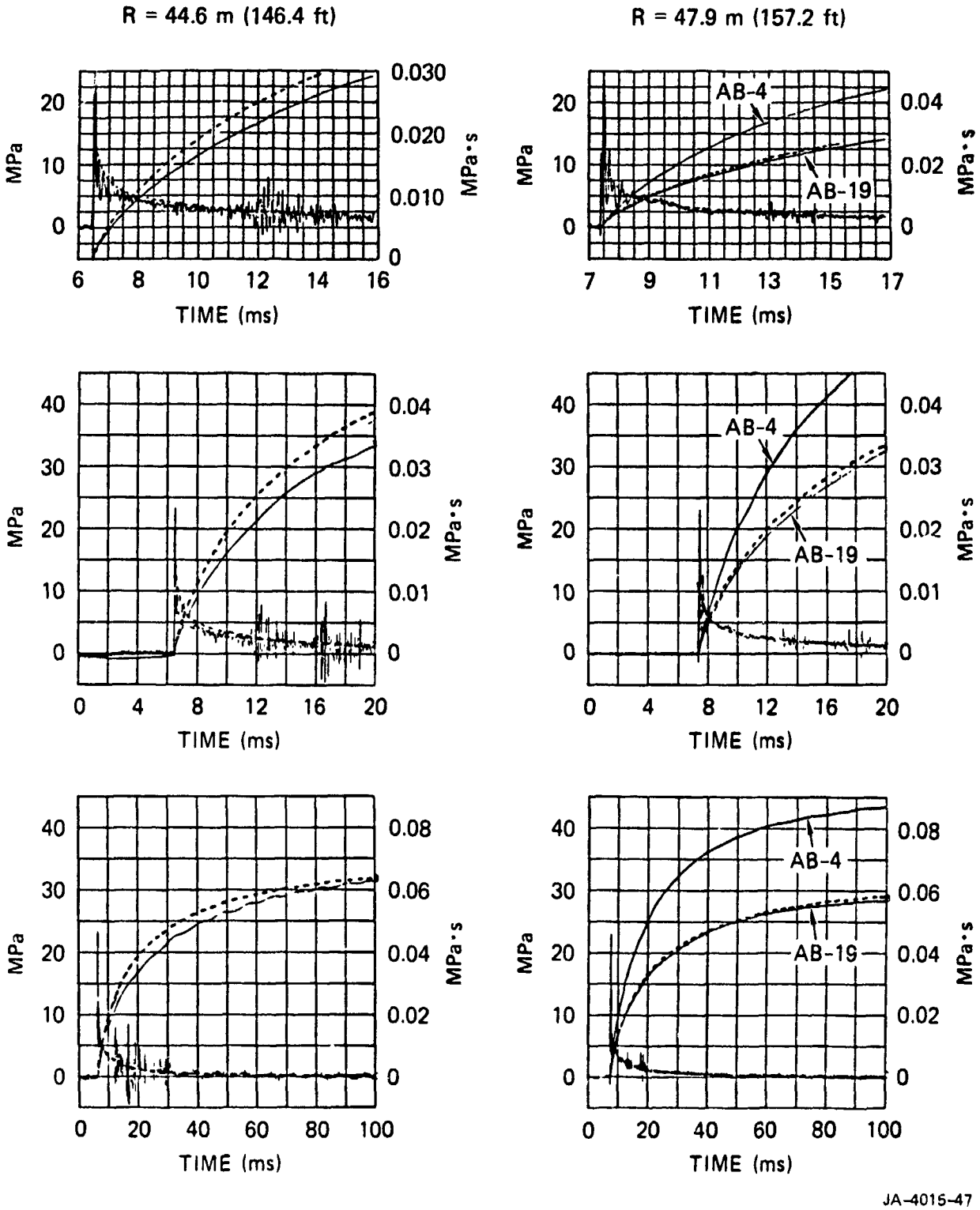

Figure 41. Airblast data from STP 3.5A experiment and simulation objectives (dashed lines). (Continued).

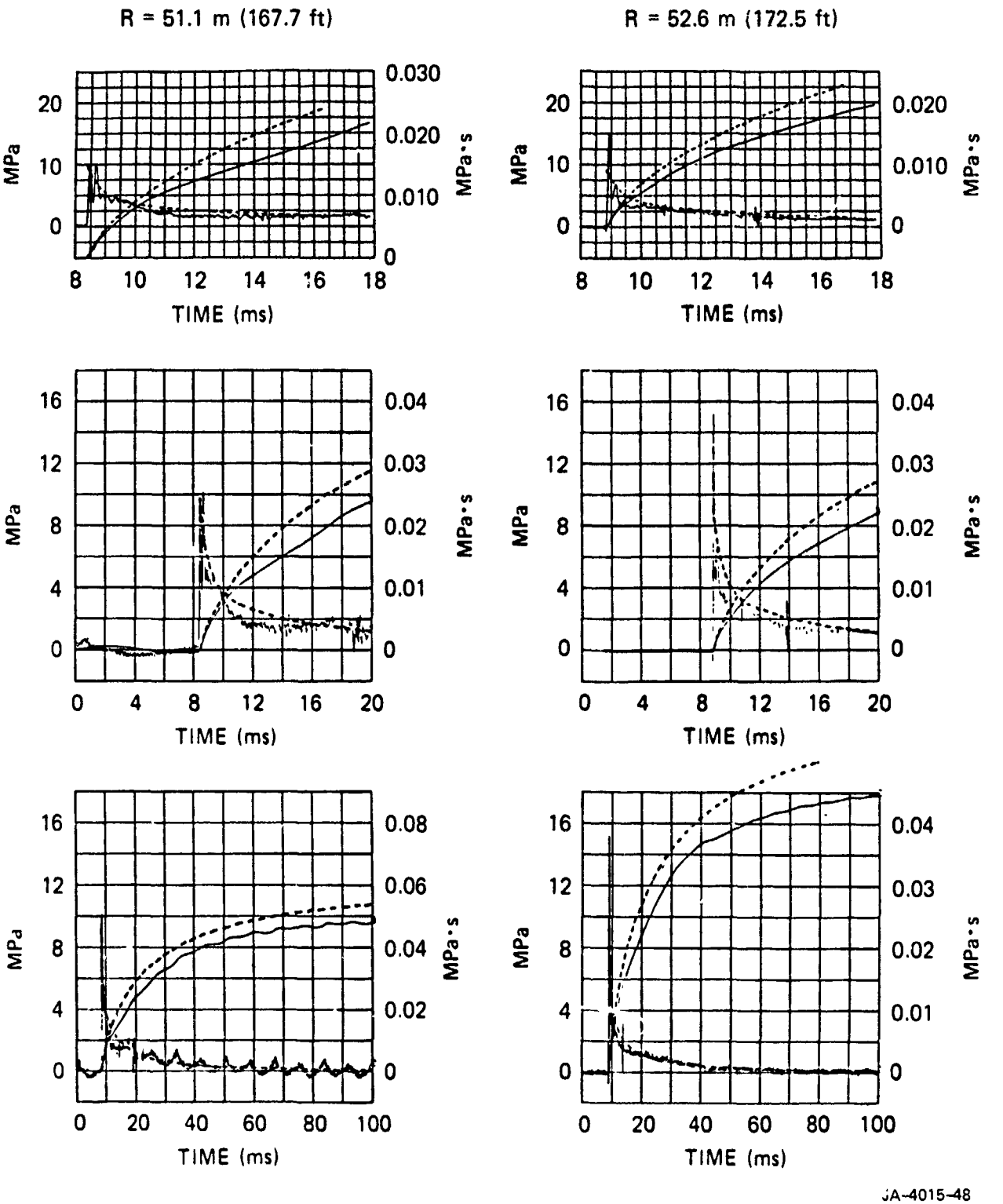

Figure 41. Airblast data from STP 3.5A experiment and simulation objectives (dashed lines). (Concluded).

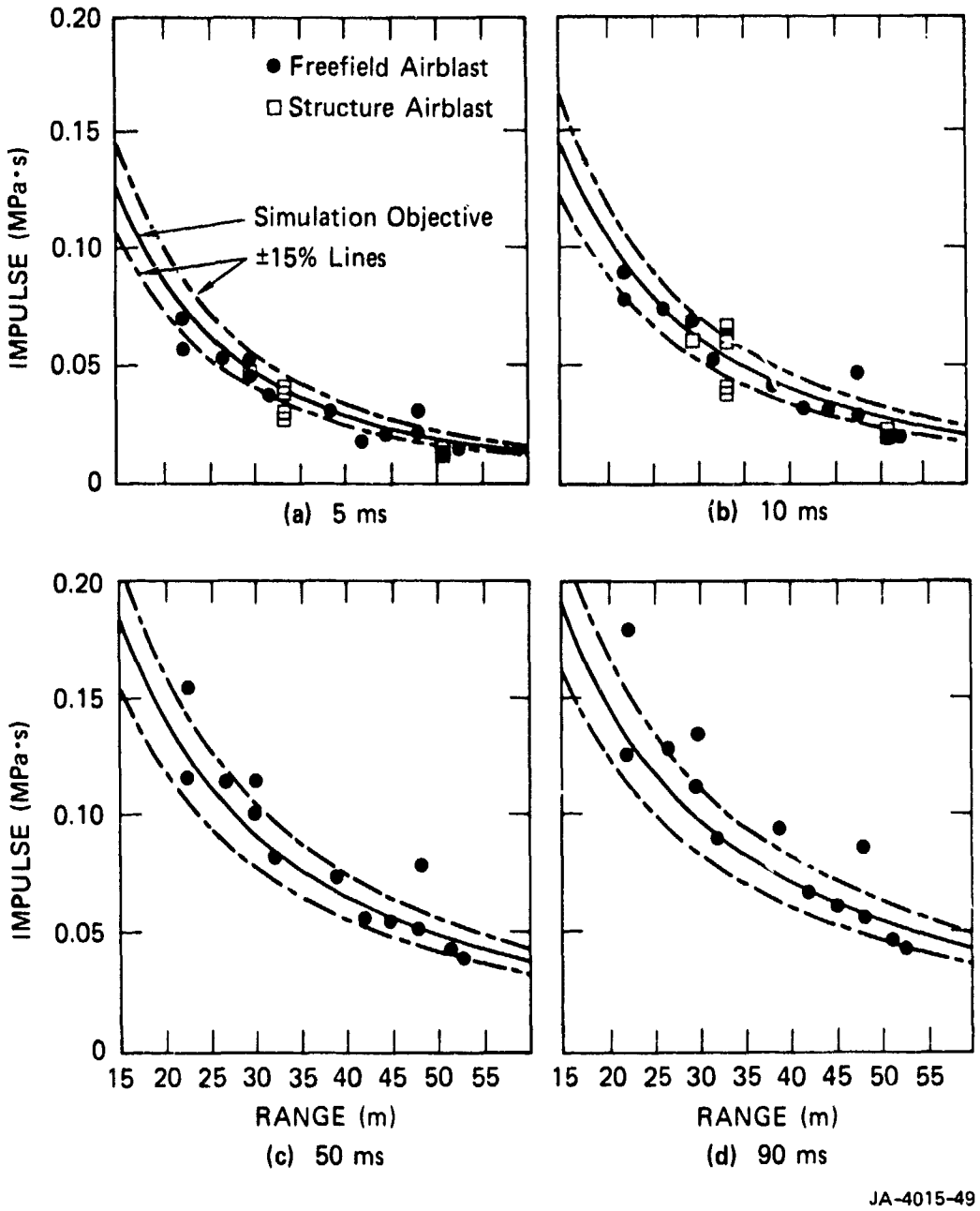

Figure 42. Impulse versus range from airblast gage measurements in STP 3.5A experiment and simulation objective at 5, 10, 50, and 90 ms after shock arrival time.

above and below the simulation objective shown as dashed lines. The data points are seen to mostly fall within the 15% band for each of the time windows, indicating satisfactory agreement with the simulation objective at all times and ranges.

5.3 DATA FROM NEAR-SURFACE STRESS GAGES

A similar conclusion is reached when the simulation objective is compared with the data obtained from the soil stress gages placed near the surface of the test bed. Figure 43 compares the simulation objective at the 28.4-m range and the impulses measured by all the horizontal and vertical stress gages that were fielded at this range to a depth of about 0.6 m (2 feet) below the test bed. Results from the airblast gages placed at the same ranges are also plotted for comparison. The horizontal and vertical stress measurements are virtually identical, indicating a state of hydrostatic loading of the soil. A good correlation of stress and airblast measurement is also found. Within the experimental errors, the measurements agree with the simulation objectives. Also, the impulse histories measured by gages 3-1 SV, 3-2 SV, and 3-3 SH under a primacord HEST are identical (to within the measurement errors) to those measured by gages 8-1 SV and 8-2 SV, which were placed under an equivalent Iremite HEST. This shows the consistency of the procedures used to design the HEST.

Figure 44 compares the measured impulses at 10 and 90 ms with the simulation objectives. Again, the data suggest a reasonable agreement with the simulation objective at all times and ranges. This conclusion also concurs with the data from the photopoles presented in Figure 45.

5.4 CONCLUSIONS ON THE SIMULATOR PERFORMANCE

The HEST simulator for the 3.5A event was designed to produce the overpressure environment from a 1.95-kt nuclear surface burst for the overpressure range of 500 MPa (5 kbar, 72,000 psi) to 7 MPa (1000 psi). Based on photopole, airblast, and near surface soil stress gage data, the impulse from the HEST agreed, to within measurement error, with the

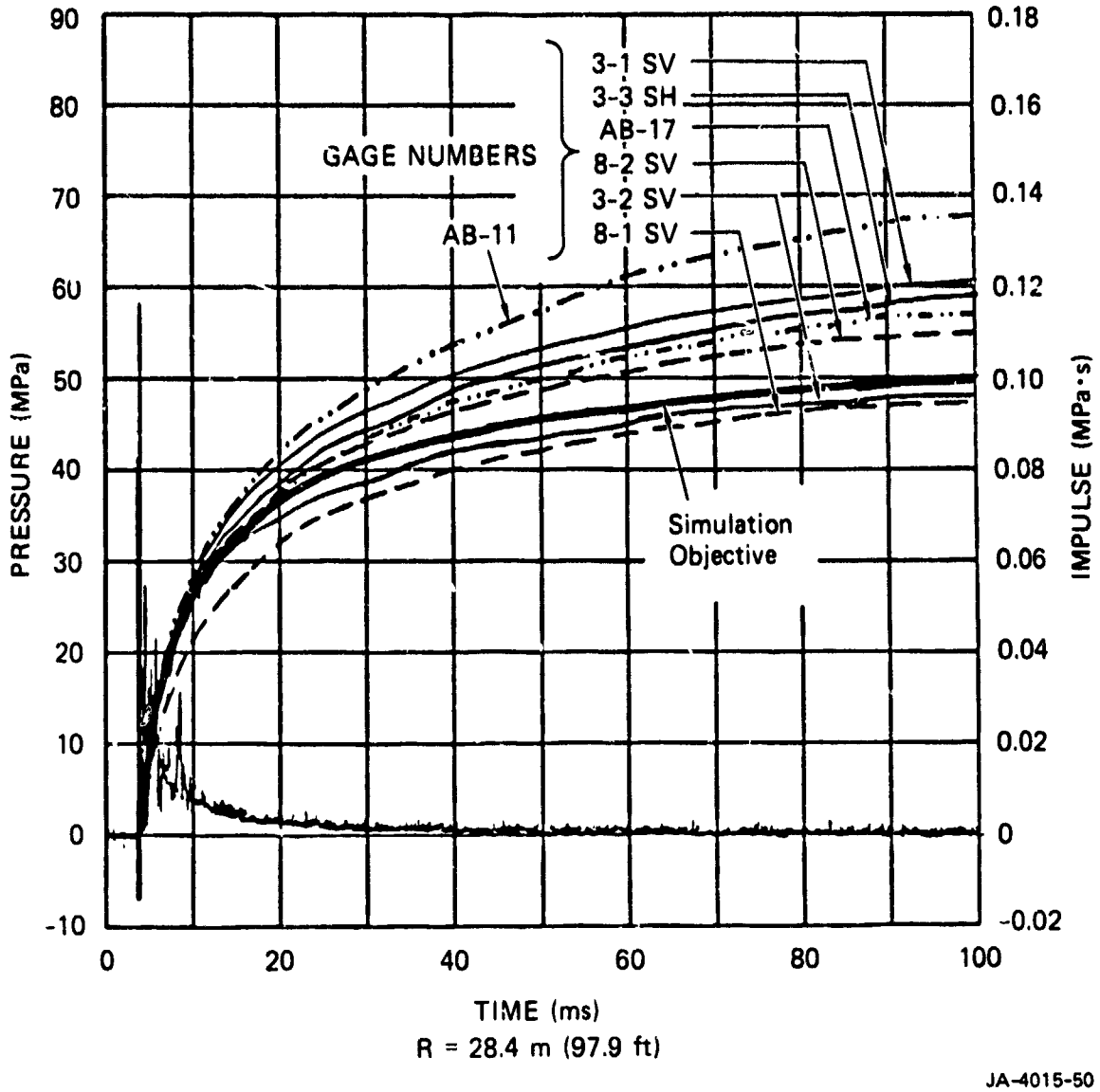

Figure 43. Simulation objective and airblast and near-surface soil stress gage measurements in STP 3.5A experiment. (Gages 3-1 SV, 3-2 SV, and 3-3 SH were located under primacord HEST, and gages 8-1 SV and 8-2 SV were under an equivalent Iremite HEST.)

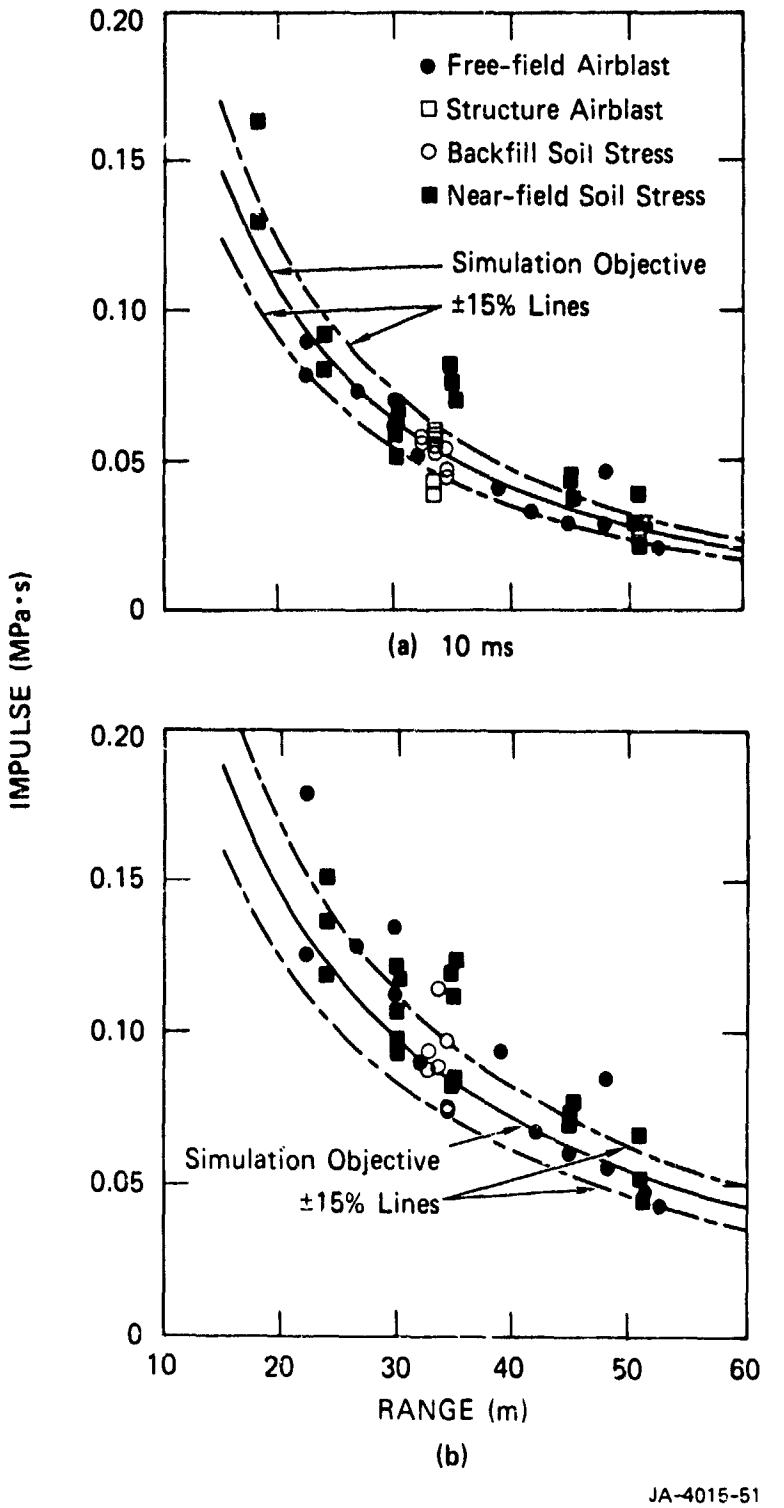

Figure 44. Simulation objective and impulse versus range from airblast and near-surface soil stress gage measurements in STP 3.5A experiment at 10 and 90 ms after shock arrival time.

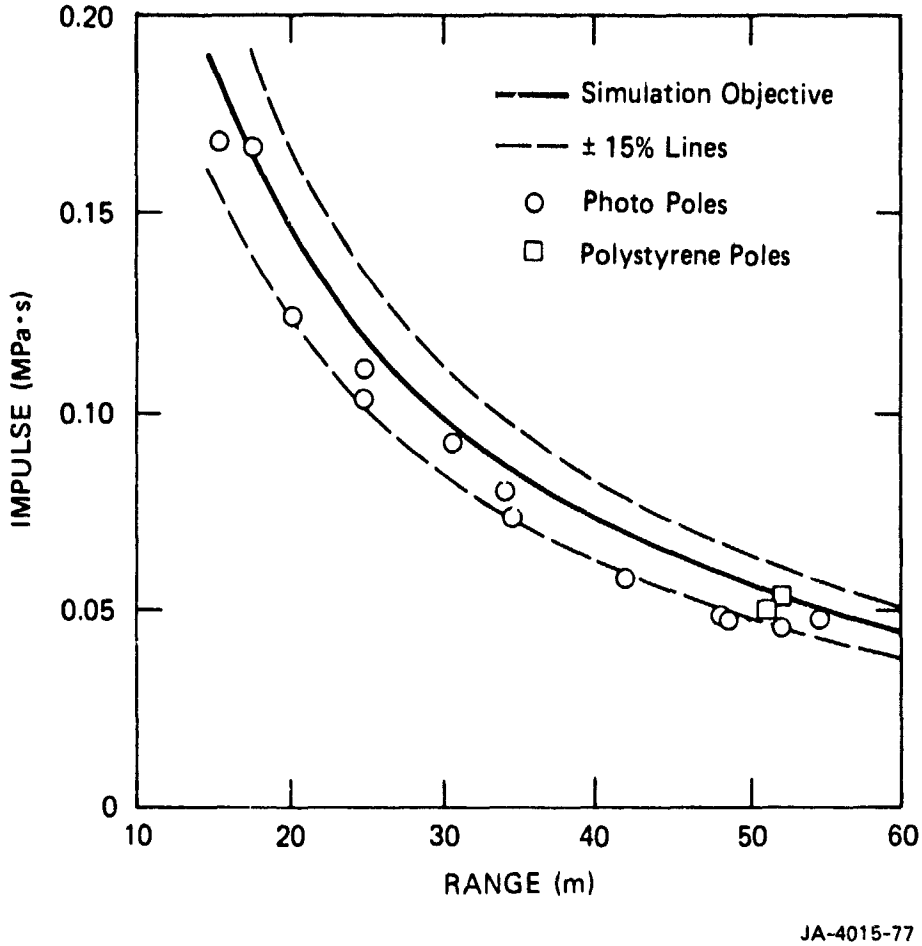

Figure 45. Photo pole total impulse versus range compared to simulation objectives at 90 ms.

design goals for both short (10-ms) and long (90-ms) times. Hence the full positive phase of a 1.95-kt surface burst was successfully simulated by the HEST.

The above conclusion also represents the concensus of the Simulation Working Group involved in the Silo Test Program.[6]

REFERENCES

1. L. Seaman and D. R. Curran, "SRI PUFF 8 Computer Program for One-Dimensional Stress Wave Propagation," SRI International Final Report on DNA Contract No. DAAK11-77-C-0083 (August 1978).

2. T. Cooper, "A Computer Code for Numerical Simulation of Shock Waves in Fluids and Solids," SVEDEFO Report No. DS 1980:16 (December 1980).

3. M. Cowperthwaite and W. H. Zwisler, "TIGER Program Documentation," SRI Publication No. 2106 (January 1973).

4. E. L. Lee, H. C. Hornig, and J. W. Kury, "Adiabatic Expansion of High Explosive Detonation Products," Lawrence Livermore National Laboratory, Livermore, CA, UCRL-50422 (1968).

5. R. J. Port, "STP HEST/BLEST Quick Look Report," R&D Associates, Marina Del Rey, CA (4 October 1982).

6. Waterways Experiment Station, "Quick Look Report on Silo Test Program 3.5A Event, Volume I: The Test Environment" (March 1983).

7. J. R. Bruce and H. E. Lindberg, "Interpretation of Airblast Simulation Tests," SRI International Final Report on DNA Contract No. DNA001-80-C-0059 (January 1982).

8. Don Simmons, "Draft Report on Pressure-Yield Estimation Techniques," R&D Associates, Marina Del Rey, CA (January 1984).

9. J. Shinn, ARA, private communication.

Appendix

CHARACTERIZATION OF HEST EXPLOSIVE CHARGE IN HIGH-PRESSURE CYLINDRICAL CALIBRATOR (HPC^2)

INTRODUCTION

To evaluate and characterize the performance of various explosives in HEST experiments, we designed and constructed a high-pressure (up to 500 MPa) expanding explosives chamber. Explosives to be tested are placed inside a thick-walled steel cylinder, and a piston is inserted from each end to confine the explosive products after detonation. The displacement histories of the pistons are measured either photographically or by time-of-arrival (TOA) pins. The initial explosion pressure is then inferred from one-dimensional calculations that match the piston displacement.

We used the above facility, designated as HPC^2 (for high-pressure cylindrical calibrator), to determine the relationship between the charge density and the effective explosion pressure of a primacord charge as used in the STP 3.5A experiments. In particular, we investigated the apparent lack of performance of a HEST charge due to the penetration of the explosive products into the soil pores.

EXPERIMENTAL SETUP

Figure A.1 shows an overview of the HPC^2 facility with typical dimensions shown in Figure A.2. The pistons and cylinders were constructed from high-strength stainless steel. Figure A.3 shows a set of four quartz TOA pins used to measure the piston displacement and Figure A.4 shows a typical oscilloscope trace from the TOA pins. The piston arrival is indicated by a sharp drop in the signal to about -40 volts.

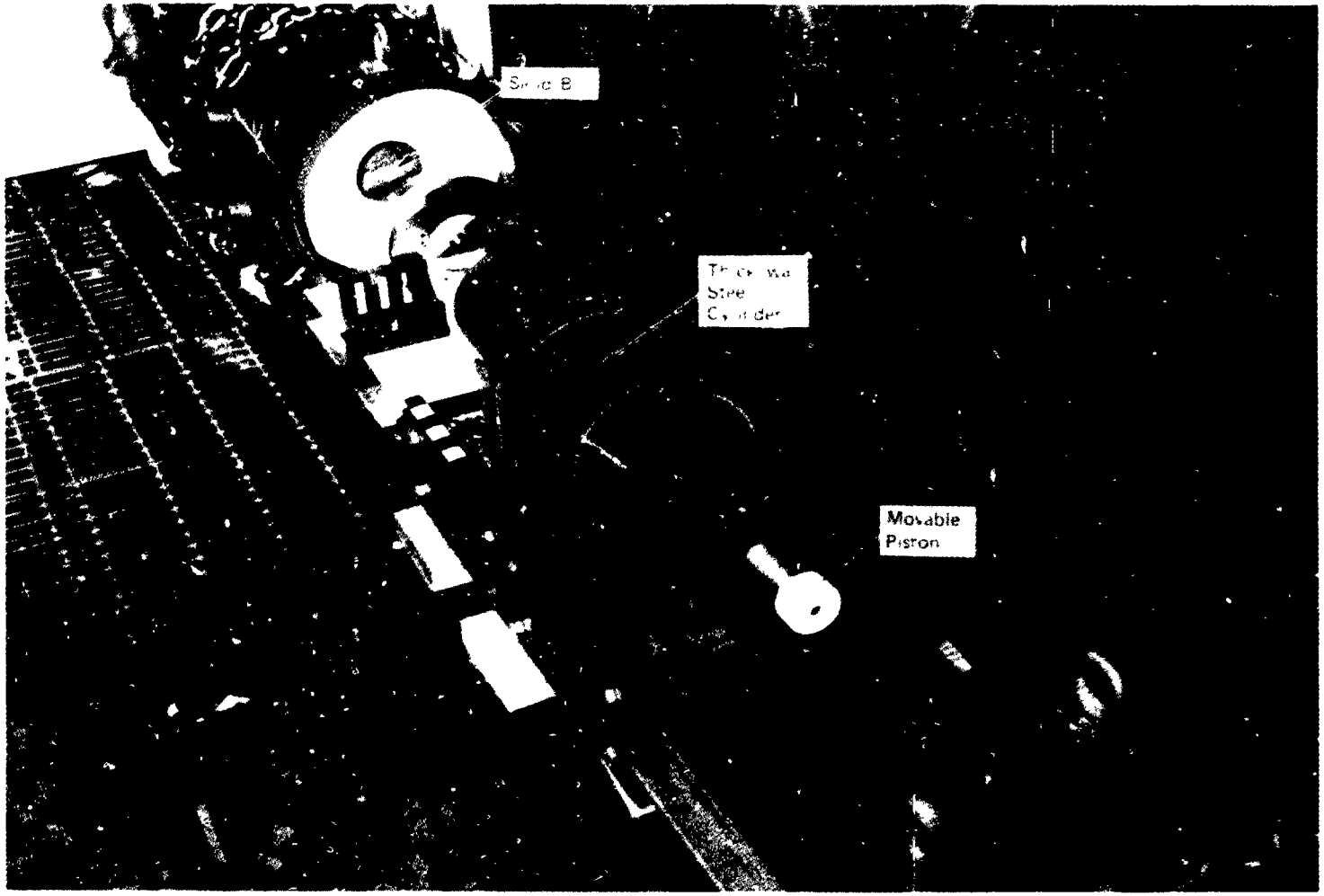

JP-4015-52

Figure A.1 An overview of the SRI high-pressure cylindrical calibrator (HPC^2).

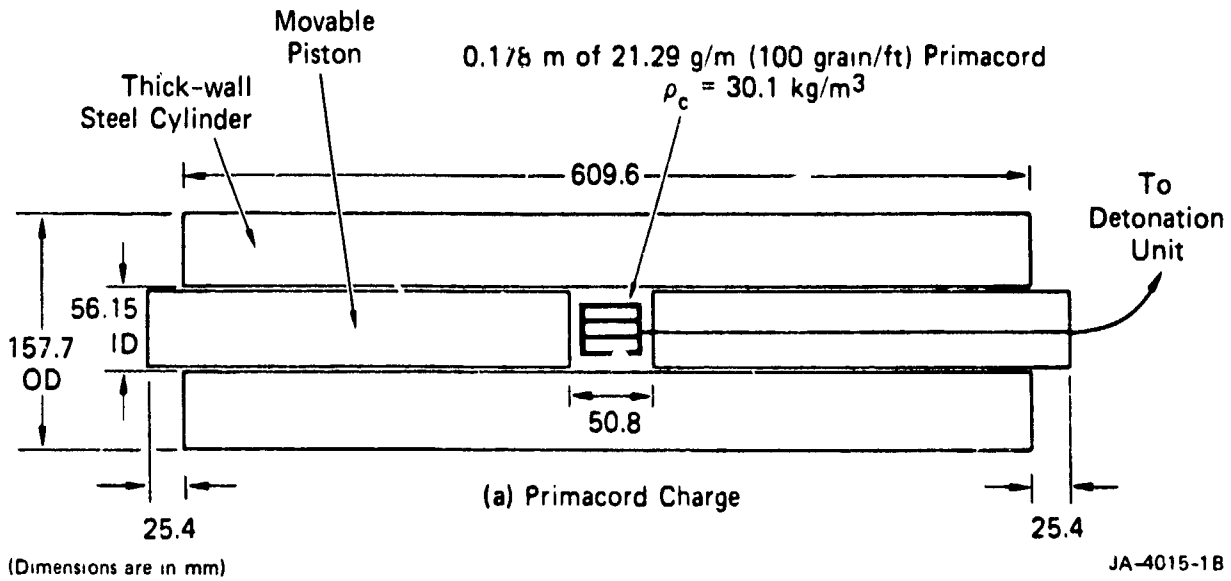

Figure A.2. Schematic of high-pressure cylindrical calibrator (HPC^2).

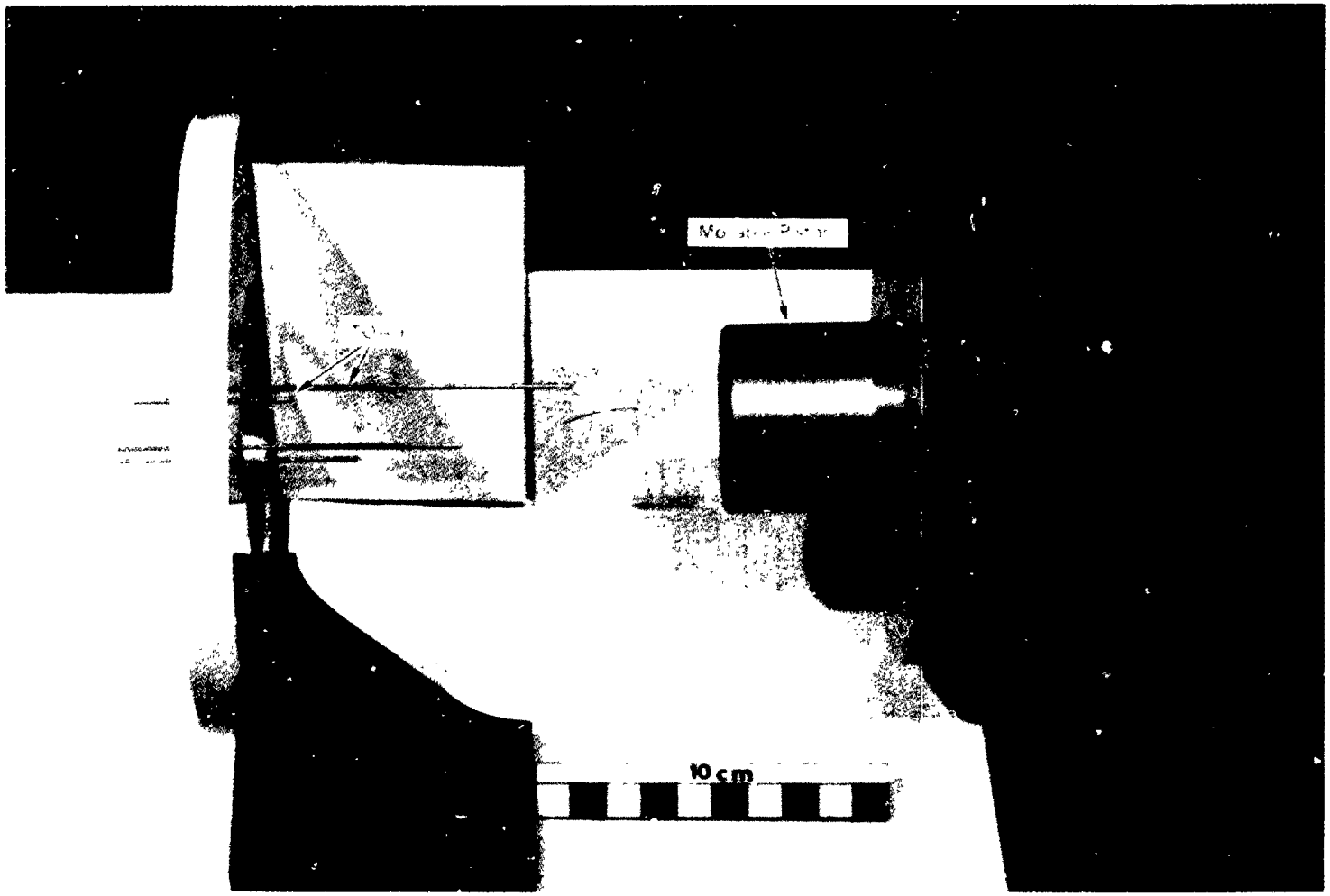

JP-4015-53

Figure A.3. Time-of-arrival pins used to measure the displacement history of the movable piston in the HPC^2 facility.

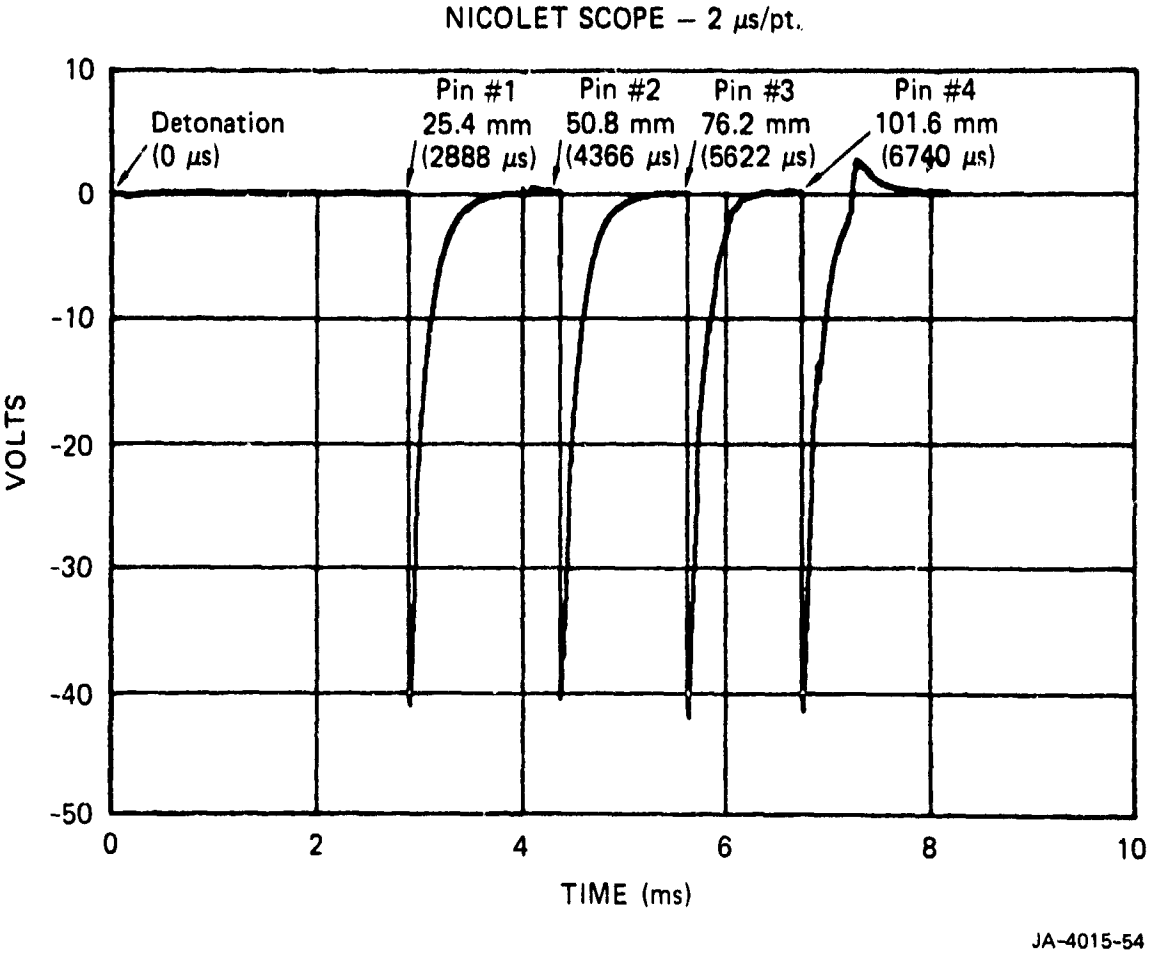

Figure A.4. Typical oscilloscope trace from a set of four TOA pins.

BACKGROUND CALCULATIONS

We used the SRI PUFF hydrocode to calculate the cavity pressure and piston displacement time histories for the setup shown in Figure A.1. Because PUFF is a one-dimensional Lagrangian hydrocode, the effects of mixing of the explosive products or leakage from the explosive chamber are not included in these calculations.

Figure A.5 shows the calculated cavity pressure as a function of time for five explosion pressures ranging from 14 to 30 MPa. The cavity length is 50.8 mm and the piston length is 304.8 mm (Figure A.2). The pressure waveforms have rounded peaks because of the piston inertia. The peaks become sharper with increasing explosion pressures.

The piston displacements calculated for the same five explosion pressures are shown in Figure A.6. The same results are shown on a log-log plot in Figure A.7. The displacement-time histories on the log-log plot form nearly a straight line with a slope of about 2. These plots facilitate the match with the piston arrival times measured in the experiments and were used to estimate the effective explosion pressures of each charge.

The explosive products in the present calculations are treated as a perfect gas. Figure A.8 shows a log-log plot of the cavity pressure (normalized with respect to the initial pressure) as a function of the cavity volume (normalized with respect to the initial cavity volume) for two values of the specific heat ratios of $\gamma = 1.1$ and $\gamma = 1.2$. The pressure-volume relationships are found to be straight lines with slopes very nearly equal to the γ initially specified in the calculations. This indicates that the explosive products expand isentropically for the pressure ranges considered (below 40 MPa).

The sensitivity of the calculated piston displacement to the choice of γ is shown in Figure A.9 by plotting piston displacements for the same two cases of $\gamma = 1.1$ and $\gamma = 1.2$. The two curves are virtually identical, although the pressure that drives the piston is proportional to $\gamma - 1$, and $\gamma - 1$ changes by a factor of two (from 0.1 to 0.2) in the

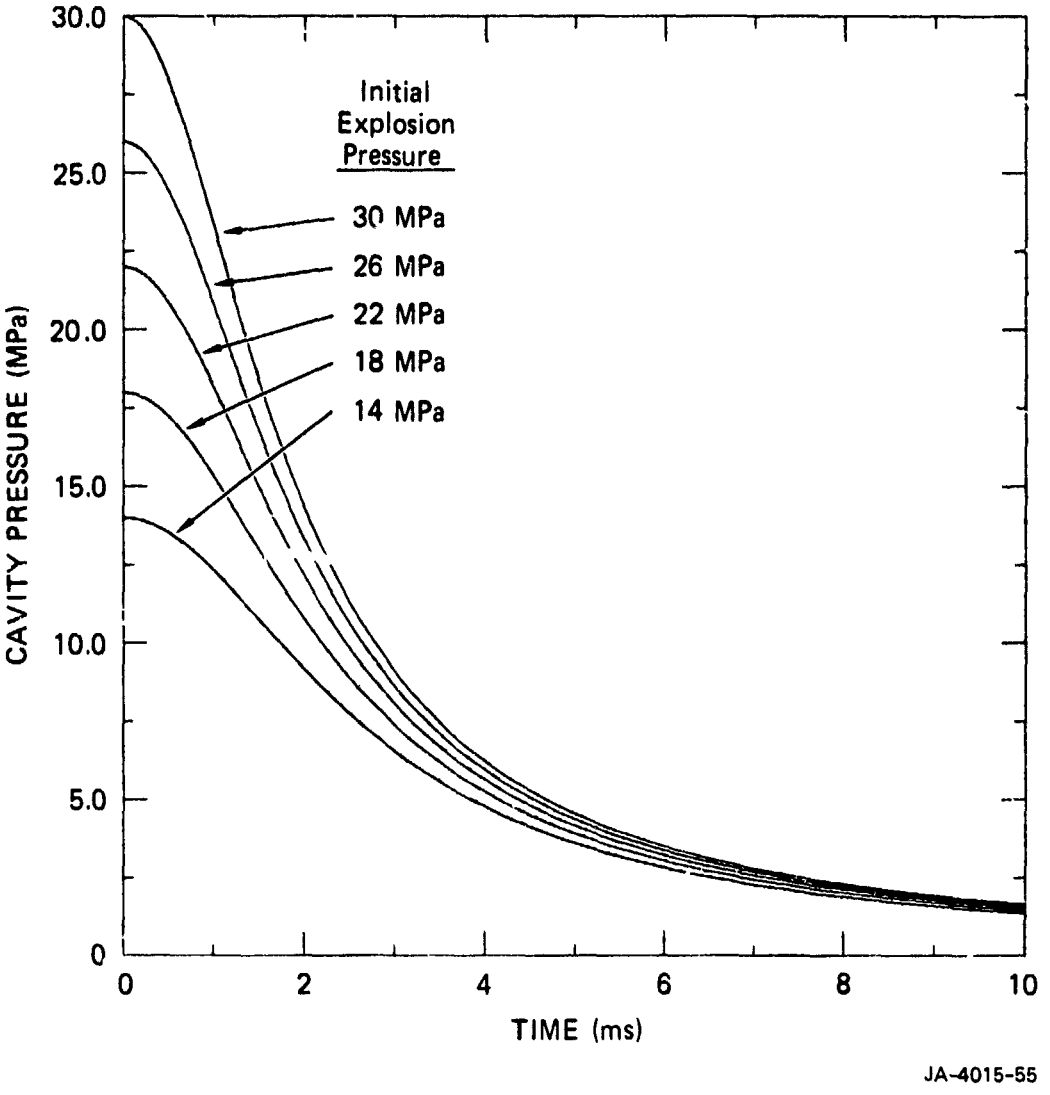

Figure A.5. Cavity pressure history for five initial explosion pressures.

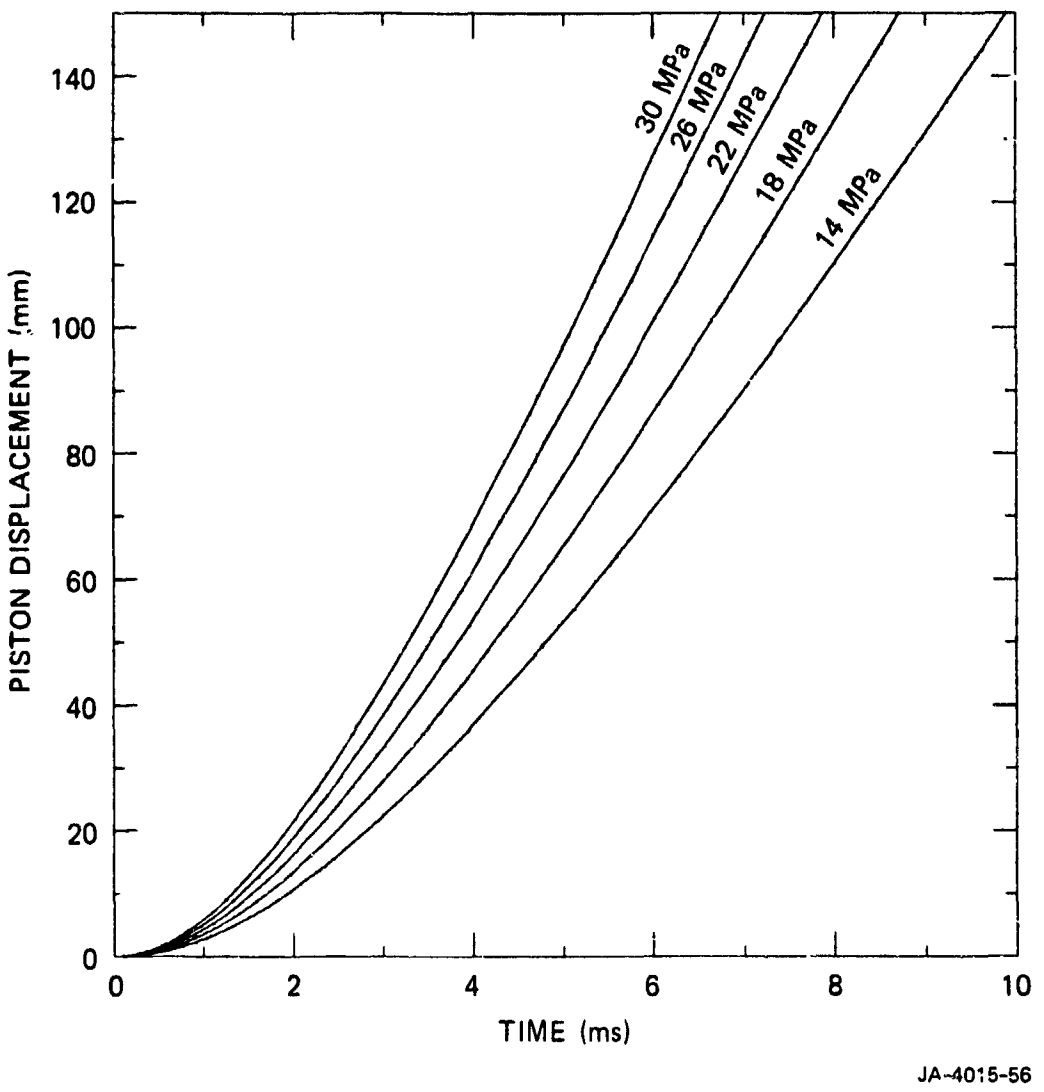

Figure A.6. Piston displacement history for five initial explosion pressures.

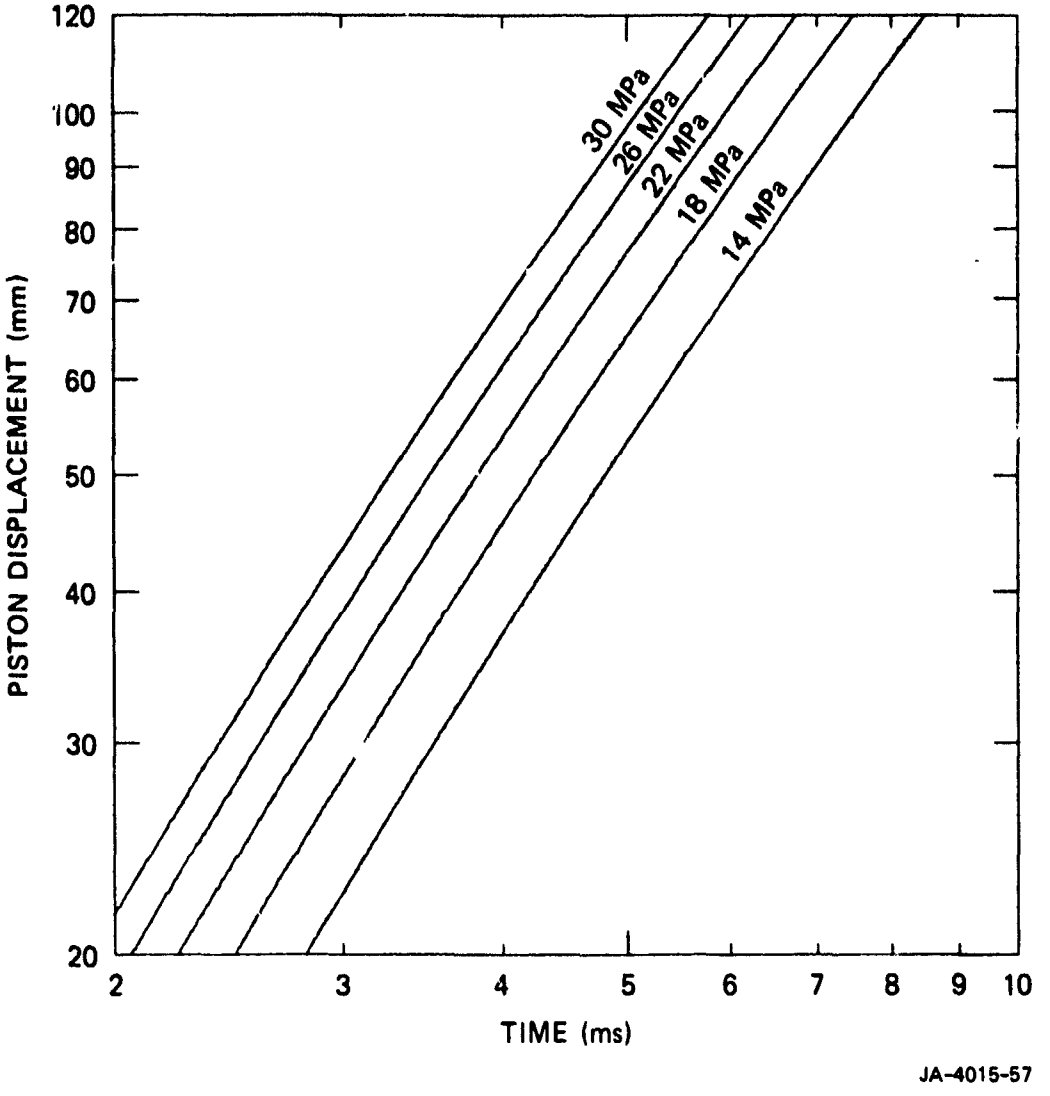

Figure A.7. Piston displacement history for five initial explosion pressures (log-log plot).

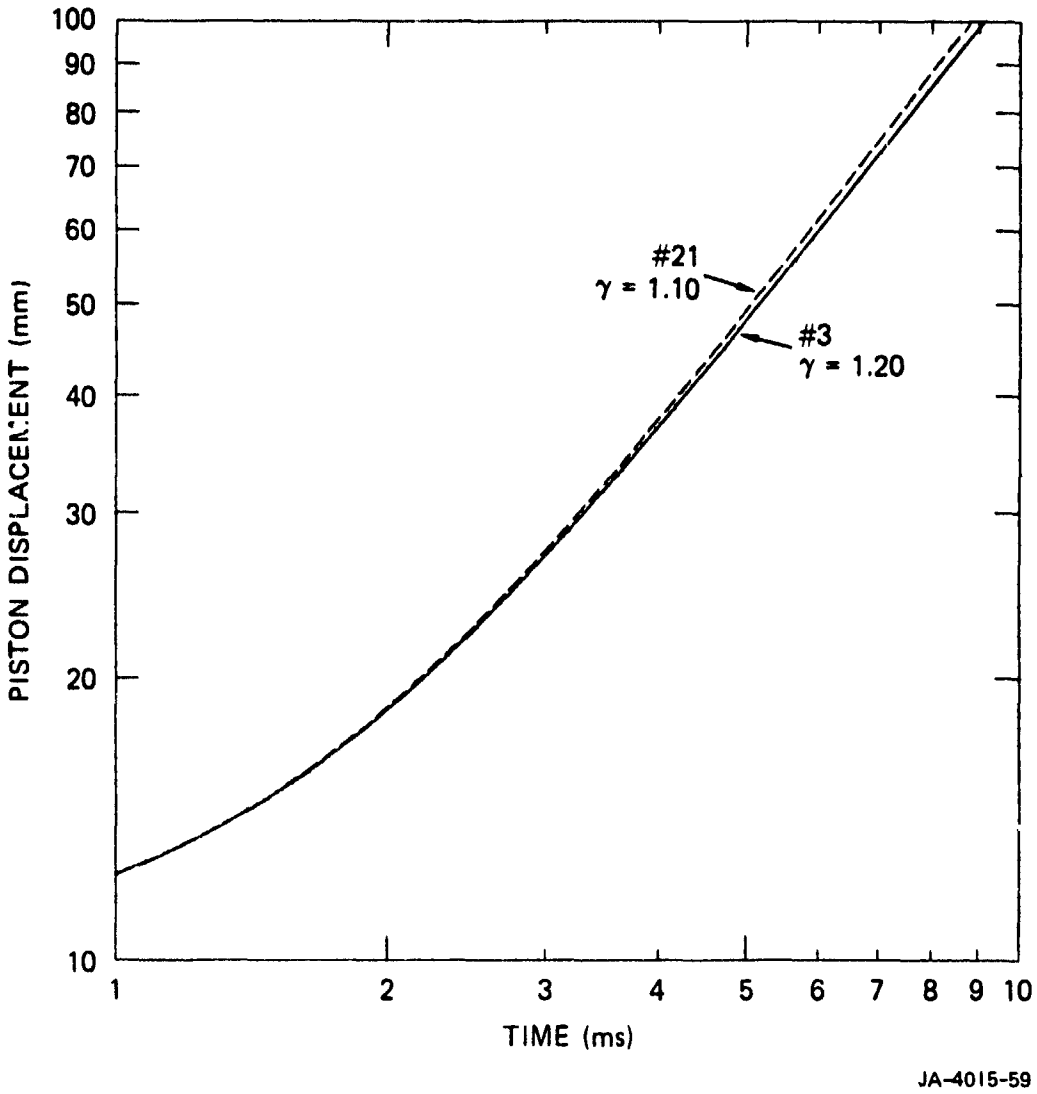

Figure A.9. Piston displacement histories for two values of the specific heat ratio, γ.

two calculations. This indicates that the explosion pressure estimated on the basis of the piston-displacement is not sensitive to the choice of γ used in the PUFF calculations.

EXPERIMENTAL RESULTS

We used the HPC^2 facility to investigate the effect of various field parameters on the HEST performance. Figure A.10 shows the schematics of the experiments performed to determine the effective explosion pressure from (a) primacord charge in an air cavity, (b) primacord charge in a foam cavity, (c) primacord charge next to a sand column, and (d) primacord charge next to a capped sand column. The experiment with the sand column was performed with both wet and dry sands.

Figure A.11 shows the piston displacement histories measured for the configurations shown in Figure A.10. The explosion pressures required in the PUFF calculations to match the measured displacement histories were found to range from a maximum of 28.5 MPa for the primacord charge in an air cavity [configuration (a) in Figure A.10] to a minimum of 18 MPa for the primacord charge next to a dry sand column [configuration (c) in Figure A.10].

Figure A.12 compares the maximum and minimum explosion pressure measured in the present experiments with the explosion pressure/charge density relationship used for the design of the STP 3.5A experiment (Figure 39). The present data roughly span the results of the TIGER calculations and the fit to HEST experiments. This comparison suggests that the field parameters in HEST experiments are responsible for the discrepancy observed between the expected explosion pressure (from TIGER calculation and C^2 experiments) and the effective explosion pressure inferred from the calibration experiments.

CONCLUSIONS

The data presented here indicate that the performance of a HEST charge (represented by its effective explosion pressure) depends not

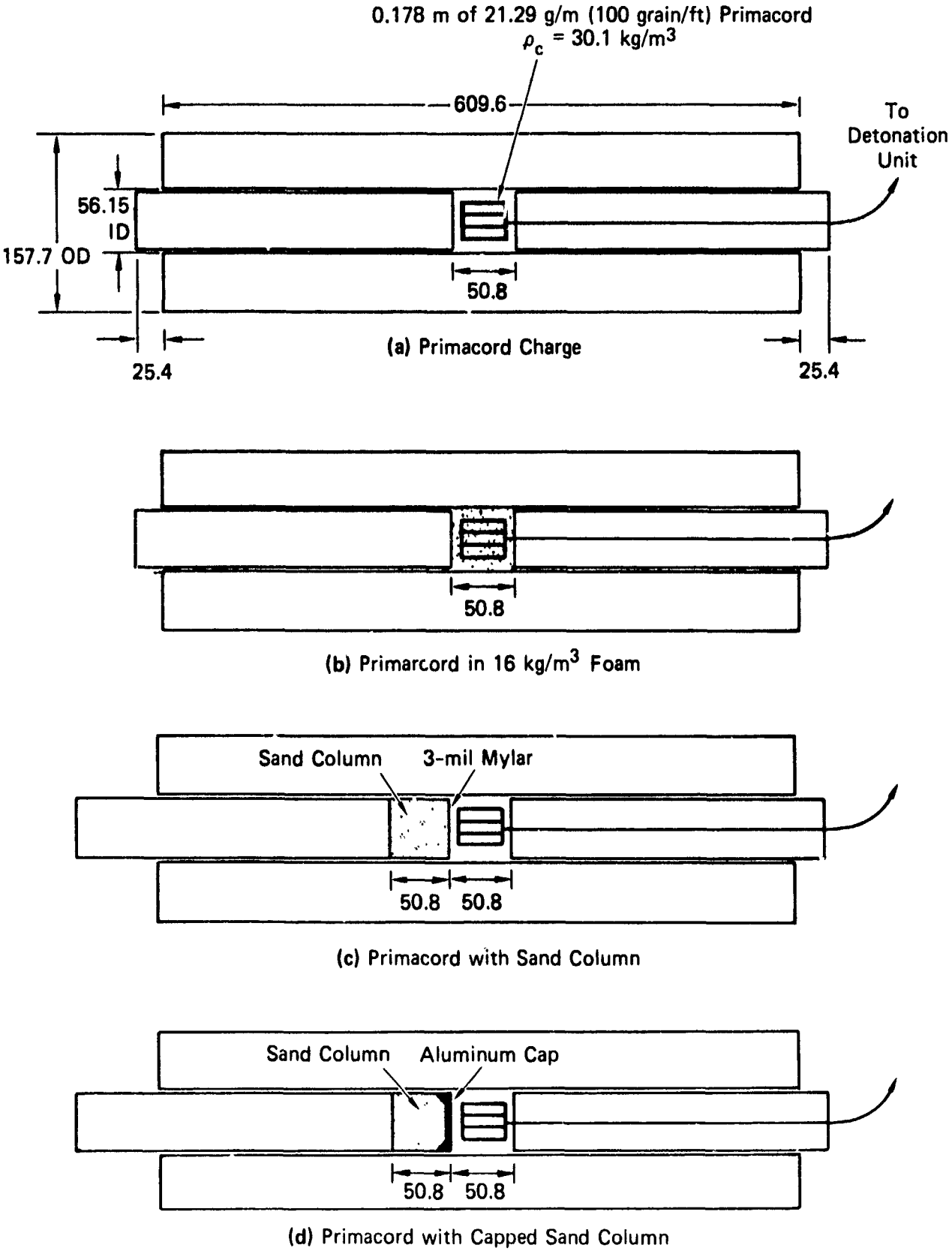

Figure A.10. Schematic of charge calibration experiments.

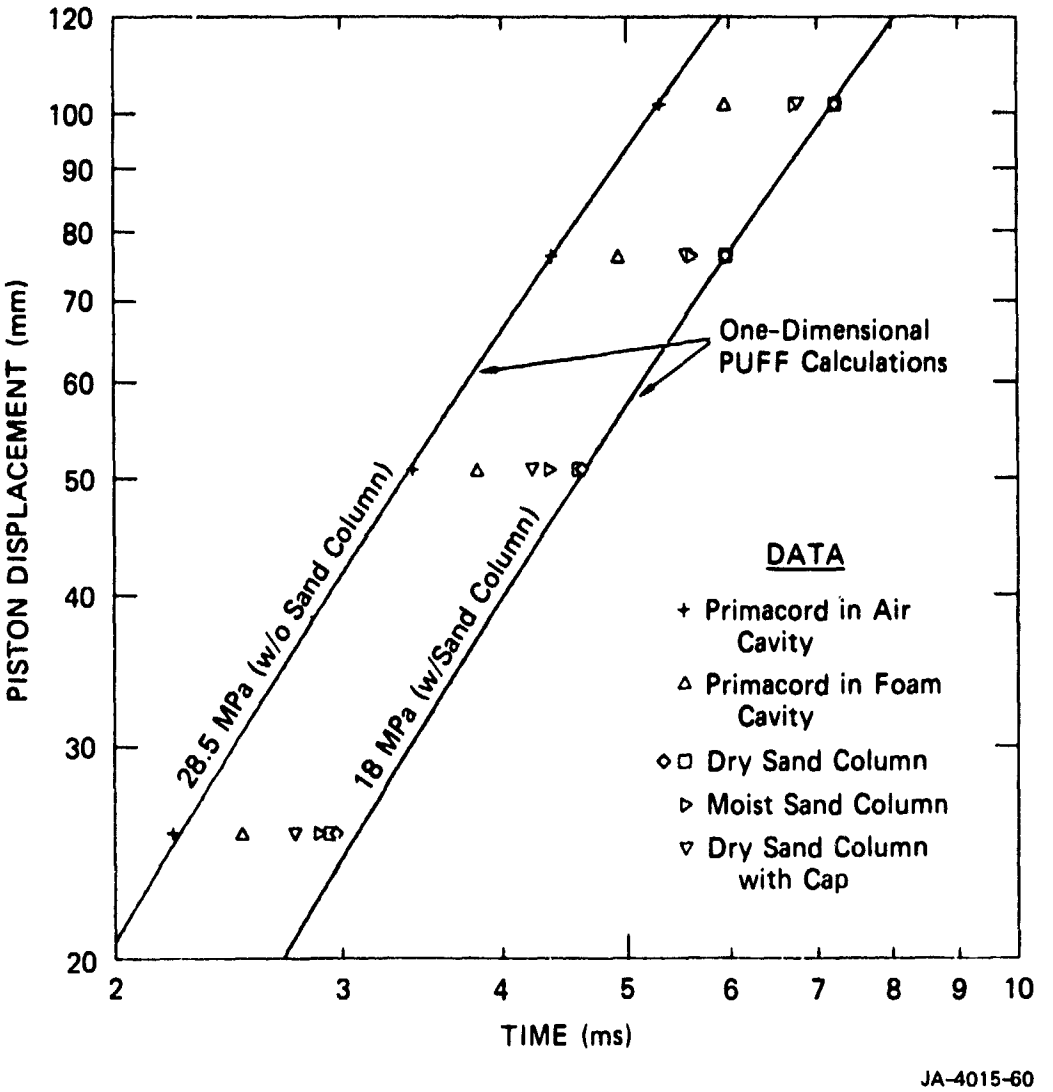

Figure A.11. Piston displacement histories measured in HPC[2] experiments.

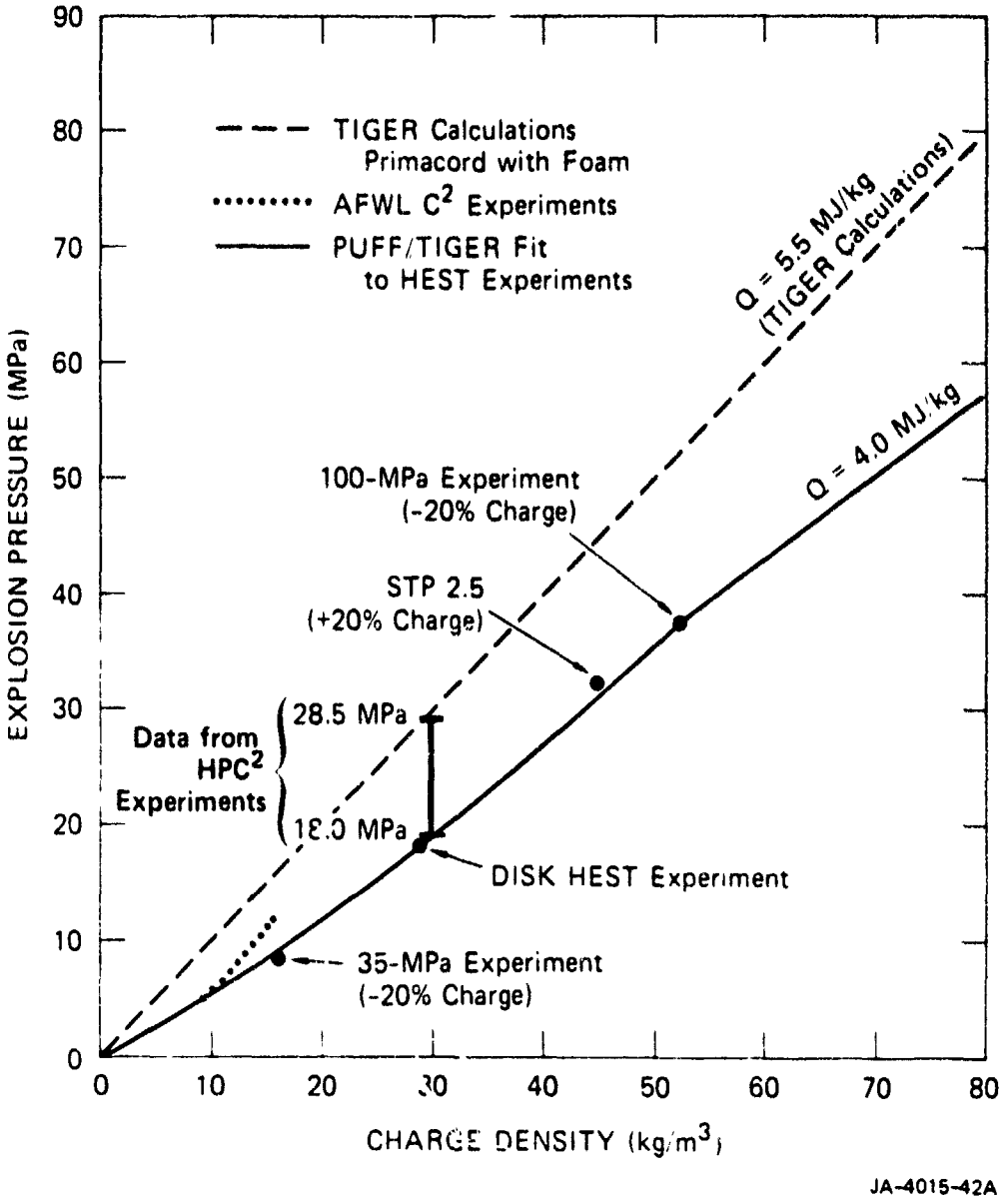

Figure A.12. Data from HPC^2 experiments compared with TIGER calculations and the fit to HEST calibration experiments.

only on the charge density but also on other field parameters such as the presence of foam in the cavity or penetration and mixing of the explosive products with the soil surrounding. We can also infer that the data obtained from conventional C^2 experiments or TIGER calculations provide only an upper bound to the performance of a HEST charge because they do not account for the field parameters mentioned above.

The results further indicate the necessity of HEST calibration experiments, such as the DISK HEST, or C^2 experiments similar to those discussed here so that the charge performance data used to validate and adjust the HEST design calculations are obtained under realistic field conditions.

DISTRIBUTION LIST

DEPARTMENT OF DEFENSE

Assist to the Sec of Def, Atomic Energy
ATTN: Exec Assist

Defense Intell Agcy
ATTN: DB-4C
ATTN: DT-1C
ATTN: DT-2
ATTN: RTS-2B

Defense Nuclear Agency
ATTN: SPTD
2 cys ATTN: SPSS
4 cys ATTN: STTI-CA

Defense Tech Info Ctr
12 cys ATTN: DD

Dept of Def Explo Safety Bd
ATTN: Chairman

Field Command, DNA, Det 2
Lawrence Livermore National Lab
ATTN: FC-1

Field Command, Defense Nuclear Agency
ATTN: FCPR
ATTN: FCT
ATTN: FCTT
ATTN: FCTT, W. Summa
ATTN: FCTXE

Field Command, Test Directorate
ATTN: FCTC

Joint Strat Tgt Planning Staff
ATTN: JLAA
ATTN: JPST

Under Secy of Def for Rsch & Engrg
ATTN: Strat & Space Sys (OS)

DEPARTMENT OF THE ARMY

Harry Diamond Laboratories
ATTN: DELHD-NW-P
ATTN: 00100 Commander/Tech Dir/Div Dir

US Army Ballistic Rsch Lab
ATTN: AMXBR-TBD, W. Taylor
ATTN: DRDAR-BLA-S, Tech Lib
ATTN: DRDAR-BLT, J. Keefer

US Army Concepts Analysis Agcy
ATTN: CSSA-ADL, Tech Lib

US Army Corps of Engineers
ATTN: DAEN-ECE-T
ATTN: DAEN-RDL

US Army Engr Waterways Exper Station
ATTN: B. Welch
ATTN: Library
ATTN: WESSD, J. Jackson

US Army Material & Mechanics Rsch Ctr
ATTN: Tech Lib

DEPARTMENT OF THE ARMY (Continued)

US Army Material Command
ATTN: DRXAM-TL, Tech Lib

US Army Mobility Equip R&D Cmd
ATTN: DRDME-WC, Tech Lib

US Army Nuc & Chem Agcy
ATTN: Library
ATTN: MONA-WPS, J. Kelley

USA Missile Command
ATTN: Doc Sect

DEPARTMENT OF THE NAVY

David Taylor Naval Ship R&D Ctr
ATTN: Code 17
ATTN: Code 1770
ATTN: Code 1844
ATTN: Tech Info Ctr, Code 522.1
2 cys ATTN: Code 1740.5, B. Whang

Naval Facs Engrg Cmd
ATTN: Code 04B

Naval Rsch Lab
ATTN: Code 2627, Tech Lib

Naval Sea Systems Cmd
ATTN: SEA-0351
ATTN: SEA-08
ATTN: SEA-09G53, Lib

Naval Surface Wpns Ctr
ATTN: Code F31
ATTN: Code R14
ATTN: Code R15
ATTN: Code R40, I. Blatstein

Naval Surface Wpns Ctr
ATTN: Tech Lib & Info Svcs Br

Ofc of the Dep Ch of Naval Ops
ATTN: NOP 03EG
ATTN: NOP 981

Office of Naval Rsch
ATTN: Code 474, N. Perrone

Space & Naval Warfare Systems Command
ATTN: PME 117-21

Strat Sys Prog
ATTN: NSP-272
ATTN: NSP-43, Tech Lib

DEPARTMENT OF THE AIR FORCE

Air Force
ATTN: Int

Air Force Geophysics Lab
ATTN: LWH, H. Ossing

DEPARTMENT OF THE AIR FORCE (Continued)

Air Force Institute of Tech
ATTN: Library

Air Force Systems Command
ATTN: DLW

Air Force Weapons Lab
ATTN: NTE, M. Plamondon
ATTN: NTED, E. Seusy
ATTN: NTEO
ATTN: NTES
ATTN: SUL

Air University Library
ATTN: AUL-LSE

Ballistic Missile Office/DAA
ATTN: ENBF, D. Gage
ATTN: PP
2 cys ATTN: ENSN

Dep Ch of Staff, Rsch, Dev & Acq
ATTN: AF/RDQI

Strategic Air Command
ATTN: DOTP
ATTN: NRI/STINFO

DEPARTMENT OF ENERGY

Department of Energy
Albuq Opns Ofc
ATTN: CTID
ATTN: D. Richmond

Department of Energy
Ofc of Mil Application, GTN
ATTN: OMA/RD&T

Department of Energy
Nevada Opns Ofc
ATTN: Doc Con for Tech Lib

OTHER GOVERNMENT AGENCY

Central Intell Agency
ATTN: OSWR/NED

NATO

NATO School, SHAPE
ATTN: US Documents Officer

DEPARTMENT OF ENERGY CONTRACTORS

University of California
Lawrence Livermore National Lab
ATTN: Tech Info Dept Library

Los Alamos National Lab
ATTN: MS P364, Reports Lib

Sandia National Labs
ATTN: Lib & Sec Class Div

Sandia National Labs
ATTN: Tech Lib, 3141

DEPARTMENT OF DEFENSE CONTRACTORS

Aerospace Corp
ATTN: Lib Acq, M1/199

Applied Rsch Assoc, Inc
ATTN: N. Higgins

Applied Rsch Assoc, Inc
ATTN: J. Shinn

Applied Rsch Assoc, Inc
ATTN: D. Piepenburg

Applied Rsch Assoc, Inc
ATTN: R. Frank

BDM Corp
ATTN: Corp Lib
ATTN: T. Neighbors

Boeing Co
ATTN: Aerospace Lib

Calif Rsch & Tech, Inc
ATTN: K. Kreyenhagen
ATTN: M. Rosenblatt

Calif Rsch & Tech, Inc
ATTN: F. Sauer

Cushing Assoc
ATTN: V. Cushing

EG&G Wash Analytical Svcs Ctr, Inc
ATTN: Library

Electro-Mech Sys, Inc
ATTN: R. Shunk

Geo Centers, Inc
ATTN: E. Marram

H-Tech Labs, Inc
ATTN: B. Hartenbaum

IIT Rsch Institute
ATTN: Doc Lib

Institute for Defense Analyses
ATTN: Class Lib

Kaman Sciences Corp
ATTN: Library

Kaman Sciences Corp
ATTN: E. Conrad

Kaman Tempo
ATTN: DASIAC

Kaman Tempo
ATTN: DASIAC

Lockheed Missiles & Space Co., Inc
ATTN: J. Bonin
ATTN: Tech Lib

DEPARTMENT OF DEFENSE CONTRACTORS (Continued)

Lockheed Missiles & Space Co., Inc
ATTN: S. Taimuty
ATTN: Tech Info Ctr, D/COLL

Mitre Corp
ATTN: MS E190

National Technical Sys
ATTN: P. Lieberman

University of New Mexico
ATTN: G. Leigh
ATTN: N. Baum
2 cys ATTN: D. Calhoun

Pacific-Sierra Rsch Corp
ATTN: H. Brode, Chairman SAGE

Pacifica Tech
ATTN: G. Kent

Physics Applications, Inc
ATTN: F. Ford

Physics International Co
ATTN: E. Moore

R & D Associates
ATTN: C. Lee
ATTN: C. Knowles
ATTN: D. Simons
ATTN: J. Lewis
ATTN: Tech Info Ctr

R & D Associates
ATTN: G. Ganong

Rand Corp
ATTN: P. Davis

Rand Corp
ATTN: B. Bennett

S-CUBED
ATTN: D. Grine
ATTN: Library

DEPARTMENT OF DEFENSE CONTRACTORS (Continued)

Science Applications Intl Corp
ATTN: Tech Lib

Science Applications Intl Corp
ATTN: J. Cockayne
ATTN: H. Knasel
ATTN: W. Layson

Southwest Rsch Institute
ATTN: A. Wenzel
ATTN: W. Baker

SRI International
ATTN: G. Abrahamson
2 cys ATTN: J. Colton
2 cys ATTN: M. Sanai

Structural Mech Associates, Inc
ATTN: R. Kennedy

Teledyne Brown Engineering
ATTN: D. Ormond
ATTN: F. Leopard

TRW Electronics & Def Sector
ATTN: D. Baer
ATTN: Tech Info Ctr
2 cys ATTN: N. Lipner

TRW Electronics & Def Sector
ATTN: E. Wong
ATTN: P. Dai

Weidlinger Assoc, Consulting Engrg
ATTN: M. Baron

Weidlinger Assoc, Consulting Engrg
ATTN: J. Isenberg

Weidlinger Assoc, Consulting Engrg
ATTN: A. Misovec